Modeling And Analysis Of A Cantilever Beam Tip Mass System

Vamsi C. Meesala

Thesis submitted to the Faculty of the
Virginia Polytechnic Institute and State University
in partial fulfillment of the requirements for the degree of

Master of Science
in
Engineering Mechanics

Muhammad R. Hajj, Chair
Saad A. Ragab
Shima Shahab

25th of April, 2018
Blacksburg, Virginia

Keywords: Parametric excitation, Cantilever beam mass systems, Boundary conditions, Perturbation methods, Method of multiple scales, Sensitivity analysis, Uncertainty quantification, Mass/gas sensing, Damage detection, Energy harvesting, Piezoelectric materials, Nonlinear constitutive relation, Parameter identification.

Modeling And Analysis Of A Cantilever Beam Tip Mass System

Vamsi C. Meesala

ABSTRACT

We model the nonlinear dynamics of a cantilever beam with tip mass system subjected to different excitation and exploit the nonlinear behavior to perform sensitivity analysis and propose a parameter identification scheme for nonlinear piezoelectric coefficients.

First, the distributed parameter governing equations taking into consideration the nonlinear boundary conditions of a cantilever beam with a tip mass subjected to principal parametric excitation are developed using generalized Hamilton's principle. Using a Galerkin's discretization scheme, the discretized equation for the first mode is developed for simpler representation assuming linear and nonlinear boundary conditions. We solve the distributed parameter and discretized equations separately using the method of multiple scales. We determine that the cantilever beam tip mass system subjected to parametric excitation is highly sensitive to the detuning. Finally, we show that assuming linearized boundary conditions yields the wrong type of bifurcation.

Noting the highly sensitive nature of a cantilever beam with tip mass system subjected to parametric excitation to detuning, we perform sensitivity of the response to small variations in elasticity (stiffness), and the tip mass. The governing equation of the first mode is derived, and the method of multiple scales is used to determine the approximate solution based on the order of the expected variations. We demonstrate that the system can be designed so that small variations in either stiffness or tip mass can alter the type of bifurcation. Notably, we show that the response of a system designed for a supercritical bifurcation can change to yield a subcritical bifurcation with small variations in the parameters. Although such a trend is usually undesired, we argue that it can be used to detect small variations induced by fatigue or small mass depositions in sensing applications.

Finally, we consider a cantilever beam with tip mass and piezoelectric layer and propose a parameter identification scheme that exploits the vibration response to estimate the nonlinear piezoelectric coefficients. We develop the governing equations of a cantilever beam with tip mass and piezoelectric layer by considering an enthalpy that accounts for quadratic and cubic material nonlinearities. We then use the method of multiple scales to determine the approximate solution of the response to direct excitation. We show that approximate solution and amplitude and phase modulation equations obtained from the method of multiple scales analysis can be matched with numerical simulation of the response to estimate the nonlinear piezoelectric coefficients.

Modeling And Analysis Of A Cantilever Beam Tip Mass System

Vamsi C. Meesala

GENERAL AUDIENCE ABSTRACT

The domain of structural dynamics involves the evaluation of the structures response when subjected to time-varying loads. This field has many applications. For instance, by observing specific variations in the response of a structure such as bridge or a structural element such as a beam, one can diagnose the state of the structure or one of its elements. At much smaller scales, one can use a device to observe small variations in the response of a beam to detect the presence of bio-materials or gas particles in air. Additionally, one can use the response of a structure to harvest energy of ambient vibrations that are freely available.

In this thesis, we develop a mathematical framework for evaluating the response of a cantilever beam with a tip mass to small variations in material properties caused by fatigue and to small variations in the tip mass caused by additional mass that gets bound to the structure. We also exploit the response of the beam to evaluate nonlinear material properties of piezoelectric materials that have been suggested for use in charging micro sensors, vibration control, load sensing and for high power energy transfer applications.

Dedication

To my parents and sister who have always wished for my best,
and to all my mentors, especially my undergraduate adviser, Dr.C.P.Vyasarayani, who is the reason I applied for Engineering Mechanics at Virginia Tech.

Acknowledgments

They say, "*There is a lesson behind every experience...a message with every person we meet...*" I believe I'm an extract of a bit of something from everyone I've met, interacted and shared experiences. I'm grateful to all the incalculable number of people including my teachers, mentors, colleagues, family, and friends who have had an enormous part in my journey so far.

First and foremost, I would like to extend my sincerest gratitude to my advisor,
Dr. Muhammad R. Hajj for taking me into his research group and providing his insightful guidance and immense support. Professor Hajj is kind, understanding, always tried to make the best out of every situation and I couldn't have imagined working with a better advisor. I have always appreciated that Professor Hajj shares my attention to conceptual and mathematical details and especially the intriguing, lengthy discussions that led to many exciting conclusions that are a part of this thesis. I cherish the time I spent with you Professor and would like to continue working with you. I can't thank Saeed Alnuaimi, a dear friend, enough for encouraging me to get in touch with Professor Hajj when I just started my masters and was looking for an advisor.

I thoroughly enjoyed attending the lectures of Profs. Romesh Batra, Shane D. Ross, Muhammad Hajj, James Hanna, Shima Shahab, Ricardo Burdisso, Saad A. Ragab and Mark Cramer, listed in the chronological order of courses taken, and interacting with them. They all have played an essential role in strengthening my basics in the concepts that they covered. I would like to thank Professor Saad A. Ragab for always welcoming me for providing his expert opinion and guidance for research and coursework. I would also like to thank Dr. Shahab for sharing her valuable expertise on modeling continuous systems, which boosted my research work. I appreciate the hard work of the staff at Department of Biomedical Engineering and Mechanics especially Jessica, Cristina, Jody, Dave, Mark, and Beverly and making the department a fantastic place to develop oneself.

I would like to thank Professor Hajj's students Dr. Yan, Saeed Alnuaimi, Hisham Shehata, Dr. Jamal ALrowaijeh, Guillermo gomez and Ahmed hussein for sharing their expertise in their respective fields and being good friends. Thanks to Dr. Ayoub Boroujeni for providing useful insights on carbon fiber/epoxy resin composites. To Manish, Aarushi, Wilson, Tapas, Shamit, Himanshu, Pavan, Manjot, and Piyush who are an extended family thank you for

your friendship and for always being there to lubricate the stressful journey and making it a memorable one. I hope to continue this remarkable bond we have for a long time. Thanks to Dr. Parag Bobade (Osman Bhai) for the Hyderabadi pun and for the laughs we shared. I'm grateful to Dr. Gary Nave, Dr. Brian Chang, Kristen, Kedar, Masoud, and Kayla for keeping me involved with Graduate Engineering Mechanics Society (GEMS), which allowed me to interact with a lot of peers in the department.

Finally, I want to thank each and everyone who is working hard to make Virginia Tech and Blacksburg a beautiful place to live with an accepting and healthy community. I enjoyed my time here so far, and it will have a special place in my heart.

VAMSI CHANDRA MEESALA

Contents

List of Figures

List of Tables

Chapter 1

Introduction

1.1 Motivation

To emphasize the importance of modeling and simulation of dynamical systems, I would like to start with the definition of ***Model*** by Professor Marvin Minsky:

"A model (M) for a system (S) and an experiment (E) is anything to which E can be applied in order to answer the questions about (S)."

Abiding by the above definition, understanding a physical system is a process that involves performing experiments to provide an insight into the principles governing the system and their respective models. Although scientists are interested in understanding the system by observing and developing a model for it, engineers are focused on applying and modifying them it to their advantage [1]. Particularly, insights from models and experiments play an important role in the prognosis of design, as they allow the designer to develop a mathematical model and simulate it. With the computational capabilities of the current digital age, these simulations can provide a quick way to predict a behavior and control it accordingly, which otherwise is done by performing time-consuming and arduous experiments.

Depending on the nature of the response, any mathematical model of a mechanical system (equation/s of motion) can be classified into linear or nonlinear dynamical system. In most cases, a complete mathematical description of the dynamical system is inherently nonlinear, which under specified conditions may be reduced to a linear description. Some of the standard examples of mechanical systems exhibiting nonlinear response or nonlinear dynamics can be found in [2–5]. In structures, the nonlinearities in the equation/s of motion arise either due to large deformations (geometric nonlinearity), or due to the inertia of motion (inertial nonlinearity) or due to the nonlinear constitutive relation between stress and strain (material nonlinearity) or all of them together. A typical free and un-damped equation of motion of a system including the inertial and geometric nonlinearities until *third* order

approximation is of the form:

$$\ddot{q(t)} + \omega^2 q(t) + \delta \left[q(t)\dot{q}(t)^2 + q(t)^2 \ddot{q}(t) \right] + \alpha q(t)^3 = 0$$

In this work, the nonlinear dynamics of a cantilever beam with tip mass are modeled and exploited for interesting objectives as will be discussed in the following paragraphs.

1.2 Background - cantilever beam and tip mass system

The cantilever beam with a tip mass is a generic system to study and assess different aspects of structural dynamics. It is utilized to model robotic arms [6,7], antenna masts [8,9], wings with store configurations [10–15], energy harvesting devices [16–22], vibrating beam gyroscopes [23, 24] and bio/chemical sensors [25–31]. In all these applications, there is a need to validate the mathematical model developed with experimental results to facilitate the analysis and optimize the design for better performance. Moreover, most of the applications mentioned above utilize the dynamic resonant response or are implicitly nonlinear, that produce large strains and induce geometric nonlinearity. This calls for accurate modeling by considering the inherently present geometric nonlinearity up to an appropriate approximation. Also, the dynamic resonant response is highly dependent on the geometric and material properties of the device. Any uncertainty in the beam's stiffness, the mass value or material properties associated with operational conditions such as environmental thermal effects, and fatigue induced by cyclic loading or manufacturing tolerances (or defects) can result in discrepancies between the proposed cantilever beam-mass model and predicted values and experimental results; thereby compromising the fidelity of the model representing the device. Such discrepancies can be anticipated by performing a sensitivity analysis of the response to small variations in the parameters, which will strengthen the model. The information of sensitivity can be precious as it can be used to detect damage or to sense a target mass using bio/mass sensors.

The problem of nonlinearity in the case of the cantilever beam with tip mass energy harvesters is even more complicated. This is because the piezoelectric material commonly employed for energy harvesting applications [17], can behave in a nonlinear manner by exhibiting amplitude dependent resonant frequency, super-harmonics in the response, saturation and hysteresis behaviors [32–34]. It is important to understand the nature of the nonlinearity by estimating the nonlinear parameters in the constitutive relations. An optimized curve fitting procedure can be used to identify the parameters causing the nonlinear behavior. Yet, there is a need for more parameter identification procedures that exploit the vibration response. We cater to all ideas and issues mentioned above in this work with the following objectives.

1.3 Objectives

The primary objectives of this work are:

- To accurately develop the governing equation of a cantilever beam tip-mass system subjected to parametric excitation with particular consideration of nonlinear boundary conditions and their effects on governing equation.
- To perform sensitivity of the parametric response of the cantilever beam tip-mass system to small variations for design purposes or for exploring specific response dynamics to detect variations.
- To propose a parameter identification scheme based on direct excitation of a cantilever beam tip-mass system to identify and quantify the nonlinear piezoelectric coefficients in constitutive relations.

We solve all the above-mentioned objectives using the framework of the method of multiple scales.

Chapter 2

Response variations of a cantilever beam tip mass system with nonlinear and linearized boundary conditions

A crucial step in the design of any structure is to understand its dynamic response. This typically includes determining its natural frequencies, corresponding mode shapes, and dynamic stresses. Such an exercise can be performed by reduced order mathematical models that predict this response. The cantilever beam with a tip mass has been used as a generic system to assess modeling needs in different applications or as a structural system whose response can be exploited for different purposes. For example, treating the boundary conditions at the free end of the cantilever beam tip mass system can shed light on how to treat wing/store configurations in flutter analysis of fighter aircraft [10–14]. In energy harvesting of ambient vibrations, the tip mass is added to cantilevered piezoelectric layered beam structure to induce large strains thereby generating high power density [16,17]. In microelectro mechanical systems, adding a tip mass decreases the natural frequency, which otherwise would be of the order of few GHz's [18–22]. In gas/mass sensors, the response of the cantilever beam in conjunction with added target mass can be used to sense the presence of bio-materials [25–31]. It is also modeled to understand coupling and energy transfer phenomenon in structures for control purposes [35–37].

The governing equations and boundary conditions of continuous systems, which are usually integro-partial differential equations, can be solved numerically using the Finite Element Methods [38]. Alternatively, a reduced-order model or representation of the system's dynamics can be treated analytically by using perturbation methods. The advantages of these methods is their flexibility to investigate stability and characteristics of nonlinear response. Direct [39–43] and Discretization [41,44,45] approaches can be used when implementing these methods. In the direct approach, the method of multiple scales is directly applied to the governing partial differential equation. By isolating the secular terms and using the adjoint

description, solvability conditions are developed from which amplitude and phase modulation equations that govern the system's response are obtained [46]. In the discretization approach, a Galerkin weighted residual method is used to develop the governing equation of n modes from the distributed system given by the partial differential equation and boundary conditions. Then, the governing equations are solved using the method of multiple scales to develop amplitude and phase modulation equations by eliminating the secular terms [41]. That is, for an excitation near a particular mode, the problem of solving a PDE and boundary conditions in the direct approach is reduced to one or more ODE in discretized approach.

It is usually assumed that linearizing the boundary conditions is justified especially when the interest is in finding linear mode shapes and natural frequency of system. On the other hand, it is fair to expect that the nature of the response of a nonlinear system may vary significantly from the true one if the boundary conditions were linearized. This chapter examines the extent of such variations in the response of a cantilever beam with tip mass system. Furthermore, particular attention is paid to the effect of linearization on the discretized governing equations and their solution. Towards this objective, we develop the distributed parameter governing equations and boundary conditions for a parametrically excited cantilever beam and tip mass system using the generalized Hamilton's principle [47]. We then employ Galerkin discretization to the distributed model and determine the governing equation of the first mode (discretized equation) to study the principal parametric resonance by considering and neglecting nonlinear boundary conditions. Thereafter, we solve the distributed parameter system and discretized equation with nonlinear boundary conditions using the method of multiple scales and compare the resulting modulation equations with those obtained from the PDE solution to validate the discretization.

2.1 Mathematical Modeling

A schematic of the cantilever beam with a tip mass subjected to parametric excitation is presented in figure 2.1. The beam with length l, width b, thickness h and mass per unit length ρ, is clamped at the base where it is subjected to a harmonic excitation at twice its natural frequency. Below, we derive the governing equation of the beam's response, with both the generalized Hamilton's principle and Newton's second law with the assumptions that the *Euler-Bernoulli beam theory* is applicable, i.e., the beam has a higher length to depth ratio so that the rotational effects of the differential element and the angular distortion can be neglected [47], and that the beam can be subjected to large bending motion without a significant axial deformation, i.e., the beam is *inextensible* [4].

2.1.1 Generalized Hamilton Principle

The generalized Hamilton's principle is expressed as:

$$\int_{t_1}^{t_2} (\delta T - \delta \Pi + \delta W_{nc})\, dt = 0 \tag{2.1}$$

where δT, $\delta \Pi$ and δW_{nc} are variations in kinetic energy, potential energy and virtual work by non-conservative forces respectively. Neglecting the gravity effects, the potential energy of the system considering only the strain energy due to bending is given by

$$\Pi = \frac{1}{2} \int_0^l \int_A E z^2 \kappa^2 \, dA \, ds \tag{2.2}$$

where E is the beam's modulus of elasticity, z is distance from the neutral axis, s is the

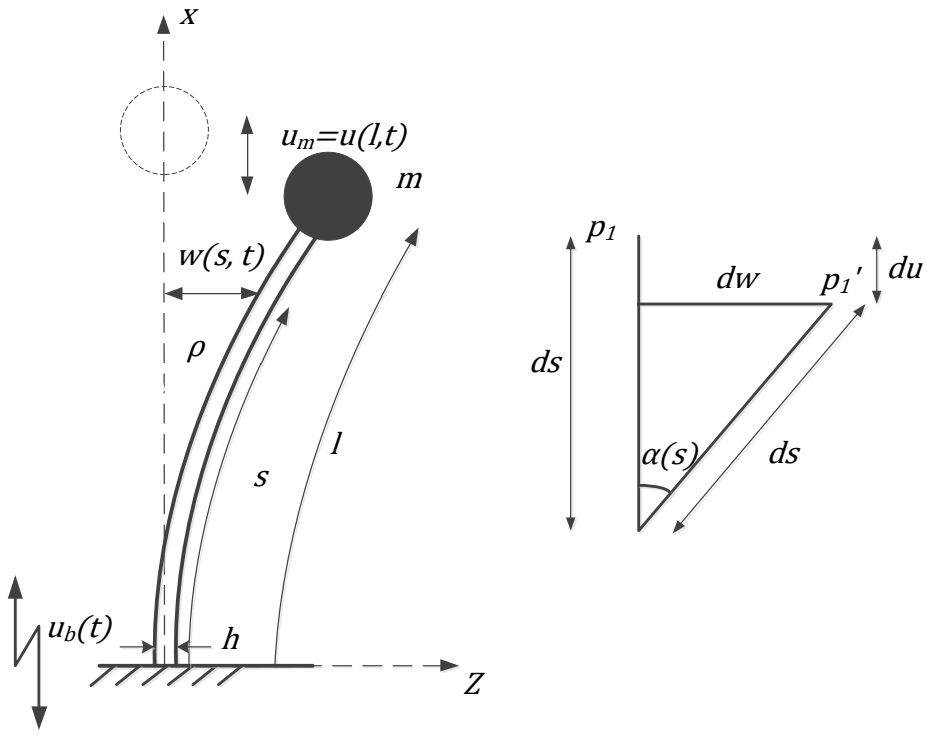

Figure 2.1: Schematic of the cantilever beam-mass system. The vertical line represents the undeformed state and the curved line represents a general deformed state. The schematic on the right hand side is used to define the geometry and depict the in-extensibility condition, $pp_1 = pp_1'$

curvilinear coordinate along the length of the beam and κ is the radius of curvature. Based

on the assumption that the beam is in extensible, the curvature is expressed as

$$\kappa = \frac{\partial}{\partial s}\alpha(s,t) = w^{(2,0)}(s,t) + \frac{1}{2}w^{(2,0)}(s,t)w^{(1,0)}(s,t)^2 + ... \tag{2.3}$$

where the notation $(.)^{(n_1,n_2)}(s,t)$ denotes n_1^{th} derivative of $(.)$ with respect to s and n_2^{th} derivative of $(.)$ with respect to t. This notation is followed quite extensively from here on. Squaring equation 2.3 yields

$$\kappa^2 = \left[w^{(2,0)}(s,t)\right]^2 + \left[w^{(2,0)}(s,t)w^{(1,0)}(s,t)\right]^2 + ... \tag{2.4}$$

Dropping all terms that give rise to nonlinearities with order larger than three, i.e., $O\left([.]^{n>3}\right) = 0$, the potential energy, $\mathit{\Pi}$ is re-written as

$$\mathit{\Pi} = \frac{1}{2}\int_0^l \int_A Ez^2 \left(\left[w^{(2,0)}(s,t)\right]^2 + \left[w^{(2,0)}(s,t)w^{(1,0)}(s,t)\right]^2\right) dA\, ds \tag{2.5}$$

and noting that the area moment of inertia about the Y-axis is given by $I_Y = \int_A z^2\, dA$, we write the potential energy as

$$\mathit{\Pi} = \frac{1}{2}\int_0^l EI_Y \left[w^{(2,0)}(s,t)\right]^2 ds + \frac{1}{2}\int_0^l EI_Y \left[w^{(1,0)}(s,t)w^{(2,0)}(s,t)\right]^2 ds \tag{2.6}$$

The kinetic energy of the beam-tip mass system is given by

$$T = \frac{1}{2}m\left([\dot{u}_m(t)]^2 + \left[\frac{\partial w(l,t)}{\partial t}\right]^2\right) + \frac{1}{2}\int_0^l \rho\left(\left[u^{(0,1)}(s,t)\right]^2 + \left[\frac{\partial w(s,t)}{\partial t}\right]^2\right) ds \tag{2.7}$$

where $u(s,t)$ and $u_m(t)$ represent respectively the vertical displacements of the beam and tip mass. The relations between these displacements is determined from the geometry of figure 2.1. We write

$$\alpha(s,t) = \sin^{-1}\left(w^{(1,0)}(s,t)\right) \text{ , and} \tag{2.8}$$

$$\cos(\alpha(s,t)) = \frac{\partial s - \partial u(s,t)}{\partial s} = 1 - u^{(1,0)}(s,t) \tag{2.9}$$

Expanding the inverse trigonometric and trigonometric functions, we re-write equations 2.8-2.9 as

$$\alpha(s,t) = w^{(1,0)}(s,t) + \frac{1}{6}\left[w^{(1,0)}(s,t)\right]^3 + ... \text{ , and} \tag{2.10}$$

$$u^{(1,0)}(s,t) = \frac{1}{2}\left[\alpha(s,t)\right]^2 - \frac{1}{24}\left[\alpha(s,t)\right]^4 - ... \tag{2.11}$$

Substituting equation 2.10 into equation 2.11, we obtain

$$u^{(1,0)}(s,t) = \frac{1}{2}\left[w^{(1,0)}(s,t)\right]^2 + O\left(\left[w^{(1,0)}(s,t)\right]^5\right) \tag{2.12}$$

where $O\left(\left[w^{(1,0)}(s,t)\right]^5\right)$ is used to represent higher order terms that are neglected in the subsequent analysis. Representing the harmonic excitation of the base by u_b, the vertical displacement of the tip mass is then given by

$$u_m(t) = \int_0^l \frac{1}{2}\left[w^{(1,0)}(s,t)\right]^2 ds - u_b(t) \tag{2.13}$$

Similarly, the vertical displacement of any element on the beam at a distance s from the base is given by

$$u(s,t) = \int_0^s \frac{1}{2}\left[w^{(1,0)}(y,t)\right]^2 dy - u_b(t) \tag{2.14}$$

Substituting the values of u_m and u_s from equations 2.13 and 2.14 into equation 2.7, we obtain

$$T = \frac{1}{2}m\left[\int_0^l \frac{1}{2}\frac{\partial}{\partial t}\left(\frac{\partial w(s,t)}{\partial s}\right)^2 ds - \dot{u}_b(t)\right]^2 + \frac{1}{2}\int_0^l \rho\left[\int_0^s \frac{1}{2}\frac{\partial}{\partial t}\left(\frac{\partial w(y,t)}{\partial y}\right)^2 dy - \dot{u}_b(t)\right]^2 ds + \frac{1}{2}m\left(\frac{\partial w(l,t)}{\partial t}\right)^2 + \frac{1}{2}\int_0^l \rho\left(\frac{\partial w(s,t)}{\partial t}\right)^2 ds \tag{2.15}$$

It has been assumed that the tip mass is treated as a point mass and, hence, the rotational effects are not included when determining the kinetic energy.

The virtual work done by the non conservative forces is given by

$$\delta W_{nc} = -\int_0^l c_1 w^{(0,1)}(s,t)\delta w(s,t)\, ds \tag{2.16}$$

where, c_1 is structural damping coefficient.

Substituting equations 2.6, 2.15 and 2.16 into equation 2.1, we obtain the equation of motion as

$$-\rho\ddot{w} - c_1\dot{w} - \frac{\rho w'}{2}\int_0^s \frac{\partial^2}{\partial t^2}\left(w'^2\right) dy + \rho\ddot{u}_b w' - EI_Y(w'''' + w''^3 + 4w'w''w''' + w'^2w'''') + w''\left(\frac{\rho}{2}\int_s^l\int_0^\theta \frac{\partial^2}{\partial t^2}\left(w'^2\right) dy\, d\theta + m\int_0^l \frac{\partial^2}{\partial t^2}\left(\frac{w'^2}{2}\right) ds - m\ddot{u}_b - (l-s)\rho\ddot{u}_b\right) = 0 \tag{2.17}$$

In deriving equation 2.17, we used the integration by parts as $\int_0^l\int_0^s G(y)\, dy\, ds = \int_0^l (l-s)G(s)\, ds$, where $G(x)$ is any continuous function.

Using $(w'(w'w'')')' = w''^3 + 4w'w''w''' + w'^2w''''$ and $\frac{\rho}{2}\left(w'\int_l^s\int_0^\theta \frac{\partial^2}{\partial t^2}\left(w'^2\right) dy\, d\theta\right)' = \frac{\rho w'}{2}\int_0^s \frac{\partial^2}{\partial t^2}\left(w'^2\right) dy + w''\frac{\rho}{2}\int_s^l\int_0^\theta \frac{\partial^2}{\partial t^2}\left(w'^2\right) dy\, d\theta$, equation 2.17 is further simplified to obtain

$$\rho\ddot{w} + c_1\dot{w} + EI_Y(w'''' + [w'(w'w'')']') + m\ddot{u}_b w'' + \frac{\rho}{2}\left(w'\int_l^s\int_0^\theta \frac{\partial^2}{\partial t^2}\left(w'^2\right)\, dy\, d\theta\right)' - \rho\ddot{u}_b\left(w' + (s-l)w''\right) - \frac{mw''}{2}\int_0^l \frac{\partial^2}{\partial t^2}\left(w'^2\right)\, ds = 0 \quad (2.18)$$

where $\ddot{u}_b = -\frac{1}{2}f\Omega^2\left[e^{j(\Omega T_0+\tau_e)} + e^{-j(\Omega T_0+\tau_e)}\right]$ and f is displacement of the excitation and Ω is the forcing frequency. The natural nonlinear boundary conditions at $s = l$ are determined from the moment and the shear boundary conditions as

$$\left(EI_Y w''w'^2 + EI_Y w''\right)|_{s=l} = 0 \quad \Longrightarrow \quad w^{(2,0)}(l,t) = 0 \quad (2.19)$$

$$\left(m\ddot{u}_b w' - mw'\int_0^l \frac{\partial^2}{\partial t^2}\left(\frac{w'^2}{2}\right)\, ds + EI_Y\left(w'''w'^2 + w''^2w' + w'''\right) - m\ddot{w}\right)\Big|_{s=l} = 0 \quad (2.20)$$

Since the beam is clamped, the geometric boundary conditions at $s = 0$ are given by

$$w(0,t) = 0 \quad (2.21)$$

$$\left.\frac{\partial w(s,t)}{\partial s}\right|_{s=0} = 0 \quad (2.22)$$

We shall note that in the above derivation, E, I_Y, l, ρ and m are assumed to be constants, that y and θ are dummy variables, and that the primes and dots represent derivatives of $w(s,t)$ with respect to the coordinate s and time t respectively. The MATHEMATICA code *Genhamilton1.0.nb*, used for the complete derivation can be found in Appendix A.

2.1.2 Newton's Second Law

The procedure of Nayfeh and Pai [4] is followed below to derive the fully nonlinear governing equations of initially straight Euler-Bernoulli beams. A local orthogonal co-ordinate system $\xi y\eta$ is considered for a better representation of the forces. The free body diagram of an element of beam of length ds is shown in the figure 2.2 where F_1 and F_2 are surface traction forces along the ξ and η directions respectively. If i_x and i_z are unit vectors along x and z axes and i_ξ and i_η are unit vectors along the ξ and η axes, there exists a transformation matrix T, such that,

$$\begin{Bmatrix} i_x \\ i_z \end{Bmatrix} = [T]\begin{Bmatrix} i_\xi \\ i_\eta \end{Bmatrix}, \qquad [T] = \begin{bmatrix} \cos\alpha & \sin\alpha \\ -\sin\alpha & \cos\alpha \end{bmatrix} \quad (2.23)$$

By considering $u(s,t)$ and $w(s,t)$ as the displacements along the x and z axes respectively and using the in-extensibility condition, we write,

$$\left[1 - u^{(1,0)}(s,t)\right]^2 + w^{(1,0)}(s,t)^2 = 1$$

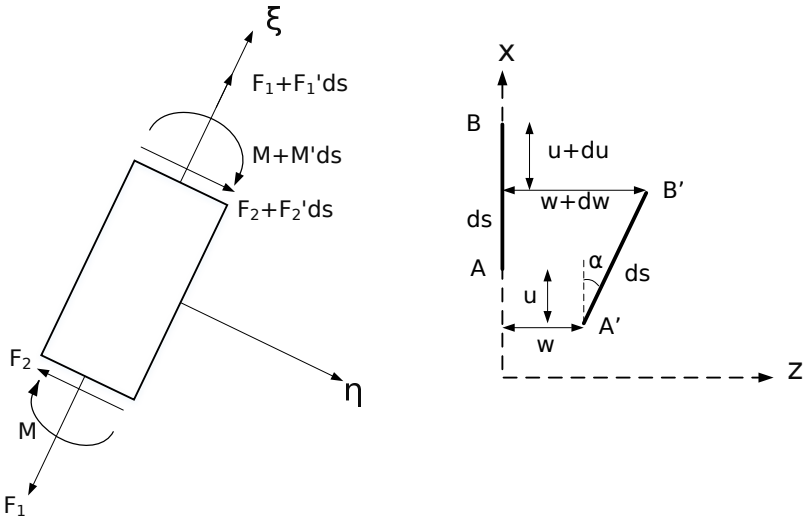

Figure 2.2: Figure showing the free body diagram of an element in the beam of length, ds and the displacements

$$\therefore \quad u(s,t) = \int_0^s \left(1 - \sqrt{1 - w^{(1,0)}(y,t)^2}\right) dy \approx \int_0^s \frac{1}{2} w^{(1,0)}(y,t)^2 \, dy \tag{2.24}$$

From figure 2.2, we have

$$\sin(\alpha(s,t)) = w^{(1,0)}(s,t) \implies \alpha(s,t) = \sin^{-1}(w^{(1,0)}(s,t)) \tag{2.25}$$

$$\cos(\alpha(s,t)) = 1 - u^{(1,0)}(s,t) = \sqrt{1 - w^{(1,0)}(s,t)^2} \tag{2.26}$$

From Newton's second law and figure 2.2, we have

$$\frac{\partial(F_1 i_\xi + F_2 i_\eta)}{\partial s} ds = \rho ds (u_g^{(0,2)}(s,t) i_x + w^{(0,2)}(s,t) i_z) \tag{2.27}$$

where $u_g(s,t) = -u(s,t) + u_b(t)$. The negative sign is the consequence of contraction of the beam due to the in-extensibility condition. Using equation 2.23 and equating the components along i_x and i_z, the above equation is rewritten as:

$$\frac{\partial}{\partial s}[F_1 \cos(\alpha(s,t))] - \frac{\partial}{\partial s}[F_2 \sin(\alpha(s,t))] = -\rho u^{(0,2)}(s,t) + \rho \ddot{u}_b(t) \tag{2.28}$$

$$\frac{\partial}{\partial s}[F_1 \sin(\alpha(s,t))] + \frac{\partial}{\partial s}[F_2 \cos(\alpha(s,t))] - c_1 w^{(0,1)}(s,t) = \rho w^{(0,2)}(s,t) \tag{2.29}$$

where c_1 is the linear structural damping coefficient.
Consistent with section 2.1.1, the rotational effects of the beam and the tip mass are neglected. Therefore, the equilibrium of moments with respect to the to $y - axis$ is,

$$ds \frac{\partial}{\partial s} M(s,t) + F_2 ds = 0 \implies F_2 = -\frac{\partial}{\partial s} M(s,t) \tag{2.30}$$

The bending moment of a beam is given by the relation, $M = EI_Y k = EI_Y \alpha^{(1,0)}(s,t)$ and equation 2.25. Equation 2.30 is re-written as

$$F_2 = -EI_Y \alpha^{(2,0)}(s,t) = -EI_Y \frac{\partial}{\partial s} \sin^{-1}(w^{(1,0)}(s,t)) \tag{2.31}$$

Since the beam is clamped at $s = 0$, the boundary conditions at $s = 0$ are

$$w(0,t) = 0$$

$$w^{(1,0)}(0,t) = 0$$

Applying the Newton's second law at $s = l$, we write

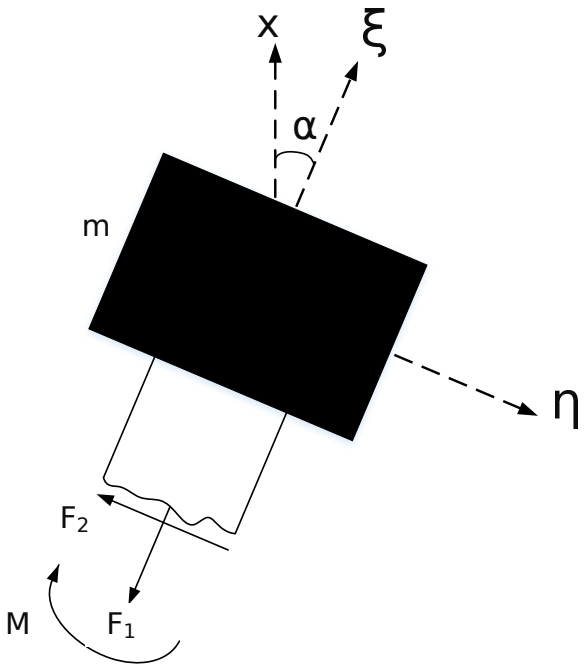

Figure 2.3: Figure showing the free body diagram at the tip of the beam, $s = l$

$$-F_1 \cos(\alpha(l,t)) + F_2 \sin(\alpha(l,t)) = -mu^{(0,2)}(l,t) + m\ddot{u}_b(t) \tag{2.32}$$

$$-F_1 \sin(\alpha(l,t)) - F_2 \cos(\alpha(l,t)) = mw^{(0,2)}(l,t) \tag{2.33}$$

From moment equilibrium, we have

$$M(l,t) = 0 \implies \alpha^{(1,0)}(l,t) = 0 \tag{2.34}$$

Integrating equation 2.28 with respect to s from l to s and using equation 2.32, we obtain

$$F_1 \cos(\alpha(s,t)) - F_2 \sin(\alpha(s,t)) - mu^{(0,2)}(l,t) + m\ddot{u}_b(t) = -\rho \int_l^s u^{(0,2)}(s,t)\, ds + (s-l)\rho\ddot{u}_b(t) \tag{2.35}$$

From equations 2.24 and 2.35, the expression for F_1 is obtained as

$$F_1 = \frac{1}{\cos(\alpha(s,t))}\left[-\frac{\rho}{2}\int_l^s\int_0^\theta \frac{\partial^2}{\partial t^2}\left(w^{(1,0)}(y,t)^2\right)\,dy\,d\theta + (s-l)\rho\ddot{u}_b(t)\right] + \frac{1}{\cos(\alpha(s,t))}\left[F_2\sin(\alpha(s,t)) + \frac{m}{2}\int_0^l \frac{\partial^2}{\partial t^2}\left(w^{(1,0)}(s,t)^2\right)\,ds - m\ddot{u}_b(t)\right] \quad (2.36)$$

Substituting the expression for F_1 in equation 2.29 and using the trigonometric relations in equations 2.25 and 2.26, we obtain

$$-\frac{\rho}{2}\frac{\partial}{\partial s}\left(\frac{w^{(1,0)}(s,t)}{\sqrt{1-w^{(1,0)}(s,t)^2}}\int_l^s\int_0^\theta \frac{\partial^2}{\partial t^2}\left(w^{(1,0)}(y,t)^2\right)\,dy\,d\theta\right) - c_1 w^{(0,1)}(s,t) - c_2 w^{(0,1)}(s,t)|w^{(0,1)}(s,t)| + \frac{\partial}{\partial s}\left(\frac{\rho\ddot{u}_b(t)(s-l)w^{(1,0)}(s,t)}{\sqrt{1-w^{(1,0)}(s,t)^2}}\right) + \frac{\partial}{\partial s}\left(\frac{F_2}{\sqrt{1-w^{(1,0)}(s,t)^2}}\right) + \frac{\partial}{\partial s}\left(\frac{w^{(1,0)}(s,t)}{\sqrt{1-w^{(1,0)}(s,t)^2}}\left[\frac{m}{2}\int_0^l \frac{\partial^2}{\partial t^2}\left(w^{(1,0)}(s,t)^2\right)\,ds - m\ddot{u}_b(t)\right]\right) = \rho w^{(0,2)}(s,t) \quad (2.37)$$

Substituting the expression for F_2 from equation 2.31, using Taylor series expansion of inverse trigonometric functions and retaining the expression up to the third order, we obtain

$$\rho\ddot{w} + c_1\dot{w} + c_2|\dot{w}|\dot{w} + EI_Y(w'''' + (w'(w'w'')')') + m\ddot{u}_b w'' + \frac{\rho}{2}\left(w'\int_l^s\int_0^\theta \frac{\partial^2}{\partial t^2}\left(w'^2\right)\,dy\,d\theta\right)' - \rho\ddot{u}_b(t)\left(w' + (s-l)w''\right) - \frac{mw''}{2}\int_0^l \frac{\partial^2}{\partial t^2}\left(w''^2\right)\,ds = 0 \quad (2.38)$$

Substituting the expressions for F_1, F_2, $\cos(\alpha(s,t))$, $\alpha^{(1,0)}(s,t)$ and $\sin(\alpha(s,t))$ into the boundary conditions at $s = l$ i.e., equations 2.33 and 2.34, we obtain the modified boundary conditions as

$$w''(l,t) = 0 \quad (2.39)$$

$$\left(m\ddot{u}_b w' - mw'\int_0^l \frac{\partial^2}{\partial t^2}\left(\frac{w'^2}{2}\right)\,ds + EI_Y\left(w'''w'^2 + w''^2w' + w'''\right) - m\ddot{w}\right)\Bigg|_{s=l} = 0 \quad (2.40)$$

The dashes and dots represent derivatives of $w(s,t)$ with respect to s and time, t respectively, and y and θ are dummy variables.

We observe that equations 2.18 - 2.20 and 2.38 - 2.40, representing governing equation and boundary conditions derived using Newton's second law exactly agree with those derived using the generalized Hamilton's principle.

2.2 Reduced order model - Galerkin discretization

Next, we perform modal analysis by solving for the exact mode shapes and orthogonal equations. Then, we use the Galerkin discretization procedure to derive and note the differences in the governing equation of the first mode when considering linearized and nonlinear boundary conditions.

2.2.1 Modal analysis

Modal analysis, used to determine the mode shapes and frequencies of the beam-mass system, is performed by considering the linear undamped free vibration problem obtained by dropping the damping, forcing and nonlinear terms in equations 2.18-2.22, which reduces the equation of motion to

$$\rho\ddot{w} + EI_Y w'''' = 0 \tag{2.41}$$

and the boundary conditions to

$$w(0,t) = 0 \tag{2.42}$$

$$\left.\frac{\partial w(s,t)}{\partial s}\right|_{s=0} = 0 \tag{2.43}$$

$$\left(EI_Y w'' w'^2 + EI_Y w''\right)|_{s=l} = 0 \implies w''|_{s=l} = 0 \tag{2.44}$$

$$\left(EI_Y w''' - m\ddot{w}\right)|_{s=l} = 0 \tag{2.45}$$

Considering equation 2.41, we observe that the spatial and temporal derivatives of $w(x,t)$ can be explicitly decomposed into two degenerate equations. So, $w(x,t)$ is decomposed into a product of independent spatial and temporal functions and written as

$$w(s,t) = \phi(s)q(t) \tag{2.46}$$

Substituting equation 2.46 into equation 2.41 and realizing that $\ddot{q} = -\omega_n^2 q$, where ω_n is the natural frequency of the n^{th}-mode, we obtain,

$$\phi'''' = \lambda^4\phi \tag{2.47}$$

whose general solution is of the form

$$\phi(s) = A\cos(\lambda s) + B\sin(\lambda s) + C\cosh(\lambda s) + D\sinh(\lambda s) \tag{2.48}$$

where $\lambda = \left(\frac{\omega_n^2\rho}{EI_Y}\right)^{\frac{1}{4}}$ and the linear boundary conditions are given by

$$\phi(0) = \phi'(0) = \phi''(l) = 0 \tag{2.49}$$

$$\left(EI_Y\phi''' + m\omega^2\phi\right)|_{s=l} = 0 \tag{2.50}$$

Substituting the general solution in the linear boundary conditions and solving for non-trivial solution yields the characteristic equation as:

$$\rho\left[\cos\left(\lambda l\right)\cosh\left(\lambda l\right)+1\right]+m\lambda\left[\cos\left(\lambda l\right)\sinh\left(\lambda l\right)-\sin\left(\lambda l\right)\cosh\left(\lambda l\right)\right]=0 \tag{2.51}$$

The characteristic equation is a transcendental equation. It has infinite solutions for λ (and ω) and, hence, an infinite number of modes. For any two distinct modes, p and q, equation 2.47 follows the orthogonality conditions [47]:

$$\begin{aligned}\int_0^l \rho\phi_p(s)\phi_q(s)\,ds+m\phi_p(l)\phi_q(l)&=\delta_{pq}\\ \int_0^l EI_Y\phi_p''(s)\phi_q''(s)\,ds&=\delta_{pq}\omega_q^2\end{aligned} \tag{2.52}$$

where δ_{pq} is the Kronecker delta, defined as unity when p is equal to q and zero otherwise. Using the above discretization, the solution is then approximated by the sum of a finite number of modes, i.e.

$$w(s,t)=\sum_{i=1}^{M}\phi_i(s)q_i(t) \tag{2.53}$$

where the basis function $\phi_i(s)$ represents the mode shape, $q_i(t)$ represents the modal coordinate, and M is the number of modes under consideration. We note that the basis function is a comparable function as it satisfies the linear boundary conditions.

2.2.2 Third order non-linear equation of motion

To develop the third order non-linear equation of motion of modal coordinates, which from now, will be referred as temporal amplitudes, we substitute $w(s,t)=\sum_{i=1}^{M}\phi_i(s)q_i(t)$ for $w(s,t)$ into equation 2.18, which yields

$$\begin{aligned}\rho\sum_{i=1}^{M}\ddot{q}_i\phi_i+c_1\sum_{i=1}^{M}\dot{q}_i\phi_i+EI_Y\left[\sum_{i=1}^{M}\phi_i''''q_i+\sum_{i,j,k=1}^{M}q_iq_jq_k(\phi_i'(\phi_j'\phi_k'')')'\right]+m\ddot{u}_b\sum_{i=1}^{M}\phi_i''q_i\\ +\frac{\rho}{2}\sum_{i,j,k=1}^{M}\left(\phi_i'q_i\int_l^s\int_0^\theta\phi_j'\phi_k'\frac{d^2}{dt^2}\left(q_jq_k\right)\,dy\,d\theta\right)'-\rho\ddot{u}_b\sum_{i=1}^{M}q_i\left(\phi_i'+(s-l)\phi_i''\right)\\ -\sum_{i,j,k=1}^{M}\frac{m\phi_i''q_i}{2}\int_0^l\phi_j'\phi_k'\frac{d^2}{dt^2}\left(q_jq_k\right)\,ds=0\end{aligned} \tag{2.54}$$

By considering only M modes, the discretization doesn't fully satisfy equation 2.18 in that the right hand side may differ from zero. One could then represent this difference in equation 2.54 by a residue R on its right hand side. We employ Galerkin's weighted residual

procedure, for the formulation of the equation/s governing temporal amplitudes $q_i(t)$ that require the residue to be orthogonal to the comparison functions $\phi_i(s)$, linear mode shapes or basis functions [48,49]. Therefore, the equation is multiplied with a mode shape $\phi_r(s)$ and integrated over the length of the beam. This procedure not only accounts for the residue but also enables us to employ the orthogonality conditions as stated in equation 2.52 to develop the governing equation/s of the temporal amplitudes.

Considering only one mode($M = 1$) and using the orthogonal properties of the linear modes, the individual terms in equation 2.54 are simplified as shown below:

$$\ddot{q}_1 \int_0^l \rho\phi_1\phi_1\, ds \;=\; \ddot{q}_1 - m\ddot{q}_1\phi_1(l)^2$$

$$c_1\dot{q}_1 \int_0^l \phi_1^2\, ds = c_1\dot{q}_1 \int_0^l \phi_1^2\, ds$$

$$EI_Y q_1 \int_0^l \phi_1\phi_1''''\, dx \;=\; \omega_1^2 q_1 + EI_Y q_1\phi_1'''(l)\phi_1(l)$$

$$EI_Y q_1^3 \int_0^l \phi_1(\phi_1'(\phi_1'\phi_1'')')'\, ds \;=\; (EI_Y q_1^3\phi_1\phi_1'^2\phi_1''')|_{s=l} - EI_Y q_1^3 \int_0^l \phi_1'^2(\phi_1'\phi_1'')'\, ds$$

$$m\ddot{u}_b q_1 \int_0^l \phi_1\phi_1''\, ds \;=\; m\ddot{u}_b\phi_1'(l)q_1\phi_1(l) - m\ddot{u}_b q_1 \int_0^l \phi_1'^2\, ds$$

$$\rho q_1(\dot{q}_1^2+q_1\ddot{q}_1) \int_0^l \phi_1 \left(\phi_1' \int_l^s \int_0^\theta \phi_1'^2\, dy\, d\theta\right)'\, ds = -\rho q_1(\dot{q}_1^2+q_1\ddot{q}_1) \int_0^l \phi_1'^2 \left(\int_l^s \int_0^\theta \phi_1'^2\, dy\, d\theta\right)\, ds$$

$$-\rho\ddot{u}_b q_1 \int_0^l \phi_1(\phi_1' + (s-l)\phi_1'')\, ds \;=\; -\rho\ddot{u}_b q_1 \int_0^l (l-s)\phi_1'^2\, ds$$

$$-mq_1(q_1\ddot{q}_1+\dot{q}_1^2) \int_0^l \phi_1\phi_1'' \left(\int_0^l \phi_1'^2\, dy\right)\, ds = mq_1(q_1\ddot{q}_1+\dot{q}_1^2) \left[-(\phi_1'\phi_1 \int_0^l \phi_1'^2\, ds)|_{s=l} + \left(\int_0^l \phi_1'^2\, ds\right)^2\right]$$

The governing equation of first modal co-ordinate, q_1, is then written as:

$$\begin{aligned}
&\ddot{q}_1 + c_1\dot{q}_1 \int_0^l \phi_1^2\, ds + \omega_1^2 q_1 - EI_Y q_1^3 \int_0^l \phi_1'^2(\phi_1'\phi_1'')' + mq_1(q_1\ddot{q}_1 + \dot{q}_1^2) \left[\int_0^l \phi_1'^2\, ds\right]^2 \\
&- m\ddot{u}_b q_1 \int_0^l \phi_1'^2\, ds - \rho q_1(q_1\ddot{q}_1 + \dot{q}_1^2) \int_0^l \phi_1'^2 \left(\int_l^s \int_0^\theta \phi_1'^2\, dy\, d\theta\right)\, ds - \rho\ddot{u}_b q_1 \int_0^l (l-s)\phi_1'^2\, ds \\
&+ \phi_1 \left(-m\ddot{q}_1\phi_1 + EI_Y q_1\phi_1'''(1+q_1^2\phi_1'^2) - mq_1(q_1\ddot{q}_1 + \dot{q}_1^2) \left[\int_0^l \phi_1'^2\, ds\right] \phi_1' + m\ddot{u}_b q_1\phi_1'\right)|_{s=l} = 0
\end{aligned} \tag{2.55}$$

The subscripts representing the mode shape are disregarded in the following sections for the sake of convenience.

2.2.3 Governing equations assuming linear boundary conditions

The linear boundary conditions corresponding to the shear balance at $s = l$ is given by

$$\left(EI_Y w''' - m\ddot{w}\right)|_{s=l} = 0 \tag{2.56}$$

Separating the variables, we rewrite equation 2.56 as

$$\left(EI_Y \phi''' q - m\phi\ddot{q}\right)|_{s=l} = 0$$

Using the linear boundary conditions, the governing equation 2.55 is re-written as

$$\begin{aligned}\ddot{q} + c_1\dot{q}\int_0^l \phi^2\,ds + \omega^2 q - EI_Y q^3\int_0^l \phi'^2(\phi'\phi'')'\,ds + mq(q_1\ddot{q}_1 + \dot{q}_1^2)\left[\int_0^l \phi'^2\,ds\right]^2 \\ - m\ddot{u}_b q\int_0^l \phi'^2\,ds - \rho q(q_1\ddot{q}_1 + \dot{q_1}^2)\int_0^l \phi'^2\left[\int_l^s\int_0^\theta \phi'^2\,dy\,d\theta\right]ds - \rho\ddot{u}_b q\int_0^l (l-s)\phi'^2\,ds \\ + \phi\left(EI_Y\phi'''\phi'^2 q_1^3 - mq(q\ddot{q} + \dot{q}^2)\left[\int_0^l \phi'^2\,ds\right]\phi' + m\ddot{u}_b q_1\phi'\right)\Big|_{s=1} = 0\end{aligned} \tag{2.57}$$

where q and ϕ are used respectively instead of q_1 and ϕ_1 for the sake of convenience.

The governing equation is then simplified to

$$\ddot{q} + \omega^2 q + 2\mu_1\dot{q} + \delta_l q(q\ddot{q} + \dot{q}^2) + \alpha_l q(t)^3 = \eta_l q f\cos(\Omega t + \tau_e) \tag{2.58}$$

where

$$\mu_1 = \frac{1}{2}\,c_1\int_0^l \phi^2\,ds,$$

$$\delta_l = -m\phi'(l)\phi(l)\left(\int_0^l \phi'^2\,ds\right) + m\left(\int_0^l \phi'^2\,ds\right)^2 + \rho\int_0^l \phi'^2\left(\int_s^l\int_0^\theta \phi'^2\,dy\,d\theta\right)ds, \text{ and} \tag{2.59}$$

$$\alpha_l = EI_Y\phi'''(l)\phi'^2(l)\phi(l) - EI_Y\int_0^l \phi'^2(\phi'\phi'')'\,ds \tag{2.60}$$

Equation 2.58 constitutes a balance of forces that includes $2\mu_1\dot{q}$ which represents the force due to linear damping, $\delta_l q(\dot{q}^2 + q\ddot{q})$ which represents the inertial force exerted by the tip mass on the beam, and is a function of the beam's displacement, and $\alpha_l q^3$ which represents the force caused by geometric nonlinearities as a result of nonlinear strains arising from large displacements. For a sinusoidal excitation with amplitude f and frequency Ω, the base

acceleration is given by $u_b = f\cos(\Omega t + \tau_e)$, which yields $\ddot{u}_b = -f\Omega^2\cos(\Omega t + \tau_e)$. As such, we have

$$\eta_l = -\Omega^2\left[m\phi'(l)\phi(l) + m\int_0^l \phi'^2\,ds + \rho\int_0^l (l-s)\phi'^2\,ds\right] \tag{2.61}$$

where $\eta_l q f\cos(\Omega t + \tau_e)$ represents the effect of the external excitation, which is a function of the displacement of the beam and tip mass.

2.2.4 Governing equations assuming non-linear boundary conditions

The nonlinear boundary condition obtained by balancing the shear force at $s = l$ is given by

$$\left(m\ddot{u}_b w' - mw'\int_0^l \frac{\partial^2}{\partial t^2}\left(\frac{w'^2}{2}\right)ds + EI_Y\left(w'''w'^2 + w''^2w' + w'''\right) - m\ddot{w}\right)\Bigg|_{s=l} = 0 \tag{2.62}$$

Separating the variables, equation 2.62 is re-written as

$$\left(-m\ddot{q}\phi + EI_Y q\phi'''(1+q^2\phi'^2) - m\phi' q(q\ddot{q}+\dot{q}^2)\left(\int_0^l \phi'^2\,ds\right) + m\ddot{u}_b q\phi'\right)|_{s=l} = 0$$

Using the nonlinear boundary conditions, the governing equation 2.55 is re-written as,

$$\ddot{q} + \omega^2 q + c_1\dot{q}\int_0^l \phi^2\,ds + q(q\ddot{q}+\dot{q}^2)\left[m\left(\int_0^l \phi'^2\,ds\right)^2 + \rho\int_0^l \phi'^2\left(\int_s^l\int_0^\theta \phi'^2\,dy\,d\theta\right)ds\right]$$
$$- EI_Y q^3\int_0^l \phi'^2(\phi'\phi'')'\,ds = q\ddot{u}_b\left[m\int_0^l \phi_1'^2\,ds + \rho\int_0^l (l-s)\phi'^2\,ds\right] \tag{2.63}$$

where q and ϕ are used to represent q_1 and ϕ_1 respectively for the sake of convenience. The governing equation is then simplified to

$$\ddot{q} + \omega^2 q + 2\mu_1\dot{q} + \delta q(q\ddot{q}+\dot{q}^2) + \alpha q^3 = \eta q f\cos(\Omega t + \tau_e) \tag{2.64}$$

where

$$\mu_1 = \frac{1}{2}c_1\int_0^l \phi^2\,ds, \tag{2.65}$$

$$\delta = m\left(\int_0^l \phi'^2\,ds\right)^2 + \rho\int_0^l \phi'^2\left(\int_s^l\int_0^\theta \phi'^2\,dy\,d\theta\right)ds, \tag{2.66}$$

$$\alpha = -EI_Y\int_0^l \phi'^2(\phi'\phi'')'\,ds, \text{ and} \tag{2.67}$$

For a sinusoidal excitation with amplitude f and frequency Ω, the base acceleration is given by, $u_b(t) = f\cos(\Omega t + \tau_e)$, which yields $\ddot{u}_b(t) = -f\Omega^2\cos(\Omega t + \tau_e)$. As such, we have

$$\eta = -\Omega^2\left[m\int_0^l \phi'^2\,ds + \rho\int_0^l (l-s)\phi'^2\,ds\right] \tag{2.68}$$

2.3 Principal parametric resonance

In this section, we determine the steady response of beam tip-mass system subjected to a principal parametric resonant excitation using the method of multiple scales. First, we attack the distributed parameter system as represented in equations 2.18 - 2.22 with MMS - which from now on will be referred as *direct approach*. Later, we attack the governing equations of the first mode represented by equations 2.64 or 2.58 with MMS - which from now on will be referred as *discretized approach*.

2.3.1 Approximate solution - Direct approach

Finding a closed form solution for the governing equation 2.18 and the boundary conditions 2.19 - 2.22 is a magnum opus, if not impossible. So, we apply the method of multiple scales directly to the partial integro-differential equations similar to Yabuno et al. [42] and study the response and stability characteristics of principle parametric response of the beam-mass system. The first step in the Method of Multiple Scales is to scale the equation of motion with a bookkeeping parameter, ϵ, that signifies the level to which the different terms in equations affect the response [46, 50]. To do so, we re-write the equations as:

$$\rho\ddot{w} + \epsilon c_1\dot{w} + EI_Y w'''' + \epsilon EI_Y[w'(w'w'')']' + \epsilon\frac{\rho}{2}\left(w'\int_l^s\int_0^\theta \frac{\partial^2}{\partial t^2}\left(w'^2\right)\,dy\,d\theta\right)' - \epsilon\frac{mw''}{2}\int_0^l \frac{\partial^2}{\partial t^2}\left(w'^2\right)\,ds + \epsilon\ddot{u}_b\left[mw'' - \rho\left(w' + (s-l)w''\right)\right] = 0 \quad (2.69a)$$

$$\left(\epsilon m\ddot{u}_b w' - \epsilon m w'\int_0^l \frac{\partial^2}{\partial t^2}\left(\frac{w'^2}{2}\right)\,ds + \epsilon EI_Y\left(w'''w'^2 + w''^2w'\right) + EI_Y w''' - m\ddot{w}\right)\Big|_{s=l} = 0 \quad (2.69b)$$

$$w^{(2,0)}(l,t) = 0, \qquad \left.\frac{\partial w(s,t)}{\partial s}\right|_{s=0} = 0, \text{ and} \qquad w(0,t) = 0 \quad (2.69c)$$

The parametric resonance of the cantilever beam mass system occurs when the excitation frequency is assumed to be close to twice of natural frequency. As such, we represent the nearness to the principal parametric resonant frequency as:

$$\Omega = 2\omega + \epsilon\sigma$$

where ω is the first natural frequency of beam and tip mass system and σ is a detuning factor, ϵ is used to signify that the excitation frequency is very close to 2ω. This representation has the advantage of identifying secular or nearly secular terms that lead to non-physical solutions [50].

To tackle the different rate of contributions in the system, we introduce two independent fast and slow time scales T_0 and T_1 defined by

$$T_n = \epsilon^n t \qquad n = 0, 1$$

It follows that $t \equiv t(T_0, T_1)$. Using the chain rule of differentiation, we let

$$\frac{D}{Dt} = \frac{\partial}{\partial T_0} + \epsilon \frac{\partial}{\partial T_1} \equiv D_0 + \epsilon D_1 \tag{2.70a}$$

and

$$\frac{D^2}{Dt^2} = \frac{\partial^2}{\partial T_0^2} + 2\epsilon \frac{\partial^2}{\partial T_1 \partial T_0} + \epsilon^2 \frac{\partial^2}{\partial T_1^2} \equiv D_0^2 + 2\epsilon D_0 D_1 + \epsilon^2 D_1^2 \tag{2.70b}$$

The solution of $w(s,t)$ is then expressed as a series in ϵ of the form

$$w(s,t,\epsilon) = w_0(s, T_0, T_1) + \epsilon w_1(s, T_0, T_1) + \epsilon^2 w_2(s, T_0, T_1) + ... \tag{2.71}$$

Next, we substitute equations 2.70a, 2.70b and 2.71 into the governing equation and boundary conditions and retain terms up-to ϵ^1. Because ϵ is a small number, terms of the order ϵ^0 and ϵ^1 on the left and right hand sides of equations after making the substitutions must be equal, which yields the $O(\epsilon^0)$ equation and boundary conditions as

$$\rho D_0^2 w_0 + E I_Y w_0'''' = 0 \tag{2.72a}$$

$$w_0|_{s=0} = 0 \qquad w_0'|_{s=0} = 0 \tag{2.72b}$$

$$w_0''|_{s=l} = 0 \qquad |E I_Y w_0''' = m D_0^2 w_0|_{s=l} \tag{2.72c}$$

Equations 2.72a - 2.72c represents a free vibration eigen value problem whose characteristic equation 2.74 is transcendental and hence the solution is an infinite series. Since, this is a principal parametric excitation, the contribution of higher modes will decay due do the damping in system. Therefore, the solution of w_0 considering only the first mode can be represented as:

$$w_0 = \phi_0(s) \left[A(T_1) e^{j\omega T_0} + cc \right] \tag{2.73a}$$

$$\phi_0(s) = \sin(\lambda_1 s) - \sinh(\lambda_1 s) - \left[\frac{\sin(\lambda_1 l) + \sinh(\lambda_1 l)}{\cos(\lambda_1 l) + \cosh(\lambda_1 l)} \right] (\cos(\lambda_1 s) - \cosh(\lambda_1 s)) \tag{2.73b}$$

where, $\lambda_1 = \left(\frac{\omega_1^2 \rho}{E I_Y} \right)$ is the smallest solution of the characteristic equation.

$$\rho \left[\cos(\lambda l) \cosh(\lambda l) + 1 \right] + m\lambda \left[\cos(\lambda l) \sinh(\lambda l) - \sin(\lambda l) \cosh(\lambda l) \right] = 0 \tag{2.74}$$

The $O(\epsilon^1)$ equation and boundary conditions are written as

$$\begin{aligned} \rho D_0^2 w_1 + E I_Y w_1'''' = & -c_1 D_0 w_0 - 2\rho D_0 D_1 w_0 - \frac{1}{2}\rho \left(w_0' \int_l^s \int_0^\theta D_0^2 w_0'^2 \, dy \, d\theta \right)' \\ & + \frac{1}{2} m w_0'' \int_0^l D_0^2 w_0'^2 \, ds - E I_Y \left(w_0''^3 + 4 w_0' w_0'' w_0''' + w_0'^2 w_0'''' \right) \\ & + \frac{1}{2} f \Omega^2 \left[e^{j(\Omega T_0 + \tau_e)} + e^{-j(\Omega T_0 + \tau_e)} \right] \left(-\rho (w_0' + (s-l) w_0'') + m w_0'' \right) \end{aligned} \tag{2.75a}$$

$$w_1|_{s=0} = 0 \qquad w_1'|_{s=0} = 0 \qquad w_1''|_{s=l} = 0 \tag{2.75b}$$

$$\Big| -mD_0^2 w_0 + EI_Y w_0''' = 2mD_0D_1w_0 + \frac{1}{2}fm\Omega^2 w_0' \left[e^{j(\Omega T_0+\tau_e)} + e^{-j(\Omega T_0+\tau_e)}\right] + \frac{1}{2}mw_0' \int_0^l D_0^2 w_0'^2\, ds - EI_Y(w_0'w_0''^2 + w_0'^2 w_0''')\Big|_{s=l} \tag{2.75c}$$

The solution of w_1 free of secular terms can be represented as:

$$w_1(s, T_0, T_1) = \phi_1(s, T_1)e^{j\omega T_0} + c.c \tag{2.76}$$

To identify secular terms and yield the solvability conditions, we multiply and integrate the equation 2.75a with $e^{-j\omega T_0}$. This treatment will retain only the secular terms in the equation 2.75a. Using $\Omega = 2\omega + \epsilon\sigma$ and $\epsilon T_0 = T_1$, we re-write the $O(\epsilon)$ equations as

$$\begin{aligned} -\rho\omega^2\phi_1 + EI_Y\phi_1'''' &= -j\omega Ac_1\phi_0 - 2j\rho\omega\phi_0A' + 2\omega^2\rho A^2\overline{A}\left(\phi_0' \int_l^s \int_0^\theta \phi_0'^2\, dy\, d\theta\right)' \\ &\quad - 2m\omega^2A^2\overline{A}\phi_0'' \int_0^l \phi_0'^2\, ds - 3EI_YA^2\overline{A}\left(\phi_0''^3 + 4\phi_0'\phi_0''\phi_0''' + \phi_0'^2\phi_0''''\right) \\ &\quad + \frac{1}{2}f(2\omega+\epsilon\sigma)^2e^{j(\sigma T_1+\tau_e)}\overline{A}\left(-\rho(\phi_0' + (s-l)\phi_0'') + m\phi_0''\right) \equiv H_1 \end{aligned} \tag{2.77a}$$

$$\phi_1(0) = 0 \qquad \phi_1'(0) = 0 \qquad \phi_1''(l) = 0 \tag{2.77b}$$

$$\Big| m\omega^2\phi_1 + EI_Y\phi_1''' = 2jm\omega\phi_0'A' + \frac{1}{2}fm(2\omega+\epsilon\sigma)^2e^{j(\sigma T_1+\tau_e)}\overline{A}\phi_0' - 2m\omega^2A^2\overline{A}\phi_0' \int_0^l \phi_0'^2\, ds - 3EI_YA^2\overline{A}\phi_0'(\phi_0''^2 + \phi_0'\phi_0''')\Big|_{s=l} \equiv H_2 \tag{2.77c}$$

Next, we multiply an adjoint solution, $u(s)$, which will be specified later, by equation 2.77a and integrate it over the domain, which yields

$$\int_0^l (-\rho\omega^2\phi_1 + EI_Y\phi_1'''')u\, ds = \int_0^l H_1u\, ds \tag{2.78a}$$

using integration by parts, the integrals are transferred to u as,

$$\int_0^l (-\rho\omega^2u + EI_Yu'''')\phi_1\, ds + [EI_Y\phi_1'''u - EI_Y\phi_1''u' + EI_Y\phi_1'u'' - EI_Y\phi_1u''']_{s=0}^{s=l} = \int_0^l H_1u\, ds \tag{2.78b}$$

The adjoint equation of the homogeneous equation of 2.77a (H_1=0) is defined as the coefficient of ϕ_1 in the integrand on left-hand side as:

$$-\rho\omega^2u + EI_Yu'''' = 0 \tag{2.78c}$$

Considering the homogeneous boundary conditions in equations 2.77b, 2.77c and 2.78c (H_2=0), equation 2.78b can simplified to

$$\left[-(m\omega^2 u + EI_Y u''')\phi_1 + EI_Y \phi_1' u''\right]_{s=l} - \left[EI_Y \phi_1''' u - EI_Y \phi_1'' u'\right]_{s=0} = 0 \tag{2.78d}$$

The available boundary conditions don't provide any information about $\phi_1(l)$, $\phi_1'(l)$, $\phi_1'''(0)$ and $\phi_1''(0)$. Nevertheless, irrespective of their values, equation 2.78d should be uniquely satisfied. This imposes the boundary condition on the adjoint solution as:

$$u(0) = 0 \qquad u'(0) = 0 \qquad u''(l) = 0 \tag{2.78e}$$

$$[m\omega^2 u + EI_Y u''']_{s=l} = 0 \tag{2.78f}$$

From the adjoint system represented by the equations 2.78c, 2.78e and 2.78f and homogeneous $O(\epsilon^1)$ system, it can be said that the $O(\epsilon^1)$ equations are a self-adjoint system. Equations 2.78c, 2.78e and 2.78f are identical to $O(\epsilon)$ equations, therefore, the non-trivial solution of the adjoint system is:

$$u(s) = \phi_0(s) \tag{2.79}$$

Because the homogeneous system has a non-trivial solution, the non-homogeneous system requires a solvability condition for determined the solution [46], which is determined as follows. Using the well-defined adjoint system from equations 2.78c - 2.78f and considering the actual boundary conditions of ϕ_1, equation 2.78b can be re-written as:

$$\int_0^l H_1 \phi_0 \, ds = H_2 \phi_0(l) \tag{2.80a}$$

$$\begin{aligned}\int_0^l \Bigg[& -j\omega A c_1 \phi_0 - c_2 g_1 \phi_0^2 - 2j\rho\omega\phi_0 A' + 2\omega^2 \rho A^2 \overline{A} \left(\phi_0' \int_l^s \int_0^\theta \phi_0'^2 \, dy \, d\theta \right)' \\ & -2m\omega^2 A^2 \overline{A} \phi_0'' \int_0^l \phi_0'^2 \, ds - 3EI_Y A^2 \overline{A} \left(\phi_0'''^3 + 4\phi_0' \phi_0'' \phi_0''' + \phi_0'^2 \phi_0'''' \right) \\ & + \frac{1}{2} f (2\omega + \epsilon\sigma)^2 e^{j(\sigma T_1 + \tau_e)} \overline{A} \left(-\rho(\phi_0' + (s-l)\phi_0'') + m\phi_0'' \right) \Bigg] \phi_0 \, ds = \phi_0 \Big[2jm\omega\phi_0 A' \\ & + \frac{1}{2} f m (2\omega + \epsilon\sigma)^2 e^{j(\sigma T_1 + \tau_e)} \overline{A} \phi_0' - 2m\omega^2 A^2 \overline{A} \phi_0' \int_0^l \phi_0'^2 \, ds - 3EI_Y A^2 \overline{A} \phi_0'^2 \phi_0''' \Big] \Bigg|_{s=l}\end{aligned} \tag{2.80b}$$

Using the polar representation of A, as $A(T_1) = \frac{1}{2} a(T_1) e^{j\beta(T_1)}$, equation 2.80b can be simpli-

fied as:

$$\int_0^l \Bigg[-\frac{1}{2} j\omega a c_1 \phi_0 - j\rho\omega\phi_0 \left(a' + j\beta' a\right) + \frac{1}{4}\omega^2 \rho a^3 \left(\phi_0' \int_l^s \int_0^\theta \phi_0'^2 \, dy \, d\theta\right)' - \frac{1}{4} m\omega^2 a^3 \phi_0'' \int_0^l \phi_0'^2 \, ds - \frac{3}{8} E I_Y a^3 \left(\phi_0'''^3 + 4\phi_0'\phi_0''\phi_0''' + \phi_0'^2 \phi_0''''\right) + \frac{1}{4} f (2\omega + \epsilon\sigma)^2 e^{j(\sigma T_1 + \tau_e)} a e^{-2j\beta} \left(-\rho(\phi_0' + (s-l)\phi_0'') + m\phi_0''\right) \Bigg] \phi_0 \, ds = \phi_0 \Big[jm\omega\phi_0 \left(a' + j\beta' a\right) + \frac{1}{4} f m (2\omega + \epsilon\sigma)^2 e^{j(\sigma T_1 + \tau_e)} a e^{-2j\beta} \phi_0' - \frac{1}{4} m\omega^2 a^3 \phi_0' \int_0^l \phi_0'^2 \, ds - \frac{3}{8} E I_Y a^3 \phi_0'^2 \phi_0''' \Big] \Big|_{s=l} \quad (2.81)$$

Separating the real and imaginary parts yields

$$a\beta' \left[\int_0^l \rho\omega\phi_0^2 \, ds + m\omega\phi_0(l)^2\right] = a^3 \Bigg[-\int_0^l \frac{1}{4}\omega^2\rho \left(\phi_0' \int_l^s \int_0^\theta \phi_0'^2 \, dy \, d\theta\right)' \phi_0 \, ds + \int_0^l \frac{1}{4} m\omega^2 \phi_0'' \left(\int_0^l \phi_0'^2 \, ds\right) \phi_0 \, ds + \frac{3}{8} \int_0^l E I_Y (\phi_0'(\phi_0'\phi_0'')')' \phi_0 \, ds - \frac{1}{4} m\omega^2 \phi_0(l) \phi_0'(l) \left(\int_0^l \phi_0'^2 \, ds\right) - \frac{3}{8} E I_Y \phi_0(l) \phi_0'^2(l) \phi_0'''(l) \Bigg] + \frac{1}{4} a f (2\omega + \epsilon\sigma)^2 \cos(\sigma T_1 + \tau_e - 2\beta) \left[\int_0^l \left(\rho[\phi_0' + (s-l)\phi_0'''] - m\phi_0''\right) \phi_0 \, ds + m\phi_0(l)\phi_0'(l)\right] \quad (2.82a)$$

$$a'\omega \left[-\int_0^l \rho\phi_0^2 \, ds - m\phi_0(l)^2\right] = \frac{1}{2} a\omega c_1 \left(\int_0^l \phi_0^2 \, ds\right) + \frac{1}{4} a f (2\omega + \epsilon\sigma)^2 \sin(\sigma T_1 + \tau_e - 2\beta) \left[\int_0^l \left(\rho[\phi_0' + (s-l)\phi_0'''] - m\phi_0''\right) \phi_0 \, ds + m\phi_0(l)\phi_0'(l)\right] \quad (2.82b)$$

Defining

$$\gamma = \sigma T_1 + \tau_e - 2\beta \implies D_1\beta = \frac{1}{2}\left[-D_1\gamma + \sigma\right]$$

$$\mu_{1D} = \frac{1}{2} \frac{c_1 \int_0^l \phi_0^2 \, ds}{\int_0^l \rho\phi_0^2 \, ds + m\phi_0(l)^2}$$

$$\alpha_D = \frac{\int_0^l E I_Y (\phi_0'(\phi_0'\phi_0'')')' \phi_0 \, ds - E I_Y \phi_0(l) \phi_0'^2(l) \phi_0'''(l)}{\int_0^l \rho\phi_0^2 \, ds + m\phi_0(l)^2} = \frac{-\int_0^l E I_Y \phi_0'^2 (\phi_0'\phi_0'')' \, ds}{\int_0^l \rho\phi_0^2 \, ds + m\phi_0(l)^2}$$

$$\delta_D = \frac{\rho \int_0^l \left(\phi_0' \int_l^s \int_0^\theta \phi_0'^2 \, dy \, d\theta\right)' \phi_0 \, ds - m\left[\int_0^l \phi_0'' \left(\int_0^l \phi_0'^2 \, ds\right) \phi_0 \, ds - \phi_0(l)\phi_0'(l) \left(\int_0^l \phi_0'^2 \, ds\right)\right]}{\int_0^l \rho\phi_0^2 \, ds + m\phi_0(l)^2}$$

which can be re-written as

$$\delta_D = \frac{\rho \int_0^l \phi_0'^2 \left(\int_s^l \int_0^\theta \phi_0'^2 \, dy \, d\theta \right) \, ds + m \left(\int_0^l \phi_0'^2 \, ds \right)^2}{\int_0^l \rho \phi_0^2 \, ds + m\phi_0(l)^2}$$

and

$$\eta_D = \frac{-(2\omega + \epsilon\sigma)^2 \left[\int_0^l \left(\rho[\phi_0' + (s-l)\phi_0''] - m\phi_0'' \right) \phi_0 \, ds + m\phi_0(l)\phi_0'(l) \right]}{\int_0^l \rho \phi_0^2 \, ds + m\phi_0(l)^2}$$

which can be re-written as

$$\eta_D = \frac{-(2\omega + \epsilon\sigma)^2 \left[\rho \int_0^l (l-s)\phi_0'^2 \, ds + m \int_0^l \phi_0'^2 \, ds \right]}{\int_0^l \rho \phi_0^2 \, ds + m\phi_0(l)^2}$$

yields the amplitude and phase modulation equations as:

$$a\left(\frac{\sigma\omega}{2} - \frac{1}{2}\omega\gamma'\right) - a^3\left(\frac{3\alpha_D}{8} - \frac{\delta_D\omega^2}{4}\right) = -\frac{1}{4}af\eta_D\cos(\gamma) \tag{2.83a}$$

$$\omega a' + a\mu_{1D}\omega = \frac{1}{4}af\eta_D\sin(\gamma) \tag{2.83b}$$

and the approximate solution is given by

$$w(s,t) \approx \frac{1}{2}\phi_0(s)ae^{\frac{1}{2}j(\Omega t + \tau_e - \gamma)} + ... \tag{2.84}$$

2.3.2 Approximate solution - Discretized approach

Next, we tackle the discretized equation of the first mode determined in the previous section 2.2.4 with the method of multiple scales. To this end, we scale equations 2.64 in a similar way to the equation 2.69 and write

$$\ddot{q} + \omega^2 q + 2\epsilon\mu_1\dot{q} + \epsilon\delta q(\dot{q}^2 + q\ddot{q}) + \epsilon\alpha q^3 = \epsilon\eta q f\cos(\Omega t + \tau_e) \tag{2.85}$$

Using the same time scales defined in section 2.3.1 and expressing the solution of $q(t)$ is then expressed as a series in ϵ of the form

$$q(t,\epsilon) = q_0(T_0,T_1) + \epsilon q_1(T_0,T_1) + \epsilon^2 q_2(T_0,T_1) + ... \tag{2.86}$$

we obtain the order ϵ^0 and ϵ^1 equations as:
$O(\epsilon^0)$ equation

$$D_0^2 q_0 + q_0\omega^2 = 0 \text{ , and} \tag{2.87}$$

$O(\epsilon^1)$ equation

$$D_0^2 q_1 + q_1\omega^2 = -\delta q_0 \left(D_0 q_0\right)^2 - \delta q_0^2 D_0^2 q_0 - 2\mu_1 D_0 q_0 - 2D_0 D_1 q_0 - \alpha q_0^3 + \frac{1}{2} f\eta q_0 e^{i\tau_e + iT_0\Omega} + \frac{1}{2} f\eta q_0 e^{-i\tau_e - iT_0\Omega} \quad (2.88)$$

The solution of linear differential equation 2.87 is of the form:

$$q_0 = A(T_1)e^{j\omega T_0} + \bar{A}(T_1)e^{-j\omega T_0} = A(T_1)e^{j\omega T_0} + cc \quad (2.89)$$

Using this solution, we rewrite the different terms that contain q_0 in equation 2.88 as

$$\begin{aligned}
-\delta q_0 \left(D_0 q_0\right)^2 &= \delta\omega^2 A^3 e^{3jT_0\omega} - \delta\omega^2 A^2 \bar{A} e^{jT_0\omega} + cc \\
-\delta q_0^2 D_0^2 q_0 &= \delta\omega^2 A^3 e^{3jT_0\omega} + 3\delta\omega^2 A^2 \bar{A} e^{jT_0\omega} + cc \\
-2\mu_1 \left(D_0 q_0\right) &= -2j\omega A\mu_1 e^{jT_0\omega} + cc \\
-2\left(D_0 D_1 q_0\right) &= -2j\omega A' e^{jT_0\omega} + cc \\
-\alpha q_0^3 &= -\alpha A^3 e^{3j\omega T_0} - 3e^{jT_0\omega}\alpha A^2 \bar{A} + cc
\end{aligned}$$

Using $\Omega = 2\omega + \epsilon\sigma$, the excitation terms are written as

$$\frac{1}{2} f\eta q_0 e^{j\tau_e + iT_0\Omega} + \frac{1}{2} f\eta q_0 e^{-j\tau_e - iT_0\Omega} = \frac{1}{2} f\eta A e^{-j\sigma T_1 - j\omega T_0 - j\tau_e} + \frac{1}{2} f\eta A e^{j\sigma T_1 + 3j\omega T_0 + j\tau_e} + cc$$

Because the solution is assumed to be periodic, the sum of all secular terms, which lead to non-periodic solutions, is equated to zero. To this end, upon substituting the above expansions into the equation 2.88, we obtain

$$-3A^2\alpha\bar{A} + \frac{1}{2} e^{j\sigma T_1 + j\tau_e} f\eta\bar{A} + 2A^2\delta\omega^2\bar{A} - 2j\omega D_1 A - 2jA\omega\mu_1 = 0, \text{ and} \quad (2.90)$$

$$-3\bar{A}^2\alpha A + \frac{1}{2} e^{-j\sigma T_1 - j\tau_e} f\eta A + 2A\delta\omega^2\bar{A}^2 + 2j\omega D_1\bar{A} + 2j\bar{A}\omega\mu_1 = 0 \quad (2.91)$$

These two equations provide valuable information about $D_1 A$ and $D_1\bar{A}$ that can be used to study the progression of the amplitude of the response in time. The two equations are complex conjugates to each other, so satisfying one equation will automatically satisfy the other.

Substituting $\frac{1}{2}ae^{j\beta}$ for A and $\frac{1}{2}ae^{-j\beta}$ for $\bar{A}$ into equation 2.90 yields,

$$-2j\omega\left(\frac{1}{2}a' + \frac{1}{2}ja\beta'\right) - \frac{3}{8}\alpha a^3 + \frac{1}{4}a^3\delta\omega^2 - ja\mu_1\omega + \frac{1}{4}af\eta e^{j\gamma} - g_1\mu_2 = 0 \quad (2.92)$$

where $-2\beta(T_1) + \tau_e + \sigma T_1$ is replaced by $\gamma(T_1)$ to remove the explicit dependence on T_1. Therefore, $\beta'(T_1) = \frac{1}{2}\left[-\gamma'(T_1) + \sigma\right]$. Substituting for the value of β' and separating the real and imaginary parts, we obtain the amplitude and phase modulation equations as

$$a\left(\frac{\sigma\omega}{2} - \frac{1}{2}\omega\gamma'\right) - a^3\left(\frac{3\alpha}{8} - \frac{\delta\omega^2}{4}\right) = -\frac{1}{4}af\eta\cos(\gamma) \tag{2.93a}$$

$$\omega a' + a\mu_1\omega = \frac{1}{4}af\eta\sin(\gamma) \tag{2.93b}$$

It is noted that the parameters μ_1,α,δ,η defined above are equivalent to μ_{1D},α_D,δ_D,η_D used in the section 2.3.1. Therefore, amplitude and phase modulation equations 2.83a and 2.83b derived using direct method by determining solvability conditions are identical to amplitude and phase modulation equations 2.93a and 2.93b derived using the Galerkin discretization and by considering nonlinear boundary conditions. This re-affirms the importance of considering the nonlinear boundary conditions while applying modal analysis.

The steady state equations are obtained by setting $\dot{a} = 0$ and $\dot{\gamma} = 0$ in equations 2.93a and 2.93b. Squaring and adding these equations yields a relation between the amplitude of the response, a, and the system's parameters as a function of the detuning parameter, σ, and the amplitude of the response f. By squaring and adding the , we obtain the amplitude response function

$$\left[\frac{\sigma\omega}{2} + a^2\left(-\frac{3\alpha}{8} + \frac{\delta\omega^2}{4}\right)\right]^2 + \omega^2\mu_1^2 = \frac{\eta^2 f^2}{16} \tag{2.94}$$

2.4 Results and discussion

In this section, we evaluate the importance of considering and neglecting nonlinear boundary conditions while developing the discretized governing equations.

2.4.1 Linear vs non-linear boundary conditions

Comparing equations 2.59 - 2.61 with equations 2.66 - 2.68, we note assuming linearized boundary conditions has resulted in additional terms for the forces related to geometric nonlinearities, inertial nonlinearities and the external excitation. As will be shown below, the options of considering or not considering these terms yield significantly differing responses. To emphasize this, we consider a carbon fiber/epoxy resin composite beam and tip mass system with the physical properties listed in Table 2.1.

Table 2.1: Material and geometric properties of the beam-tip mass system.

Parameter [units]	**Value**
Mass per unit length, ρ [g/m]	21
Young's modulus, E) [GPa]	43
Length, l [mm]	150
Thickness, h [mm]	0.5
Width, b [mm]	30
Tip mass, m [gm]	5
Area moment of inertia, $I_Y = \frac{1}{12}bh^3$ [mm^4]	312.5

Using the characteristic equation 2.51 and modal analysis presented in section 2.2.1, we determine that

$$\phi(s) \approx 14.67\,[\,\sinh(7.55s) - \sin(7.55s)\,] + 15.76\,[\,\cos(7.55s) - \cosh(7.55s)\,]$$

Using equations 2.59 - 2.61 and the expression for $\phi(s)$, we obtain

$$\delta_l \approx -1149.91\,\mathrm{Kg^{-1}m^{-2}}, \qquad \alpha_l \approx -1.48\times10^7\,\mathrm{Kg^{-1}m^{-2}s^{-2}}, \text{and} \quad \eta_l \approx -16.91\Omega^2\,\mathrm{m^{-1}s^{-2}} \tag{2.95}$$

Using equations 2.66 - 2.68 and the expression for $\phi(s)$, we obtain

$$\delta \approx 10776.1\,\mathrm{Kg^{-1}m^{-2}}, \qquad \alpha \approx 1.6\times10^7\,\mathrm{Kg^{-1}m^{-2}s^{-2}}, \text{and} \quad \eta \approx -8.31\Omega^2\,\mathrm{m^{-1}s^{-2}} \tag{2.96}$$

Although there are considerable differences between the parameter values generated by considering linear or nonlinear boundary conditions, we note that the coefficients of cubic nonlinearities are affected the most. Particularly we note the change in its sign that suggests a change from a softening response when linear boundary conditions are assumed to hardening response when nonlinear boundary conditions are accounted for. From equations 2.59, 2.60, 2.66 and 2.67, the change in sign of coefficient of cubic nonlinearities can be attributed to the fact that $\phi'''(l)\phi'^2(l)\phi(l) << \int_0^l \phi'^2(\phi'\phi'')'\,ds$ and $m\phi'(l)\phi(l)\left(\int_0^l \phi'^2\,ds\right) > m\left(\int_0^l \phi'^2\,ds\right)^2 + \rho\int_0^l \phi'^2\left(\int_s^l\int_0^\theta \phi'^2\,dy\,d\theta\right)ds$. Also, we note that the change in this behavior is independent of E and I_Y but has an implicit dependence on ρ, m and l. From equation 2.94, the steady state amplitude response relation is determined as:

$$\mu_1^2 + \frac{1}{4}\left(\sigma + 17316.63a^2\right)^2 = 8.6\Omega^2 f^2\times10^{-3} \tag{2.97}$$

when assuming linearized boundary conditions, and

$$\mu_1^2 + \frac{1}{4}\left(\sigma - 217475.36a^2\right)^2 = 2.07\Omega^2 f^2 \times 10^{-3} \tag{2.98}$$

when the nonlinearities are accounted for in the boundary conditions.

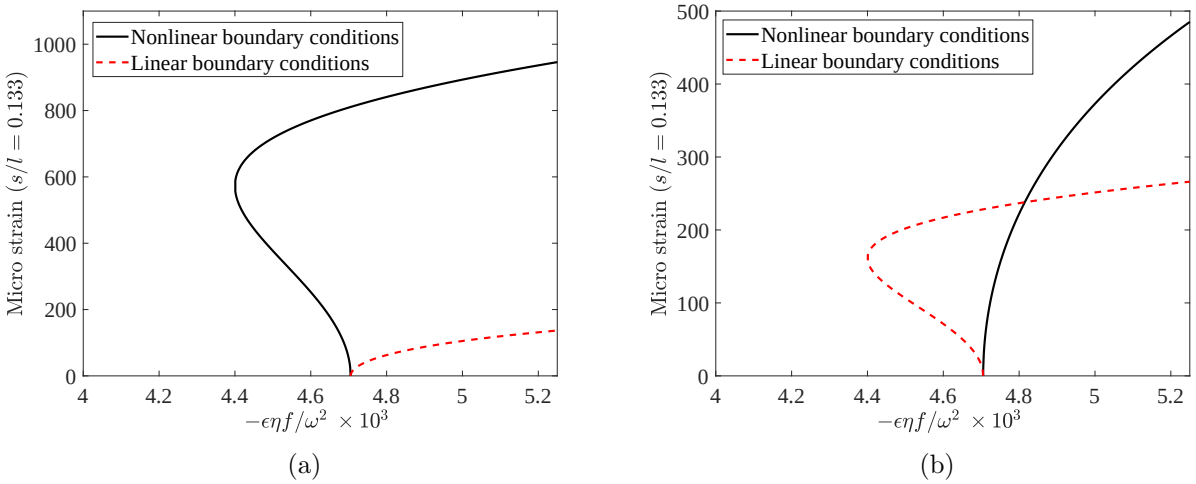

Figure 2.4: Principal parametric response of beam and tip mass system when $\mu_1 = 0.05$ s^{-1} and for (a) positive detuning $\epsilon\sigma = 0.038$ rad/s and (b) negative detuning $\epsilon\sigma = -0.038$ rad/s. The response is represented as micro strain at 2 cm from the base excitation and appropriate η or η_l has been chosen to nondimensionalize the forcing.

Figure 2.4(a) shows comparison the response of beam with a tip mass system for a positive detuning, $\sigma = 0.038$ rad/s for linearized and nonlinear boundary conditions. It is noted that the response assuming nonlinear boundary conditions is of sub-critical bifurcation type and that of assuming linear boundary conditions is of supercritical bifurcation type. The nature of response is reversed when considering a negative detuning, $\sigma = -0.038$ rad/s as shown in figure 2.4(b).

2.5 Conclusions

In this chapter, we presented an extensive theoretical modeling of beam with a tip mass system subjected to parametric excitation. We showed that the modulation equations determined when the PDE and boundary conditions are directly attacked with the method of multiple scales are equivalent to those determined when implementing the method of multiple scales onto discretized ODE which is developed by assuming full nonlinear description of boundary conditions. We also showed that neglecting the nonlinear boundary conditions

while developing the discretized governing equation of temporal modes can significantly alter the response. In particular, we demonstrated that for the problem under consideration, the sign of the cubic nonlinearity coefficients are opposite to the one obtained when assuming linearized boundary conditions are neglected to that of when considered. From figure 2.4(a) and 2.4(b) we showed that, nature of Hopf bifurcation is exactly opposite and the amplitudes of response are considerably different when considering linearized and nonlinear boundary conditions. From the analysis and results discussed in this chapter, it can be concluded that, though neglecting nonlinear boundary conditions can simplify the math in determining the governing equations, the representation of response can be significantly altered.

Chapter 3

Parameter sensitivity of cantilever beam with tip mass to parametric excitation

The cantilever beam with a tip mass configuration has been used to model robotic arms [6,7], antenna masts [8,9], wings with store configurations [10–15], energy harvesting devices [16–22], vibrating beam gyroscopes [23,24] and bio/chemical sensors [25–31]. In all of these applications, there is a need for matching the system's response with a predicted value in order to determine a quantity of interest. For instance, in a bio/chemical sensor, the objective would be to detect the presence of target bio-materials by assessing a very small change in the static or dynamic response of the beam-mass system caused by the binding of the bio-material mass to the beam. In the static response, the bending or deflection of the beam is related to the value of the additional mass. In the dynamic resonant response, the presence of the added mass is detected by measuring a shift in the resonance frequency of the cantilever beam. Although the analysis seems straightforward, determining the resonance frequency may require additional evaluation because the dynamic resonant response depends on small variations in the beam's dimensions, material properties, operational conditions such as environmental thermal effects, and fatigue induced by cyclic loading. Subsequently, any uncertainty in the beam's dimensions, the mass value or material properties can result in inaccurate estimates of the natural frequency, which may induce discrepancies between the proposed cantilever beam-mass model and predicted values and experimental results, thereby compromising the fidelity of the model representing the device.

The effects of discrepancies in representative parameters on the response of a beam mass system can be quantified by performing a sensitivity analysis of the response to variations in these parameters. Alternatively, one may think of exploiting these effects in order to detect changes in the parameters that can be associated with additional mass and manufacturing or operational conditions such as the ones discussed above. The sensitivity analysis becomes

more challenging in applications where nonlinear effects cannot be neglected or are of primary interest. For example in the case of the bio mass sensor, Younis and Nayfeh [51] noted that accurate frequency response requires accurate representation of the nonlinearities of an electrically actuated micro beam subjected to axial loading. Zhang et al. [30] and Zhang and Turner [31] showed that the jump phenomenon in the principal parametric resonance of a micro cantilever can be utilized for mass sensing with significantly higher sensing capability in comparison to linear resonant type sensors. Often, when considering a nonlinear response, the type and point of bifurcation are highly sensitive to the system's nonlinearities. Perturbation analysis around this point provides a capability to assess the sensitivity of the response to small variations in the model parameters.

In this chapter, we consider a cantilever beam with a tip mass under parametric excitation and use the mathematical model developed in chapter 2 to assess its nonlinear response and perform sensitivity analysis of the nonlinear response to variations in the elasticity (stiffness) and additional mass of the beam and tip mass system. Using a discretized form of the governing equation, we evaluate this sensitivity by implementing the Method of Multiple Scales [46, 50]. We choose the discretized equation as the analysis is more intuitive in comparison to the direct approach, which involves solving five nonlinear integro-partial differential equations. Particular attention is paid to determining the effects of varying the system's parameter on changing the type of bifurcation under different resonance conditions. Although nonlinear and damping terms in the governing equation are of $O(\epsilon)$ and hence one could assume that a solution considering the modulation equations up to $O(\epsilon)$ is appropriate, the small uncertainties in the nonlinear parameter are of the order $O(\epsilon^2)$ in the governing equation, which requires a solution considering the modulation equations up to $O(\epsilon^2)$. To be consistent and identify the sensitivity of the response from equilibrium solution, we will compare the $O(\epsilon^2)$ solutions for the governing equations with and without small variations in their parameters.

3.1 Governing equations

A schematic of the cantilever beam with a tip mass subjected to parametric excitation is presented in figure 3.1. The beam with length l, width b, thickness h, and mass per unit length ρ, is clamped at the base where it is subjected to a harmonic excitation at twice its natural frequency. Assuming that the beam is in-extensible and that the Euler-Bernoulli beam theory is applicable the governing equation, derived in chapter 2, is written as

$$\rho\ddot{w} + c_1\dot{w} + EI_Y(w'''' + [w'(w'w'')']') + m\ddot{u}_b w'' + \frac{\rho}{2}\left(w'\int_l^s\int_0^\theta \frac{\partial^2}{\partial t^2}\left(w'^2\right)\, dy\, d\theta\right)' - \rho\ddot{u}_b\left(w' + (s-l)w''\right) - \frac{mw''}{2}\int_0^l \frac{\partial^2}{\partial t^2}\left(w'^2\right)\, ds = 0 \quad (3.1)$$

where the modulus of elasticity E, the damping coefficient c_1, the second moment of the area I_Y, l, ρ, and tip mass m are assumed to be constants, and $\ddot{u}_b$ is the base acceleration. The primes and dots represent respectively the derivatives of $w(s,t)$ with respect to the coordinate s and time t, and y and θ are used as dummy variables. The natural nonlinear boundary conditions at $s = l$ are determined from the moment and the shear boundary conditions and are given by

$$\left(EI_Y w'' w'^2 + EI_Y w''\right)|_{s=l} = 0 \quad \Longrightarrow \quad w''(l,t) = 0 \quad (3.2)$$

$$\left(m\ddot{u}_b w' - mw'\int_0^l \frac{\partial^2}{\partial t^2}\left(\frac{w'^2}{2}\right) ds + EI_Y\left(w''' w'^2 + w''^2 w' + w'''\right) - m\ddot{w})\right|_{s=l} = 0 \quad (3.3)$$

At $s = 0$, the essential boundary conditions are written as

$$w(0,t) = 0 \qquad \left.\frac{\partial w(s,t)}{\partial s}\right|_{s=0} = 0 \quad (3.4)$$

Implementing the Galerkin discretization, the governing equation of the first mode is written as:

$$\ddot{q} + \omega^2 q + q(q\ddot{q} + \dot{q}^2)\left[m\left(\int_0^l \phi'^2\, ds\right)^2 + \rho\int_0^l \phi'^2\left(\int_s^l\int_0^\theta \phi'^2\, dy\, d\theta\right) ds\right] - EI_Y q^3\int_0^l \phi'^2(\phi'\phi'')'\, ds + c_1\dot{q}\int_0^l \phi^2\, ds = q\ddot{u}_b\left[m\int_0^l \phi_1'^2\, ds + \rho\int_0^l (l-s)\phi'^2\, ds\right] \quad (3.5)$$

where q and ϕ are respectively the temporal modal displacement and linear mode shape corresponding to the first mode. The governing equation is alternatively written as:

$$\ddot{q} + \omega^2 q + 2\mu_1\dot{q} + \delta q(q\ddot{q} + \dot{q}^2) + \alpha q^3 = \eta q f\cos(\Omega t + \tau_e) \quad (3.6)$$

where

$$\mu_1 \;=\; \frac{1}{2}c_1\int_0^l \phi^2\, ds \equiv \zeta\omega, \quad (3.7)$$

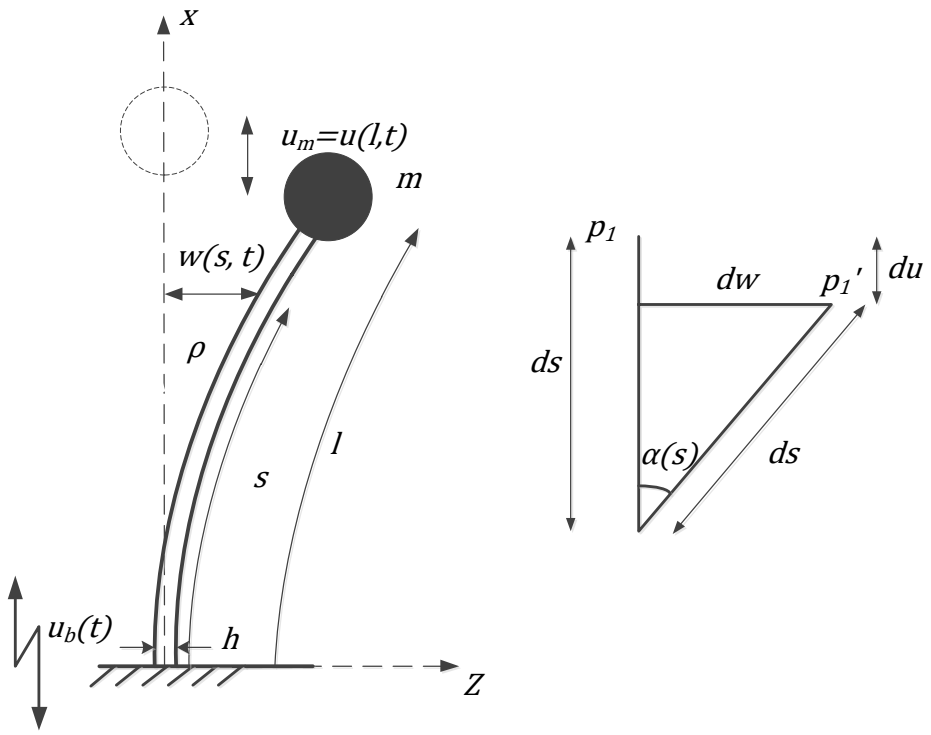

Figure 3.1: Schematic of the beam with tip mass system. The vertical line represents the undeformed state and the curved line represents a general deformed state. The schematic on the right hand side is used to define the geometry and depict the in-extensibility condition, $pp_1 = pp_1'$

$$\delta \;=\; m\left(\int_0^l \phi'^2\,ds\right)^2 + \rho\int_0^l \phi'^2\left(\int_s^l\int_0^\theta \phi'^2\,dy\,d\theta\right)\,ds, \tag{3.8}$$

$$\alpha \;=\; -EI_Y\int_0^l \phi'^2(\phi'\phi'')'\,ds, \text{ and} \tag{3.9}$$

For a sinusoidal excitation with amplitude f and frequency Ω, the base acceleration is given by $u_b(t) = f\cos(\Omega t + \tau_e)$, which yields $\ddot{u}_b(t) = -f\Omega^2\cos(\Omega t + \tau_e)$. As such, we write

$$\eta = -\Omega^2\left[m\int_0^l \phi'^2\,ds + \rho\int_0^l (l-s)\phi'^2\,ds\right] \tag{3.10}$$

3.2 Sensitivity analysis

Next, we employ the method of multiple scales to determine the approximate solution and to study the stability characteristics of the response governed by equation 3.6 when subjected to small variations in elasticity and tip mass. First, we investigate the principal parametric resonance response characteristics of the beam tip mass system without any variations in its parameters by appropriately scaling contributions of the different terms in the governing equation 3.6 as:

$$\ddot{q} + \omega^2 q + 2\epsilon\mu_1\dot{q} + \epsilon\delta q\left(\dot{q}^2 + q\ddot{q}\right) + \epsilon\alpha q^3 = \epsilon\eta q f\cos(\Omega t + \tau_e) \tag{3.11}$$

where the forcing frequency is given by $\Omega = 2\omega + \epsilon\sigma$. Here, $\epsilon\sigma$ is a small detuning parameter that quantifies the difference between the excitation frequency and twice the natural frequency of the first mode of the beam and tip mass system.

As discussed above, any small uncertainty in the nonlinear parameters due to variations in elasticity and tip mass is of order $O(\epsilon^2)$ in the governing equation 3.11, which requires the derivation of the modulation equations up to $O(\epsilon^2)$ to capture their influence. As such, we first compare the approximate solutions and response functions of the original system, with no parameter variations, when implementing $O(\epsilon)$ and $O(\epsilon^2)$ approximations.

3.2.1 Approximate solution

To obtain an approximate solution using the method of multiple scales, we introduce three independent time scales T_0, T_1 and T_2 defined by

$$T_n = \epsilon^n t \qquad n = 0, 1, 2$$

Using the chain rule of differentiation, we expand the derivatives up to $O(\epsilon^2)$ and write:

$$\frac{D}{Dt} = \frac{\partial}{\partial T_0} + \epsilon\frac{\partial}{\partial T_1} + \epsilon^2\frac{\partial}{\partial T_2} \equiv D_0 + \epsilon D_1 + \epsilon^2 D_2 \tag{3.12a}$$

and

$$\frac{D^2}{Dt^2} = \frac{\partial^2}{\partial T_0^2} + 2\epsilon\frac{\partial^2}{\partial T_1\partial T_0} + \epsilon^2\left(2\frac{\partial^2}{\partial T_0\partial T_2} + \frac{\partial^2}{\partial T_1^2}\right) \equiv D_0^2 + 2\epsilon D_0 D_1 + \epsilon^2\left(D_1^2 + 2D_0 D_2\right) \tag{3.12b}$$

The solution of $q(t)$ is then expressed as

$$q(t,\epsilon) = q_0(T_0, T_1, T_2) + \epsilon q_1(T_0, T_1, T_2) + \epsilon^2 q_2(T_0, T_1, T_2) + ... \tag{3.13}$$

Substituting equations 3.12a, 3.12b and 3.13 into the equation 3.11, retaining terms up-to $O(\epsilon^2)$ and equating terms of the order ϵ^0, ϵ^1 and ϵ^2 on the left and right hand sides of equation 3.11, we obtain

ϵ^0- *order equation:*

$$D_0^2 q_0 + q_0\omega^2 = 0 \ , \tag{3.14}$$

ϵ^1- *order equation:*

$$D_0^2 q_1 + q_1\omega^2 = -2D_0D_1q_0 - \delta q_0 D_0 q_0^2 - \delta q_0^2 D_0^2 q_0 - \delta q_0 \left(D_0 q_0\right)^2 - \alpha q_0^3 - 2\mu_1 D_0 q_0 + \frac{1}{2} f\eta q_0 e^{i\tau_e + iT_0\Omega} + \frac{1}{2} f\eta q_0 e^{-i\tau_e - iT_0\Omega}, \text{ and} \tag{3.15}$$

ϵ^2- *order equation:*

$$D_0^2 q_2 + q_2\omega^2 = -2D_0D_1q_1 - D_1^2 q_0 - 2D_0D_2q_0 - 2\delta q_0 D_0 q_0 D_0 q_1 - 2\delta q_0 D_0 q_0 D_1 q_0 - \delta q_1 D_0 q_0^2 - 2\delta q_0^2 D_0 D_1 q_0 - \delta q_1 D_0 q_0^2 - 2\delta q_0 q_1 D_0^2 q_0 - 3\alpha q_1 q_0^2 - 2\mu_1 D_0 q_1 - 2\mu_1 D_1 q_0 + \frac{1}{2} f\eta q_1 e^{i\tau_e + iT_0\Omega} + \frac{1}{2} f\eta q_1 e^{-i\tau_e - iT_0\Omega} \tag{3.16}$$

By eliminating the secular terms that result from substituting the solution of q_0 from equation 3.14 into the ϵ^1-*order* equation 3.15, we obtain the amplitude and phase modulation equations as:

$$\dot{a} = \epsilon \frac{f\eta}{4\omega} a \sin\gamma - \epsilon\mu_1 a, \text{ and} \tag{3.17a}$$

$$\dot{\gamma} = \epsilon\sigma + \epsilon \frac{f\eta}{2\omega} \cos\gamma - \epsilon \frac{(3\alpha - 2\delta\omega^2)}{4\omega} a^2 \tag{3.17b}$$

where the steady state equations are obtained by setting $\dot{a} = 0$ and $\dot{\gamma} = 0$. Squaring and adding these equations yields a relation between amplitude of the response, a, and the system's parameters as a function of the detuning parameter, σ, and the amplitude of the response f.

$$\mu_1^2 + \left[\frac{1}{2}\sigma - \frac{(3\alpha - 2\delta\omega^2)}{8\omega} a^2\right]^2 = \frac{f^2\eta^2}{16\omega^2} \tag{3.18}$$

Carrying the same procedure to the ϵ^2-*order*, i.e., finding the solution of q_1, and substituting it in equation 3.16, we obtain the following amplitude and phase modulation equations

$$\dot{a} = m_{11} a \sin\gamma + m_{21} a^3 \sin\gamma + m_{31} a^3 + m_{41} a, \text{ and} \tag{3.19a}$$

$$\dot{\gamma} = \epsilon\sigma - m_{12}\cos\gamma - m_{22} a^2 \cos\gamma - m_{32} a^2 - m_{42} - m_{52} a^4 \tag{3.19b}$$

where

$$m_{11} = -\epsilon \frac{f\eta(\epsilon\sigma - 2\omega)}{8\omega^2}, \qquad m_{21} = -\epsilon^2 \frac{f\eta(5\alpha + 6\delta\omega^2)}{64\omega^3},$$

$$m_{31} = \epsilon^2 \frac{(3\alpha + 2\delta\omega^2)\mu_1}{8\omega^2}, \qquad m_{41} = -\epsilon\mu_1, \qquad m_{12} = \epsilon \frac{f\eta(\epsilon\sigma - 2\omega)}{4\omega^2},$$
$$m_{22} = -\epsilon^2 \frac{f\eta(\alpha - 6\delta\omega^2)}{16\omega^3}, \qquad m_{32} = \epsilon \frac{(3\alpha - 2\delta\omega^2)}{4\omega},$$
$$m_{42} = \epsilon \frac{3\epsilon f^2\eta^2 - 32\epsilon\omega^2\mu_1^2}{32\omega^3}, \quad \text{and} \quad m_{52} = 3\epsilon^2 \frac{-5\alpha^2 - 12\alpha\delta\omega^2 + 12\delta^2\omega^4}{128\omega^3}. \tag{3.20a}$$

Squaring the steady state equations, obtained by setting $\dot{a} = 0$ and $\dot{\gamma} = 0$ and neglecting the higher order terms [52], we obtain

$$\frac{32\mu_1^2\omega^2\left[a^2\epsilon\left(3\alpha + 2\delta\omega^2\right) - 4\omega^2\right]}{\left[a^2\epsilon\left(5\alpha + 6\delta\omega^2\right) + 8\omega(\sigma\epsilon - \omega)\right]} - \frac{a^2\left(3\alpha - 2\delta\omega^2\right) - 4\sigma\omega}{16\left[a^2\epsilon\left(\alpha - 6\delta\omega^2\right) + 4\omega(\omega - \sigma\epsilon)\right]}\left[3\epsilon\left(5a^4\alpha^2 - 4f^2\eta^2\right) + 12a^2\alpha\omega^2\left(3a^2\delta\epsilon - 4\right) + 4a^2\delta\omega^4\left(8 - 9a^2\delta\epsilon\right) + 64\sigma\omega^3 + 128\mu_1^2\omega^2\epsilon\right] = f^2\eta^2 \tag{3.21}$$

Table 3.1: Material and geometric properties of the beam-tip mass system.

Parameter [units]	**Value**
Mass per unit length, ρ [g/m]	21
Young's modulus, E) [GPa]	43
Length, l [mm]	150
Thickness, h [mm]	0.5
Width, b [mm]	30
Tip mass, m [gm]	5
Area moment of inertia, $I_Y = \frac{1}{12}bh^3$ [mm^4]	312.5

The sensitivity of the approximate solution to solving for the steady state amplitude of response, a_0, up to $O(\epsilon)$ and $O(\epsilon^2)$ can be determined by comparing the amplitude response functions of equations 3.18 and 3.21 with numerical solutions of the governing equations as shown in figures 3.2(a) and 3.2(b). The goemetric and material propoerties of the beam and tip mass are presented in Table 3.1. Figure 3.2(a) shows the sub-critical type principal parametric response of the beam and tip mass system for a positive detuning, $\epsilon\sigma = 0.038$ rad/s and figure 3.2(b) shows the supercritical type response for a negative detuning $\epsilon\sigma = -0.038$ rad/s. The plots also show that the response predicted from the numerical simulations are in excellent agreement with the steady state response predicted with equation 3.21.

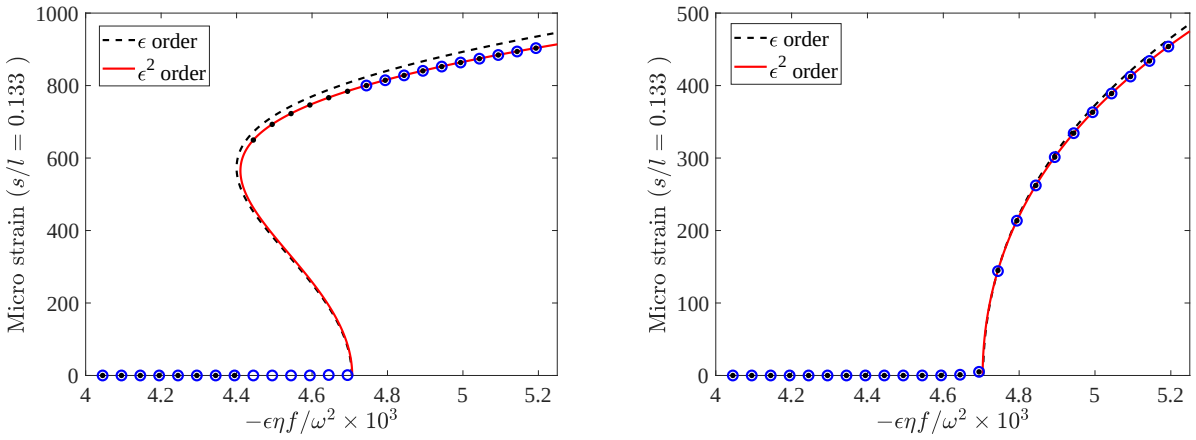

Figure 3.2: Principal parametric response of the beam and tip mass, represented as micro strain at 2 cm from the base excitation where $s/l = 0.133$, when (a) $\epsilon\sigma = 0.038$ rad/s, (b) $\epsilon\sigma = -0.038$ rad/s. The dots and circles represent respectively the numerically simulated results of backward and forward sweeps.

3.2.2 Sensitivity to stiffness variation

From the linear eigenvalue problem and equation 3.9, the natural frequency and geometric non linearity coefficients are a function of the linear stiffness through the following relations

$$\omega = \left(\frac{EI_Y\lambda^4}{\rho}\right)^{\frac{1}{2}}, \text{ and} \tag{3.22}$$

$$\alpha = -EI_Y \int_0^l \phi'^2(\phi'\phi'')'\, ds \tag{3.23}$$

Given that the beam is in-extensible and the tip-mass and density of the beam are not altered, the mode shape should not be affected. For the sake of analysis, we vary the elasticity and write

$$E' = E(1 + \epsilon\sigma_E)$$

where, $\epsilon\sigma_E$ represents the non dimensional change in the elasticity and ϵ denotes that the term is smaller than 1. Consequently, we write

$$\omega'^2 = \omega^2 + \omega^2\epsilon\sigma_E = \omega^2(1 + \epsilon\sigma_E), \text{ and} \tag{3.24}$$

$$\alpha' = \alpha + \alpha\epsilon\sigma_E = \alpha(1 + \epsilon\sigma_E) \tag{3.25}$$

The forcing frequency is based on the natural frequency of the system and such that $\Omega = 2\omega + \epsilon\sigma$. Incorporating the change in the parameters into the governing equation, we rewrite the governing equation of the first mode as,

$$\ddot{q} + \omega'^2 q + 2\epsilon\mu_1\dot{q} + \epsilon\delta q\left(\dot{q}^2 + q\ddot{q}\right) + \epsilon\alpha' q^3 = \epsilon\eta q f\cos(\Omega t + \tau_e) \tag{3.26}$$

where α' and ω'^2 have been defined in equations 3.24 and 3.25.

Implementing the method of multiple scales as explained in the previous section, we obtain the

ϵ^0- *order equation:*

$$D_0^2 q_0 + q_0\omega^2 = 0\ , \tag{3.27}$$

ϵ^1- *order equation:*

$$\begin{aligned} D_0^2 q_1 + q_1\omega^2 = {} & -2D_0D_1q_0 - \delta q_0^2 D_0^2 q_0 - \delta q_0\left(D_0 q_0\right)^2 - \alpha q_0^3 - q_0\sigma_E\omega^2 - 2\mu_1 D_0 q_0 \\ & + \frac{1}{2}f\eta q_0 e^{i\tau_e + iT_0\Omega} + \frac{1}{2}f\eta q_0 e^{-i\tau_e - iT_0\Omega},\ \text{and} \end{aligned} \tag{3.28}$$

ϵ^2- *order equation:*

$$\begin{aligned} D_0^2 q_2 + q_2\omega^2 = {} & -2D_0D_1q_1 - D_1^2 q_0 - 2D_0D_2q_0 - 2\delta q_0 D_0 q_0 D_0 q_1 - 2\delta q_0 D_0 q_0 D_1 q_0 \\ & - \delta q_1 D_0 q_0^2 - 2\delta q_0^2 D_0 D_1 q_0 - \delta q_1 D_0 q_0^2 - 2\delta q_0 q_1 D_0^2 q_0 - 3\alpha q_1 q_0^2 - \alpha q_0^3\epsilon\sigma_E - q_1\sigma_E\omega^2 \\ & - 2\mu_1 D_0 q_1 - 2\mu_1 D_1 q_0 + \frac{1}{2}f\eta q_1 e^{i\tau_e + iT_0\Omega} + \frac{1}{2}f\eta q_1 e^{-i\tau_e - iT_0\Omega} \end{aligned} \tag{3.29}$$

By finding the solution of q_0 and q_1 while eliminating the secular terms that result from substituting q_0 and q_1 respectively into the ϵ-*order* equation 3.28 and ϵ^2-*order* equation 3.29, we obtain the amplitude and phase modulation equations as:

$$\dot{a} = m_{11}a\sin\gamma + m_{21}a^3\sin\gamma + m_{31}a^3 + m_{41}a,\ \text{and} \tag{3.30a}$$

$$\dot{\gamma} = \epsilon\sigma - m_{12}a\cos\gamma - m_{22}a^3\cos\gamma - m_{32}a^3 - m_{42}a - m_{52}a^5 \tag{3.30b}$$

where

$$m_{11} = -\epsilon\frac{f\eta(\epsilon\sigma - 2\omega)}{8\omega^2},\quad m_{21} = -\epsilon^2\frac{f\eta(5\alpha + 6\delta\omega^2)}{64\omega^3},$$

$$m_{31} = \epsilon^2\frac{(3\alpha + 2\delta\omega^2)\mu_1}{8\omega^2},\qquad m_{41} = -\epsilon\mu_1,\qquad m_{12} = \epsilon\frac{f\eta(\epsilon\sigma - 2\omega)}{4\omega^2},$$

$$m_{22} = -\epsilon^2\frac{f\eta(\alpha - 6\delta\omega^2)}{16\omega^3},\qquad m_{32} = \epsilon\frac{(3\alpha - 2\delta\omega^2)(2 + \epsilon\sigma_E)}{8\omega},$$

$$m_{42} = \epsilon\frac{3\epsilon f^2\eta^2 + 32\omega^4\sigma_E - 8\epsilon\omega^4\sigma_E^2 - 32\epsilon\omega^2\mu_1^2}{32\omega^3},\ \text{and}$$

$$m_{52} = 3\epsilon^2 \frac{-5\alpha^2 - 12\alpha\delta\omega^2 + 12\delta^2\omega^4}{128\omega^3}. \tag{3.30c}$$

Squaring the steady state equations, obtained by setting $\dot{a} = 0$ and $\dot{\gamma} = 0$ in equations 3.30a and 3.30b, we obtain:

$$\begin{aligned}\frac{32\mu_1^2\omega^2\left[a^2\epsilon\left(3\alpha + 2\delta\omega^2\right) - 4\omega^2\right]}{a^2\epsilon\left(5\alpha + 6\delta\omega^2\right) + 8\omega(\sigma\epsilon - \omega)} - \frac{a^2\left(3\alpha - 2\delta\omega^2\right) + 4\sigma_E\omega^2 - 4\sigma\omega}{16\left[a^2\epsilon\left(\alpha - 6\delta\omega^2\right) + 4\omega(\omega - \sigma\epsilon)\right]}\left[3\epsilon\left(5a^4\alpha^2\right.\right.\\ \left.-4f^2\eta^2\right) + 12a^2\alpha\omega^2\left(3a^2\delta\epsilon - 4\right) + 4a^2\delta\omega^4\left(8 - 9a^2\delta\epsilon\right)\\ +16\omega^2\left[\sigma_E\left(a^2\epsilon\left(2\delta\omega^2 - 3\alpha\right) + 2\sigma_E\omega^2\epsilon - 4\omega^2\right) + 8\mu_1^2\epsilon\right] + 64\sigma\omega^3\Big] = f^2\eta^2\end{aligned} \tag{3.31}$$

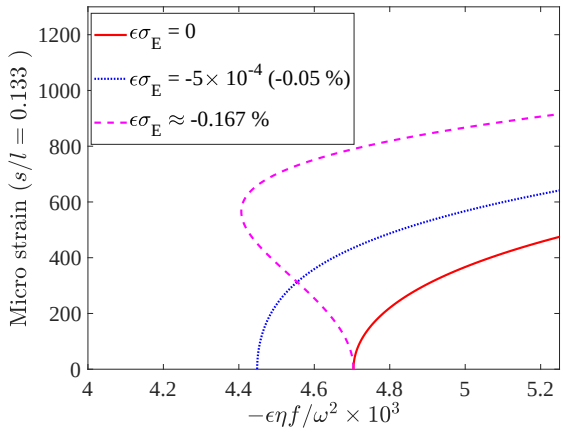

Figure 3.3: Sensitivity of the parametric response of the beam-tip mass system to small variations in elasticity $E = 43$ GPa and $\Omega = 2\omega - 0.038$ rad/s

Figure 3.3 shows the change in the amplitude response function when the modulus of elasticity is varied. Of particular interest is the notion that small variations can induce a drastic change in the response in terms of the type of bifurcation. For properties used in this particular problem, a decrease in elasticity by 0.167% of the actual value (i.e., $\epsilon\sigma_E \approx -1.67 \times 10^{-3}$) changes the behavior from a supercritical Hopf bifurcation to a sub-critical one. In other words, the extent of damage, represented by small reduction in the beam's stiffness of a beam-tip mass system that is designed for a supercritical response can be quantified by testing it for a subcritical response under the same detuning conditions.

It is important to note the closeness of the bifurcation points for the original system and for the one where the modulus of elasticity is reduced by 0.167%. It can be explained by investigating the change in parameters governing the response of system. When the elasticity is decreased by 0.167%, the value of modulus of elasticity is changed from $E = 43$ GPa to $E' = 42.928$ GPa causing the natural angular frequency to decrease from $\omega = 45.596$ rad/s

to $\omega' = 45.558$ rad/s. Because the set detuning is, $\epsilon\sigma = -0.038$ rad/s and the excitation frequency is $\Omega = 2\omega + \epsilon\sigma = 91.154$ rad/s, the change in natural frequency alters the detuning that is being exerted on the system, which is hereafter referred as the effective detuning. This effective detuning (σ_{eff}) can be calculated from $\omega' = 45.558$ rad/s, which yields, $\epsilon\sigma_{eff} = \Omega - 2\omega' = 0.038$ rad/s $\approx |\epsilon\sigma|$. The minimum excitation amplitude that is required to produce a non-zero response depends on the absolute magnitude of the detuning that is being exerted on the system. As demonstrated above, since $\epsilon\sigma_{eff} \approx |\epsilon\sigma|$, the bifurcation point, representing the excitation amplitude at which the system produces a non-zero response in the original system and when the elasticity decreases by 0.167% are approximately the same.

3.2.3 Sensitivity to variations in tip mass

The tip mass affects the natural frequency and mode shapes in a complicated way. Because the mode shape influences all the coefficients in the governing equation, we develop the governing equation for each value of the tip mass. Figures 3.4(a) and 3.4(b) show the sensitivity of response to small variations in the tip mass for a particular forcing frequency in each case. In particular, figure 3.4(a) presents the sensitivity of the response to changes in the tip mass without changing the forcing frequency when the unaltered system ($m = 5$ gm) has a positive detuning of $\epsilon\sigma = 0.038$ rad/s. As the tip-mass is slightly increased it can be seen that the limits of the sub-critical response change. This change can be attributed to the fact that the increase in mass decreases the natural frequency of the system, thereby increasing the effective detuning for a constant forcing frequency. Figure 3.4(b) presents the sensitivity of response to a small change in the tip mass without changing the forcing frequency when the unaltered system has a negative detuning of $\epsilon\sigma = -0.038$ rad/s. As explained above, increasing the tip mass increases the effective detuning of the system. For a system that initially had a negative detuning, an increase in the tip mass can potentially make the effective detuning positive and thereby alters the bifurcation from a supercritical Hopf bifurcation to a subcritical one as seen when the tip mass is increased to $m = 5.0096$ gm. This is quite drastic change in the behavior for a very small change in tip mass (about 0.19% in this case) and can potentially be exploited in MEMS application for mass sensing or detection.

Couple of sample MATHEMATICA files, *mass vary.nb* and *mass vary 0p0096.nb* are in the Appendix A.

3.3 Shift in bifurcation behavior - summary

In figures 3.3 and 3.4(b), we noted that a system excited with an expected response that follows a supercritical bifurcation behavior can shift to a sub-critical behavior due to a reduction in stiffness or the addition of tip mass. Next, we examine the extent to which this

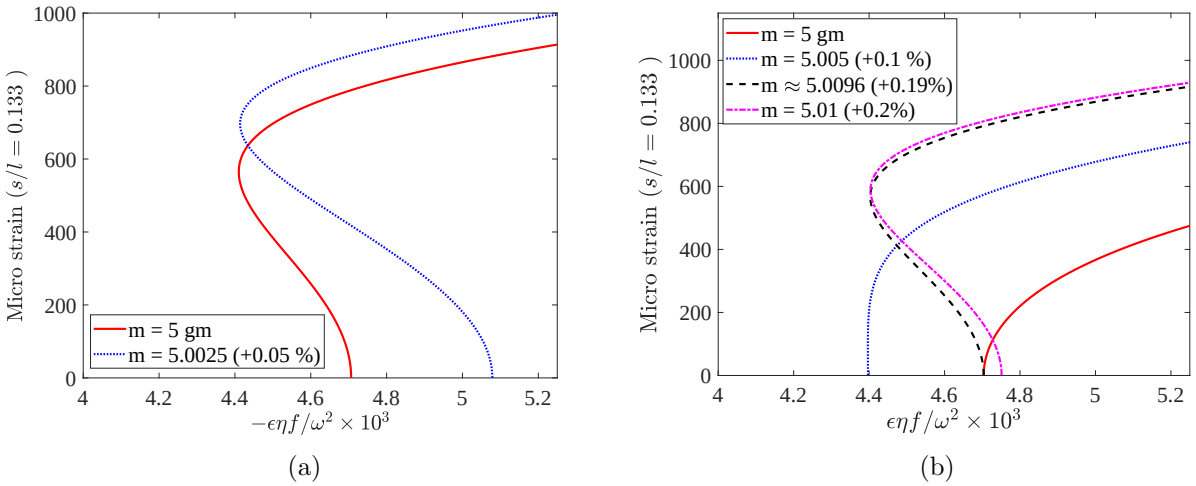

Figure 3.4: Sensitivity of parametric response of the beam-tip mass system to small variations in tip mass when the excitation frequency (a) $\Omega = 2\omega_{m=5} + 0.038$ rad/s and (b) $\Omega = 2\omega_{m=5} - 0.038$ rad/s. The parameters chosen for nondimensionalizing acceleration are $\omega = 45.596$ rad/s and $\eta = -69127.320$ $\mathrm{m^{-1}s^{-2}}$ for postive detuning and $\eta = -69012.193$ $\mathrm{m^{-1}s^{-2}}$ for negative detuning.

change can be exploited to detect and quantify mass or stiffness variations. To this end, we consider that a shift in bifurcation behavior can be detected when the bifurcation point of the sub-critical curve meets the bifurcation point of actual supercritical curve exhibited by the system. For instance, in the case of sensitivity of response to small variations in tip mass retaining the stiffness as $E = 43$ GPa, as represented in figure 3.4(b), we consider the shift in bifurcation behavior to be detectable when the tip mass is increased by 0.19%.

For a fixed stiffness, tip-mass values and a given initial detuning value, $\epsilon\sigma$, figure 3.5 shows the range by which E, m or both of them should change to yield the change in the type of bifurcation behavior. The results show that at higher detuning values, a larger change must take place before a shift in the type of bifurcation takes place.

3.4 Conclusions

We performed a sensitivity analysis of the beam with a tip mass system subjected to parametric excitation for small variations in the values of the elasticity and tip mass. The analysis was carried out by solving the system using the method of multiple scales with the objective of detecting small variations in nonlinear parameters due small uncertainty in elasticity and tip mass. For the problem considered, we illustrated that a decrease in elasticity can alter

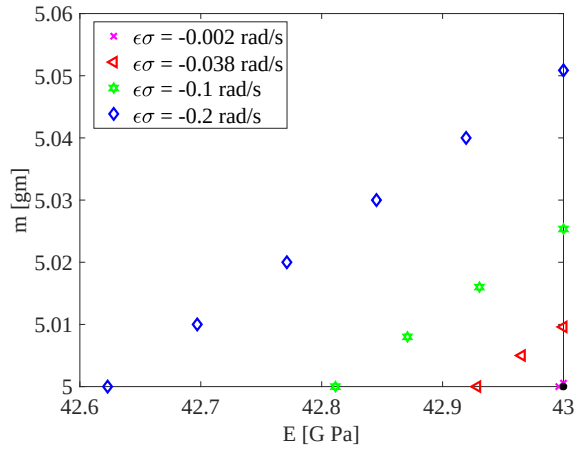

Figure 3.5: Required variation in stiffness and tip-mass to observe the change in the type of bifurcation behavior for the considered beam and tip mass system ($E = 43$ GPa and $m = 5$ gm) for various values of initial detuning in the system.

the response of a system that is designed to yield a supercritical bifurcation to result in a sub-critical bifurcation. We explained this change in the response by defining effective detuning, which accounts for the fact that the change in elasticity affects the natural frequency of the system and thereby affects the actual detuning. From the sensitivity analysis of tip mass, we showed that a very small change of the order of 0.19% in the tip mass can cause an appreciable effect in the response by changing the type of bifurcation. This observation can potentially be applied for using parametrically excited micro-cantilever beams as sensing devices. Introspecting the definition of effective detuning suggests that the sensitivity to change in the tip mass is directly proportional to the closeness of the excitation frequency to twice the natural frequency of original system, i.e., the detuning parameter σ. In the light of this observation, we noted that the sensitivity of tip mass can be increased by decreasing σ.

Chapter 4

Identification of nonlinear piezoelectric coefficients

Attention to piezoelectric materials has increased dramatically in recent years. This interest rises from their potential for their use in many applications for various objectives. They have been suggested for developing self powered micro systems and sensors [53–58], active-passive vibration control and damping systems [59–64], broadband energy harvesters [65–68] and impedance based structural health monitoring devices [57, 69, 70]. In more recent studies, piezoelectric/ceramic materials have been proposed in biomedical applications as load and wear sensors for knee joints [71, 72] and as receivers to oxygenate tumors and charge pacemakers [73–75]. To augment the power generated, specific designs have been proposed that produce large strains and thereby generating more power [76–78]. Extending the realm of applications of piezoelectric materials comes with a price, as large strains can cause the material to behave in a nonlinear manner and exhibit amplitude-dependent resonant frequencies, super-harmonics in the response, saturation and hysteresis behaviors. As such, identification of the nonlinear electromechanical constitutive relation must be performed to design, analyze, optimize and/or exploit such behaviors.

Aurelle et al. [32] and Guyomar et al. [33] presented a nonlinear electromechanical constitutive relation to study the saturation and hysteresis behavior that they observed in their experiments on ultrasonic transducers. Wagner and Hagedorn [34] derived an equation for the electric enthalpy density that accounts for nonlinearities in piezoelectric response. They demonstrated that a bi-morph cannot be used to study the quadratic nonlinearities because the symmetrical nature of the bi-morph eliminates the effects of quadratic nonlinearities. A review of the nonlinear behavior of piezoelectric materials was presented by Leadenham and Erturk [79]. We note that the most common approach employed to estimate the parameters governing the nonlinear behavior in the above mentioned references has consisted of an optimized curve fitting procedure and, postulate that there is a need to develop a holistic parameter identification scheme that utilizes the vibration behavior.

Analyzing the vibration behavior is probably the most insightful and physical way for parameter identification. Free vibration tests are commonly used for estimating damping ratio of a structure and in piezoelectric energy harvesters. The frequency response functions of displacement and voltage generated are used to identify characteristic capacitance and electromechanical coupling of the harvester. Nayfeh [80] presented a parameter identification procedure for a generic nonlinear coupled oscillator that exploits the hysteresis and sub critical bufurcation exhibited by a generic oscillator. Zavodney [81] generalized the theory to identify and estimate the nonlinearity in the system from random excitations and forcing and frequency sweeps. Hajj et al. [82] combined perturbation techniques and bispectral analysis to characterize nonlinear damping from experimental data of three beam and two mass system. A concise review of nonlinear system identification in structural dynamics is presented by Kerschen et al. [83]. To date, the parameter identification work for smart and intelligent systems has concentrated on micro resonators, where the system is represented as a Duffing oscillator with geometric nonlinearity [84, 85] without a specific approach to identify nonlinear piezoelectric coefficients.

In this paper, we consider an unsymmetrical piezoelectric energy harvester and propose a parameter identification scheme to identify nonlinear piezoelectric coefficients by exploiting the principal mode resonant response. We consider a beam with tip mass and a single piezoelectric layer subjected to direct excitation as an unsymmetrical piezoelectric energy harvester and first derive the governing equations of the first mode using the electric enthalpy density representation introduced by Wagner and Hagedorn [34]. We then use the method of multiple scales [46, 50] to determine the approximate solution of the response to a principal mode resonant excitation and under open circuit conditions (i.e., high load resistance). We argue that the characteristic nonlinear response of the harvester predicted by the method of multiple scales as approximate solution and steady state amplitude response relations can be used for estimating nonlinear parameters and propose a holistic parameter identification scheme. By choosing a numerical example, we validate the proposed parameter identification scheme and estimate the material parameters governing the nonlinear behavior.

4.1 Mathematical Modeling

A cantilever beam system with a tip mass m, partially covered with piezoelectric layer, subjected to direct excitation is considered for the analysis as shown in the figure 2.1. The beam with length l, width b_p, thickness h_s and mass per unit length ρ_s is bonded with a piezoelectric layer of length l_1, width b, thickness h_p and mass per unit length ρ_p that is connected to a load resistance, R. To derive the governing equation and energy harvested, we employ the generalized Hamilton principle for electronic transducers [34, 86–89], which is written as:

$$\int_{t_1}^{t_2} (\delta T - \delta \Delta + \delta W_{nc})\, dt = 0 \tag{4.1}$$

Assuming that the beam is in-extensible, the horizontal displacement, $u(s,t)$ can be represented as $u(s,t) = \frac{1}{2}\int_0^s w'^2\, ds$ [4]. Therefore, the kinetic energy of the system can be written as:

$$T = \frac{1}{2}m\left[\int_0^l \frac{1}{2}\frac{\partial}{\partial t}\left(w'^2\right)\, ds\right]^2 + \frac{1}{2}\int_0^{l_1}\rho_{eq}\left[\int_0^s \frac{1}{2}\frac{\partial}{\partial t}\left(w'^2\right)\, dy\right]^2 ds + \frac{1}{2}\int_{l_1}^{l}\rho_s\left[\int_0^s \frac{1}{2}\frac{\partial}{\partial t}\left(w'^2\right)\, dy\right]^2 ds + \frac{1}{2}m\left[\frac{\partial w(l,t)}{\partial t} + \dot{u}_b\right]^2 + \frac{1}{2}\int_0^{l_1}\rho_{eq}\left[\dot{w}+\dot{u}_b\right]^2 ds + \frac{1}{2}\int_{l_1}^{l}\rho_s\left[\dot{w}+\dot{u}_b\right]^2 ds \quad (4.2)$$

where $\rho_{eq} = \rho_s + \rho_p$. The neutral axis of the system is discontinuous because of the presence

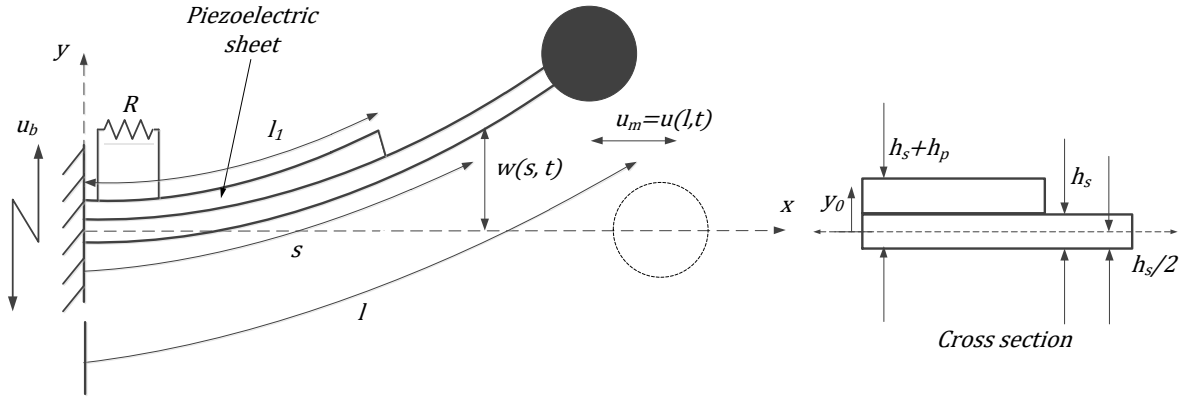

Figure 4.1: Schematic of the beam and tip mass system with a piezoelectric layer. The dashed circle represents the initial undeformed position of the tip mass.

of partial piezoelectric layer and as such, it can be derived by recalling that the stresses through the cross section must be in equilibrium. By defining the neutral axis y_0, as shown in figure 4.1, we write:

$$y_0 = \begin{cases} \frac{Y_{11}^p h_p(h_s+h_p)}{2\left(Y_{11}^s h_s + Y_{11}^p h_p\right)} & 0 \le s \le l_1 \\ 0 & l_1 < s \le l \end{cases} \quad (4.3)$$

The corresponding strain up to the third order approximation can be written as [4],

$$\varepsilon_{11} = -\left[y - y_0\right]\kappa = -\left[y-y_0\right] w''\left(1 + \frac{1}{2}w'^2\right)$$

As discussed above, we wish to identify nonlinear coefficients in the constitutive relation of the piezoelectric material, which can be represented by the electric enthalpy. To accomplish

this, we account for the potential energy and use the electric enthalpy derived by Wagner and Hagedorn [34] and write

$$\Delta = \int \left(\frac{1}{2} Y_{11}^{s} \varepsilon_{11}^{2} + \frac{1}{2} Y_{11}^{p} \varepsilon_{11}^{2} - e_{31} \varepsilon_{11} E_3 - \frac{1}{2} \alpha_3 E_3 \varepsilon_{11}^{2} - \frac{1}{2} \epsilon_{33}^{S} E_3^{2} + \frac{1}{6} \alpha_1 \varepsilon_{11}^{3} - \frac{1}{6} \alpha_2 \varepsilon_{11}^{3} E_3 + \frac{1}{8} \alpha_4 \varepsilon_{11}^{4} \right) dv \tag{4.4}$$

where Y_{11}^{s}, Y_{11}^{p}, e_{31} and ϵ_{33}^{S} are respectively the Young's modulus of elasticity of the beam (substrate), Young's modulus of piezoelectric material, piezoelectric coupling co-efficient and dielectric (or piezoelectric permittivity) constant. E_3 is the induced electric field and is given by

$$E_3 = \begin{cases} -\frac{V_H}{h_p} & \frac{h_s}{2} \leq y \leq \frac{h_s}{2} + h_p \\ 0 & -\frac{h_s}{2} \leq y < \frac{h_s}{2} \end{cases} \tag{4.5}$$

where $V_H(s,t) = V(t)\left[H(s) - H(s-l_1)\right] = V(t)Hf(s)$, $V_H(s,t)^n = V(t)^n\left[H(s) - H(s-l_1)\right] = V(t)^n Hf(s)$ and $H(x)$ is Heaviside step function.

The electric enthalpy in equation 4.4 can be re-written as:

$$\begin{aligned} \Delta = \frac{1}{2}\int_0^{l_1} YI_{eq} w''^2 \left[1 + w'^2\right] ds - \int_0^{l_1} e_{31}\Lambda_1 w''(1 + \frac{1}{2}w'^2)\frac{V_H}{h_p} ds + \frac{1}{2}\int_0^{l_1} \alpha_3 I_p w''^2 \frac{V_H}{h_p} ds \\ - \frac{1}{2}\int_0^{l_1} \epsilon_{33}^{S}\frac{V_H^2 b}{h_p} ds - \frac{1}{6}\int_0^{l_1} \alpha_1 \Lambda_2 w''^3 ds - \frac{1}{6}\int_0^{l_1} \alpha_2 \frac{V_H}{h_p}\Lambda_2 w''^3 ds \\ + \frac{1}{8}\int_0^{l_1} \alpha_4 \Lambda_3 w''^4 ds + \frac{1}{2}\int_{l_1}^{l} Y_{11}^{s} I_s w''^2 \left[1 + w'^2\right] ds \end{aligned} \tag{4.6}$$

where $YI_{eq} = (YI)_s + Y_{11}^{p} I_p$,

$$(YI)_s = \int_{-\frac{h_s}{2}}^{\frac{h_s}{2}} Y_{11}^{s} b\,(y - y_0)^2\, dy = Y_{11}^{s}\frac{b}{3}\left[\left(\frac{h_s}{2} - y_0\right)^3 + \left(\frac{h_s}{2} + y_0\right)^3\right], \tag{4.7a}$$

$$I_p = \int_{\frac{h_s}{2}}^{\frac{h_s}{2}+h_p} b_p\,(y - y_0)^2\, dy = \frac{b_p}{3}\left[\left(\frac{h_s}{2} + h_p - y_0\right)^3 - \left(\frac{h_s}{2} - y_0\right)^3\right], \tag{4.7b}$$

$$\Lambda_1 = \frac{b_p}{2}\left[\left(\frac{h_s}{2} + h_p - y_0\right)^2 - \left(\frac{h_s}{2} - y_0\right)^2\right], \qquad \Lambda_2 = \frac{b_p}{4}\left[\left(\frac{h_s}{2} + h_p - y_0\right)^4 - \left(\frac{h_s}{2} - y_0\right)^4\right], \tag{4.7c}$$

$$\Lambda_3 = \frac{b_p}{5}\left[\left(\frac{h_s}{2} + h_p - y_0\right)^5 - \left(\frac{h_s}{2} - y_0\right)^5\right], \text{ and} \qquad I_s = \frac{b}{12}h_s^3. \tag{4.7d}$$

The virtual work done by the non conservative forces is represented by

$$\delta W_{nc} = -\int_0^{l} c_1 w^{(0,1)}(s,t)\delta w(s,t)\, ds \tag{4.8}$$

where c_1 is structural damping coefficient. Substituting equations 4.2, 4.6, and 4.8 into equation 4.1, we obtain the piece-wise distributed parameter governing equation of motions as

$$\begin{aligned}
&-\rho_{eq}\ddot{w} - c_1\dot{w} - YI_{eq}(w'''' + [w'(w'w'')']') - \frac{\rho_{eq}}{2}\left[w'\int_{l_1}^{s}\int_0^{\theta}\frac{\partial^2}{\partial t^2}\left(w'^2\right)\,dy\,d\theta\right]' \\
&\qquad + \frac{mw''}{2}\int_0^{l}\frac{\partial^2}{\partial t^2}\left(w'^2\right)\,ds + e_{31}II_p\left[\frac{w'^2VHf''}{2h_p} + \frac{w''w'VHf'}{h_p} + \frac{VHf''}{h_p}\right] \\
&+ \alpha_2\Lambda_2\left[\frac{VHf''w''^2}{2h_p} + \frac{2w''w'''VHf'}{h_p} + \frac{w'''^2VHf}{h_p} + \frac{w''''w''VHf}{h_p}\right] + \alpha_1\Lambda_2\left[w'''^2 + w''w''''\right] \\
&\qquad - \alpha_3 I_p\left[\frac{VHf''w''}{h_p} + \frac{2Vhf'w'''}{h_p} + \frac{VHfw''''}{h_p}\right] + \alpha_4\Lambda_3\left[-3w''w'''^2 - \frac{3}{2}w''^2w''''\right] \\
&\qquad\qquad + \frac{\rho_s}{2}w''\int_{l_1}^{l}\int_0^{\theta}\frac{\partial^2}{\partial t^2}\left(w'^2\right)\,dy\,d\theta - \rho_{eq}\ddot{u}_b = 0 \quad (4.9)
\end{aligned}$$

for $0 < s < l_1$,

$$\begin{aligned}
&-\rho_s\ddot{w} - c_1\dot{w} - Y_{11}^s I_s(w'''' + [w'(w'w'')']') \\
&\qquad - \frac{\rho_s}{2}\left[w'\int_{l}^{s}\int_0^{\theta}\frac{\partial^2}{\partial t^2}\left(w'^2\right)\,dy\,d\theta\right]' + \frac{mw''}{2}\int_{1_1}^{l}\frac{\partial^2}{\partial t^2}\left(w'^2\right)\,ds - \rho_s\ddot{u}_b = 0 \quad (4.10)
\end{aligned}$$

for $l_1 < s < l$, and the corresponding electrical equation is

$$\begin{aligned}
&e_{31}\Lambda_1\left[\int_0^{l_1}\frac{w''}{h_p}\,ds + \int_0^{l}\frac{w'^2w''}{2h_p}\,ds\right] + \alpha_2\Lambda_2\int_0^{l_1}\frac{w''^3}{6h_p}\,ds \\
&\qquad\qquad + \int_0^{l_1}\frac{\varepsilon_{33}Vb}{h_p}\,ds - \alpha_3 I_p\int_0^{l_1}\frac{w''^2}{2h_p}\,ds = Q(t) \quad (4.11)
\end{aligned}$$

Since the beam is clamped at $s = 0$, the essential boundary conditions at $s = 0$ are given by

$$w(0,t) = 0 \qquad w^{(1,0)}(0,t) = 0 \tag{4.12}$$

and the natural nonlinear boundary conditions at $s = l$, which are moment and shear force balance equations, obtained from the generalized Hamilton principle are written as

$$Y_{11}^s I_s\left(w''w'^2 + w''\right)\Big|_{s=l} = 0 \implies w''(l,t) = 0 \tag{4.13}$$

$$-m\ddot{u}_b + Y_{11}^s I_s\left(w'''w'^2 + w''^2w' + w'''\right) - mw'\int_0^{l}\frac{\partial^2}{\partial t^2}\left(\frac{w'^2}{2}\right)\,ds - m\ddot{w}\Big|_{s=l} = 0 \tag{4.14}$$

The generalized Hamilton's principle also yields us the moment and shear force balance equations at $s = l_1$, which serve as the compatibility conditions at $s = l_1$ and are written as

$$e_{31}\Lambda_1\left[\frac{w'^2VHf}{2h_p}+\frac{VHf}{h_p}\right]+\frac{1}{2}\alpha_1\Lambda_2w''^2+\frac{1}{2h_p}\alpha_2\Lambda_2HfVw''^2-\frac{1}{2}\alpha_4\Lambda_3w''^3 \\ -\alpha_3I_p\frac{w''VHf}{h_p}-YI_{eq}\left(w''w'^2+w''\right)+Y_{11}^sI_s\left(w''w'^2+w''\right)\Big|_{s=l_1}=0 \quad (4.15)$$

$$-e_{31}\Lambda_1\left(\frac{w'^2VHf'}{2h_p}+\frac{VHf'}{h_p}\right)+YI_{eq}\left(w'''w'^2+w''^2w'+w'''\right)-Y_{11}^sI_s\left(w'''w'^2+w''^2w'+w'''\right) \\ -\alpha_2\Lambda_2\left(\frac{w''^2VHf'}{2h_p}+\frac{VHfw''w'''}{h_p}\right)-\alpha_1\Lambda_2w''w'''+\alpha_3I_p\left(\frac{w''VHf'}{h_p}+\frac{w'''VHf}{h_p}\right) \\ +\frac{3}{2}\alpha_4\Lambda_3w''^2w'''\Big|_{s=l_1}=0 \quad (4.16)$$

4.1.1 Reduced order model - Galerkin discretization

To simplify the representative model and to study the response to a principal mode resonance excitation, we employ a Galerkin discretization and perform weighted residual method to determine the governing equation of the first mode. To this end, we determine the linear mode shapes of the system by considering the undamped, unforced, short circuited $[V(t) = 0]$ and linear free vibration description of motion as

$$\begin{cases} \rho_{eq}\ddot{w}+YI_{eq}w''''=0 & 0<s<l_1 \\ \rho_s\ddot{w}+Y_{11}^sI_sw''''=0 & l_1<s<l \end{cases} \quad (4.17)$$

Assuming the discretization as

$$w(s,t)=\begin{cases} \sum_{i=1}^{M}\phi_i(s)q_i(t) & 0<s<l_1 \\ \sum_{i=1}^{M}\psi_i(s)q_i(t) & l_1<s<l \end{cases} \quad (4.18)$$

and substituting into equation 4.17, while realizing that $\ddot{q} = -\omega_n^2 q$, where ω_n is the natural frequency of the n^{th}-mode, we obtain

$$\phi_i'''' = \lambda_{1i}\phi_i \qquad 0<s<l_1 \quad (4.19a)$$

$$\psi_i'''' = \lambda_{2i}^4\psi_i \qquad l_1<s<l \quad (4.19b)$$

whose general solution is of the form

$$\phi_i(s)=A_1\cos(\lambda_{1i}s)+B_1\sin(\lambda_{1i}s)+C_1\cosh(\lambda_{1i}s)+D_1\sinh(\lambda_{1i}s) \qquad 0<s<l_1 \quad (4.20a)$$

$$\psi_i(s) = A_2\cos(\lambda_{2i}s) + B_2\sin(\lambda_{2i}s) + C_2\cosh(\lambda_{2i}s) + D_2\sinh(\lambda_{2i}s) \qquad l_1 < s < l \quad (4.20b)$$

where $\lambda_{1i} = \left(\frac{\omega_i^2\rho_{eq}}{YI_{eq}}\right)^{\frac{1}{4}}$, $\lambda_{2i} = \left(\frac{\omega_i^2\rho_s}{Y_{11}^s I_s}\right)^{\frac{1}{4}}$ and the linear short circuited boundary conditions are given by

$$\phi(0) = \phi'(0) = 0, \qquad \psi''(l) = 0, \text{ and} \quad (4.21a)$$

$$\left(Y_{11}^s I_s\psi''' + m\omega^2\psi\right)|_{s=l} = 0. \quad (4.21b)$$

The continuity relations and linear compatibility conditions are written as

$$\phi(l_1) = \psi(l_1), \qquad \phi'(l_1) = \psi'(l_1), \quad (4.22a)$$

$$YI_{eq}\phi''(l_1) = Y_{11}^s I_s\psi''(l_1), \text{ and} \qquad YI_{eq}\phi'''(l_1) = Y_{11}^s I_s\psi'''(l_1). \quad (4.22b)$$

Moreover, for any two distinct modes, p and q, we assume

$$\omega_p^2\int_0^{l_1}\rho_{eq}\phi_p\phi_q\,ds = YI_{eq}\phi_p'''\phi_q\big|_{s=0}^{s=l_1} - YI_{eq}\phi_p''\phi_q'\big|_{s=0}^{s=l_1} + \int_0^{l_1}YI_{eq}\phi_p''\phi_q''\,ds \quad (4.23a)$$

$$\omega_p^2\int_{l_1}^{l}\rho_s\psi_p\psi_q\,ds = Y_{11}^s I_s\psi_p'''\psi_q\big|_{s=l_1}^{s=l} - Y_{11}^s I_s\psi_p''\psi_q'\big|_{s=l_1}^{s=l} + \int_{l_1}^{l}Y_{11}^s I_s\psi_p''\psi_q''\,ds \quad (4.23b)$$

Adding equations 4.23a and 4.23b and using the compatibility conditions, the orthogonality relations are written as

$$\begin{gathered}\int_0^{l_1}\rho_{eq}\phi_p(s)\phi_q(s)\,ds + \int_{l_1}^{l}\rho_s\psi_p(s)\psi_q(s)\,ds + m\psi_p(l)\psi_q(l) = \delta_{pq} \\ \int_0^{l_1}YI_{eq}\phi_p''(s)\phi_q''(s)\,ds + \int_{l_1}^{l}Y_{11}^s I_s\psi_p''(s)\psi_q''(s)\,ds = \delta_{pq}\omega_q^2\end{gathered} \quad (4.24)$$

where δ_{pq} is the Kronecker delta, defined as unity when p is equal to q and zero otherwise. Using the above discretization, the solution is approximated as the sum of a finite number of modes, i.e.,

$$w(s,t) = \begin{cases}\sum_{i=1}^{M}\phi_i(s)q_i(t) & 0 < s < l_1 \\ \sum_{i=1}^{M}\psi_i(s)q_i(t) & l_1 < s < l\end{cases} \quad (4.25)$$

where the basis functions $\phi_i(s)$ and $\psi_i(s)$ represent the mode shape, $q_i(t)$ represents the modal coordinate (temporal amplitude) and M is the number of modes under consideration. For any given problem, the natural frequency ω_i and mass normalized mode shapes can be uniquely determined by solving for non-trivial solution of eight equations 4.21a - 4.22b in conjunction with the orthogonality relations represented by equation 4.24.

Using the piece-wise description of $w(s,t)$ from the equation 4.25, and the Galerkin-weighted residual method, the equation of motion is written as

$$
\begin{aligned}
&-\rho_{eq}\sum_{i=1}^{M}\phi_i\ddot{q}_i - c_1\sum_{i=1}^{M}\phi_i\dot{q}_i - YI_{eq}\left(\sum_{i=1}^{M}\phi_i''''q_i + \sum_{i,j,k=1}^{M}q_iq_jq_k[\phi_i'(\phi_j'\phi_k'')']'\right)\\
&-\frac{\rho_{eq}}{2}\sum_{i,j,k=1}^{M}\left[\phi_i'q_i\int_{l_1}^{s}\int_0^{\theta}\phi_j'\phi_k'\frac{\partial^2}{\partial t^2}(q_jq_k)\,dy\,d\theta\right]' + \sum_{i,j,k=1}^{M}\frac{m\phi_i''q_i}{2}\frac{\partial^2}{\partial t^2}(q_jq_k)\left[\int_0^{l_1}\phi_j'\phi_k'\,ds + \int_{l_1}^{l}\psi_j'\psi_k'\,ds\right]\\
&\qquad + e_{31}II_p\left[\sum_{i,j=1}^{M}q_iq_j\phi_i'\phi_j'\frac{VHf''}{2h_p} + \sum_{i,j=1}^{M}q_iq_j\phi_i''\phi_j'\frac{VHf'}{h_p} + \frac{VHf''}{h_p}\right]\\
&+\alpha_2\Lambda_2\left[\sum_{i,j=1}^{M}q_iq_j\phi_i''\phi_j''\frac{VHf''}{2h_p} + \sum_{i,j=1}^{M}q_iq_j\phi_i''\phi_j'''\frac{2VHf'}{h_p} + \sum_{i,j=1}^{M}q_iq_j\phi_i'''\phi_j'''\frac{VHf}{h_p} + \sum_{i,j=1}^{M}q_iq_j\phi_i''''\phi_j''\frac{VHf}{h_p}\right]\\
&+\alpha_1\Lambda_2\sum_{i,j=1}^{M}q_iq_j\left[\phi_i'''\phi_j''' + \phi_i''\phi_j''''\right] - \alpha_3I_p\left[\sum_{i=1}^{M}\phi_i''q_i\frac{VHf''}{h_p} + \sum_{i=1}^{M}q_i\phi_i'''\frac{2VHf'}{h_p} + \sum_{i=1}^{M}q_i\phi_i''''\frac{VHf}{h_p}\right]\\
&\quad + \alpha_4\Lambda_3\sum_{i,j,k=1}^{M}q_iq_jq_k\left[-3\phi_i''\phi_j'''\phi_k''' - \frac{3}{2}\phi_i''\phi_j''\phi_k''''\right] + \sum_{i,j,k=1}^{M}\frac{\rho_s}{2}\phi_i''q_i\int_{l_1}^{l}\int_0^{\theta}\psi_j'\psi_k'\frac{\partial^2}{\partial t^2}(q_jq_k)\,dy\,d\theta\\
&\qquad\qquad - \rho_{eq}\ddot{u}_b = 0 \quad (4.26)
\end{aligned}
$$

$$
\begin{aligned}
&-\rho_s\sum_{i=1}^{M}\psi_i\ddot{q}_i - c_1\sum_{i=1}^{M}\psi_i\dot{q}_i - Y_{11}^sI_s\left(\sum_{i=1}^{M}\psi_i''''q_i + \sum_{i,j,k,l=1}^{M}q_iq_jq_k[\psi_i'(\psi_j'\psi_k'')']'\right)\\
&-\frac{\rho_s}{2}\sum_{i,j,k,l=1}^{M}\left[\psi_i'q_i\int_{l}^{s}\int_0^{\theta}\psi_j'\psi_k'\frac{\partial^2}{\partial t^2}(q_jq_k)\,dy\,d\theta\right]' + \sum_{i,j,k=1}^{M}\frac{m}{2}\psi_i''q_i\int_{1_1}^{l}\psi_j'\psi_k'\frac{\partial^2}{\partial t^2}(q_jq_k)\,ds - \rho_s\ddot{u}_b = 0
\end{aligned}
\quad (4.27)
$$

and the corresponding electrical equation is written as

$$
\begin{aligned}
&e_{31}\Lambda_1\left[\sum_{i=1}^{M}q_i\int_0^{l_1}\phi_i''\frac{1}{h_p}\,ds + \sum_{i,j,k=1}^{M}q_iq_jq_k\int_0^{l_1}\phi_i'\phi_j'\phi_k''\frac{1}{2h_p}\,ds\right] + \alpha_2\Lambda_2\sum_{i,j,k=1}^{M}q_iq_jq_k\int_0^{l_1}\phi_i''\phi_j''\phi_k''\frac{1}{6h_p}\,ds\\
&\qquad + \int_0^{l_1}\frac{\varepsilon_{33}Vb}{h_p}\,ds - \alpha_3I_p\sum_{i,j=1}^{M}q_iq_j\int_0^{l_1}\phi_i''\phi_j''\frac{1}{2h_p}\,ds = Q(t) \quad (4.28)
\end{aligned}
$$

By considering only one mode($M = 1$) and using the orthogonal properties of the linear modes, the individual terms in equation 4.26 and 4.27 are simplified as shown below:

$$YI_{eq}q_1\int_0^{l_1}\phi_1\phi_1''''\,dx \;=\; YI_{eq}q_1\int_0^{l_1}\phi_1''\phi_1''\,ds + YI_{eq}q_1\phi_1'''(l_1)\phi_1(l_1) - YI_{eq}q_1\phi_1''(l_1)\phi_1'(l_1) \quad (4.29)$$

$$YI_{eq}q_1^3\int_0^{l_1}\phi_1(\phi_1'(\phi_1'\phi_1'')')'\,ds \;=\; (YI_{eq}q_1^3\phi_1\phi_1'^2\phi_1''' + YI_{eq}q_1^3\phi_1\phi_1'\phi_1''^2)|_{s=l_1} - (YI_{eq}q_1^3\phi_1'^3\phi_1'')|_{s=l_1} + 2YI_{eq}q_1^3\int_0^{l_1}\phi_1'^2\phi_1''^2\,ds \quad (4.30)$$

$$\rho_{eq}q_1(\dot{q}_1^2+q_1\ddot{q}_1)\int_0^{l_1}\phi_1\left(\phi_1'\int_{l_1}^{s}\int_0^{\theta}\phi_1'^2\,dy\,d\theta\right)'\,ds = -\rho_{eq}q_1(\dot{q}_1^2+q_1\ddot{q}_1)\int_0^{l_1}\phi_1'^2\left(\int_{l_1}^{s}\int_0^{\theta}\phi_1'^2\,dy\,d\theta\right)ds \quad (4.31)$$

$$\begin{aligned} -mq_1(q_1\ddot{q}_1+\dot{q}_1^2)\int_0^{l_1}\phi_1\phi_1''\left(\int_0^{l_1}\phi_1'^2\,dy+\int_{l_1}^{l}\psi_1'^2\,dy\right)ds \;=\; & \\ mq_1(q_1\ddot{q}_1+\dot{q}_1^2)\left[-(\phi_1'\phi_1)|_{s=l_1}\int_{l_1}^{l}\psi_1'^2\,ds+\int_0^{l_1}\phi_1'^2\,ds\int_{l_1}^{l}\psi_1'^2\,ds\right] & \\ +mq_1(q_1\ddot{q}_1+\dot{q}_1^2)\left[-\left(\phi_1'\phi_1\int_0^{l_1}\phi_1'^2\,ds\right)\Big|_{s=l_1}+\left(\int_0^{l_1}\phi_1'^2\,ds\right)^2\right] & \quad (4.32) \end{aligned}$$

$$\begin{aligned} -e_{31}II_pq_1^2\frac{V}{2h_p}\int_0^{l_1}\phi_1\phi_1'^2Hf''\,ds = & -e_{31}\Lambda_1q_1^2\frac{V}{2h_p}\phi_1'^2\phi_1Hf'\,|_{s=l_1}+e_{31}\Lambda_1q_1^2\frac{V}{h_p}\int_0^{l_1}\phi_1\phi_1'\phi_1''Hf'\,ds \\ & +e_{31}\Lambda_1q_1^2\frac{V}{2h_p}\int_0^{l_1}\phi_1'^3Hf'\,ds \\ = & -e_{31}\Lambda_1q_1^2\frac{V}{2h_p}\phi_1'^2\phi_1Hf'\,|_{s=l_1}+e_{31}\Lambda_1q_1^2\frac{V}{h_p}\int_0^{l_1}\phi_1\phi_1'\phi_1''Hf'\,ds \\ & +e_{31}\Lambda_1q_1^2\frac{V}{2h_p}\phi_1'^3Hf\,|_{s=l_1}-e_{31}\Lambda_1q_1^2\frac{3V}{2h_p}\int_0^{l_1}\phi_1'^2\phi_1''Hf\,ds \quad (4.33) \end{aligned}$$

$$-e_{31}\Lambda_1\frac{V}{h_p}\int_0^{l_1}\phi_1Hf''\,ds = -\,e_{31}\Lambda_1\frac{V}{h_p}\phi_1Hf'\Big|_{s=l_1}+e_{31}\Lambda_1\frac{V}{h_p}\phi_1'Hf.\Big|_{s=l_1}-e_{31}\Lambda_1\frac{V}{h_p}\int_0^{l_1}\phi_1''Hf\,ds \quad (4.34)$$

$$-\alpha_2\Lambda_2 q_1^2\frac{V}{2h_p}\int_0^{l_1}\phi_1\phi_1''^2 Hf''\,ds = -\alpha_2\Lambda_2 q_1^2\frac{V}{2h_p}\phi_1\phi_1''^2 Hf'|_{s=l_1} + \alpha_2\Lambda_2 q_1^2\frac{V}{h_p}\int_0^{l_1}\phi_1\phi_1''\phi_1''' Hf'\,ds + \alpha_2\Lambda_2 q_1^2\frac{V}{2h_p}\phi_1'\phi_1''^2 Hf\Big|_{s=l_1} - \alpha_2\Lambda_2 q_1^2\frac{V}{2h_p}\int_0^{l_1}\left(\phi_1'''^3 + 2\phi_1'\phi_1''\phi_1'''\right)Hf\,ds \quad (4.35)$$

$$-\alpha_2\Lambda_2 q_1^2\frac{V}{h_p}\int_0^{l_1}\phi_1\phi_1''\phi_1''' Hf'\,ds = -\alpha_2\Lambda_2 q_1^2\frac{V}{h_p}\phi_1\phi_1''\phi_1''' Hf\Big|_{s=l_1} + \alpha_2\Lambda_2 q_1^2\frac{V}{h_p}\int_0^{l_1}\left(\phi_1'\phi_1''\phi_1''' + \phi_1\phi_1'''^2 + \phi_1\phi_1''\phi_1''''\right)Hf\,ds \quad (4.36)$$

$$-\alpha_1\Lambda_2 q_1^2\int_0^{l_1}\phi_1\phi_1''\phi_1''''\,ds = -\alpha_1\Lambda_2 q_1^2\phi_1\phi_1''\phi_1'''\big|_{s=l_1} + \alpha_1\Lambda_2 q_1^2\int_0^{l_1}\phi_1\phi_1'''^2\,ds + \alpha_1\Lambda_2 q_1^2\phi_1'\phi_1''\phi_1''\big|_{s=l_1} - \alpha_1\Lambda_2 q_1^2\int_0^{l_1}\left(\phi_1''^2 + \phi_1'\phi_1'''\right)\phi_1''\,ds$$

$$since, -\alpha_1\Lambda_2 q_1^2\int_0^{l_1}\phi_1'\phi_1''\phi_1'''\,ds = -\frac{1}{2}\alpha_1\Lambda_2 q_1^2\phi_1'\phi_1''^2|_{s=l_1} + \frac{1}{2}\alpha_1\Lambda_2 q_1^2\int_0^{l_1}\phi_1''^3\,ds$$

$$-\alpha_1\Lambda_2 q_1^2\int_0^{l_1}\phi_1\phi_1''\phi_1''''\,ds = -\alpha_1\Lambda_2 q_1^2\phi_1\phi_1''\phi_1'''\big|_{s=l_1} + \alpha_1\Lambda_2 q_1^2\int_0^{l_1}\phi_1\phi_1'''^2\,ds + \alpha_1\Lambda_2 q_1^2\phi_1'\phi_1''\phi_1''\big|_{s=l_1} - \frac{1}{2}\alpha_1\Lambda_2 q_1^2\phi_1'\phi_1''^2|_{s=l_1} - \frac{1}{2}\alpha_1\Lambda_2 q_1^2\int_0^{l_1}\phi_1''^3\,ds \quad (4.37)$$

$$\alpha_3 I_p\frac{V}{h_p}q_1\int_0^{l_1}\phi_1\left(\phi_1''Hf'' + \phi_1''''Hf + 2Hf'\phi_1'''\right)ds = -\alpha_3 I_p\frac{V}{h_p}q_1 Hf\phi_1'\phi_1''\Big|_{s=l_1} + \alpha_3 I_p\frac{V}{h_p}q_1\left(Hf'\phi_1\phi_1'' + Hf\phi_1\phi_1'''\right)\Big|_{s=l_1} + \alpha_3 I_p\frac{V}{h_p}q_1\int_0^{l_1}Hf\phi_1''^2\,ds \quad (4.38)$$

$$\alpha_4\Lambda_3 q_1^3\int_0^{l_1}\left(3\phi_1\phi_1''\phi_1'''^2 + \frac{3}{2}\phi_1\phi_1''^2\phi_1''''\right)ds = \frac{3}{2}\alpha_4\Lambda_3 q_1^3\phi_1\phi_1''^2\phi_1'''\Big|_{s=l_1} - \frac{1}{2}\alpha_4\Lambda_3 q_1^3\phi_1'\phi_1''^3\Big|_{s=l_1} + \frac{1}{2}\alpha_4\Lambda_3 q_1^3\int_0^{l_1}\phi_1''^4\,ds \quad (4.39)$$

$$-\rho_s(\dot{q}_1^2+q_1\ddot{q}_1)\int_0^{l_1}\phi_1\phi_1''q_1\left(\int_{l_1}^{l}\int_0^{\theta}\psi_1'^2\,dy\,d\theta\right)ds=-\rho_s(\dot{q}_1^2+q_1\ddot{q}_1)\phi_1(l_1)\phi_1'(l_1)\left(\int_{l_1}^{l}\int_0^{\theta}\psi_1'^2\,dy\,d\theta\right)$$
$$+\rho_s(\dot{q}_1^2+q_1\ddot{q}_1)\left[\int_0^{l_1}\phi_1{}'^2\,ds\right]\left(\int_{l_1}^{l}\int_0^{\theta}\psi_1'^2\,dy\,d\theta\right) \quad (4.40)$$

$$Y_{11}^sI_sq_1\int_{l_1}^{l}\psi_1\psi_1''''\,ds \;=\; Y_{11}^sI_sq_1\int_{l_1}^{l}\psi_1''\psi_1''\,ds+Y_{11}^sI_sq_1\psi_1'''\psi_1|_{s=l_1}^{s=l}-Y_{11}^sI_sq_1\psi_1''\psi_1'|_{s=l_1}^{s=l} \quad (4.41)$$

$$Y_{11}^sI_sq_1^3\int_{l_1}^{l}\psi_1(\psi_1'(\psi_1'\psi_1'')')'\,ds \;=\; (Y_{11}^sI_sq_1^3\psi_1\psi_1'^2\psi_1'''+Y_{11}^sI_sq_1^3\psi_1\psi_1'\psi_1''^2)|_{s=l_1}^{s=l}$$
$$-(Y_{11}^sI_sq_1^3\psi_1'^3\psi_1'')|_{s=l_1}^{s=l}+2Y_{11}^sI_sq_1^3\int_{l_1}^{l}\psi_1'^2\psi_1''^2\,ds \quad (4.42)$$

$$\rho_sq_1(\dot{q}_1^2+q_1\ddot{q}_1)\int_{l_1}^{l}\psi_1\left(\psi_1'\int_l^{s}\int_0^{\theta}\psi_1'^2\,dy\,d\theta\right)'ds=-\rho_sq_1(\dot{q}_1^2+q_1\ddot{q}_1)\int_{l_1}^{l}\psi_1'^2\left(\int_l^{s}\int_0^{\theta}\psi_1'^2\,dy\,d\theta\right)ds$$
$$+\rho_sq_1(\dot{q}_1^2+q_1\ddot{q}_1)\psi_1(l_1)\psi_1'(l_1)\left(\int_{l_1}^{l}\int_0^{\theta}\psi_1'^2\,dy\,d\theta\right) \quad (4.43)$$

$$-mq_1(q_1\ddot{q}_1+\dot{q}_1^2)\int_{l_1}^{l}\psi_1\psi_1''\left(\int_0^{l_1}\phi_1'^2\,dy+\int_{l_1}^{l}\psi_1'^2\,dy\right)ds\;=$$
$$mq_1(q_1\ddot{q}_1+\dot{q}_1^2)\left[-(\psi_1'\psi_1)|_{s=l_1}^{s=l}\int_0^{l_1}\phi_1'^2\,ds+\int_{l_1}^{l}\psi_1'^2\,ds\int_0^{l_1}\phi_1'^2\,ds\right]$$
$$+mq_1(q_1\ddot{q}_1+\dot{q}_1^2)\left[-\left(\psi_1'\psi_1\int_{l_1}^{l}\psi_1'^2\,ds\right)\Big|_{s=l_1}^{s=l}+\left(\int_{l_1}^{l}\psi_1'^2\,ds\right)^2\right] \quad (4.44)$$

From continuity, compatibility and the nonlinear boundary conditions along with normal-

ization conditions, we write the equation of motion of the first mode as

$$\begin{aligned}
&\ddot{q}_1 + c_1\dot{q}_1\left(\int_0^{l_1}\phi_1^2\,ds + \int_{l_1}^{l}\psi_1^2\,ds\right) + \omega_1^2 q_1 \\
&\qquad + 2q_1^3\left(YI_{eq}\int_0^{l_1}\phi_1'^2\phi_1''^2\,ds + Y_{11}^s I_s\int_{l_1}^{l}\psi_1'^2\psi_1''^2\,ds\right) \\
&\quad + mq_1(q_1\ddot{q}_1+\dot{q}_1^2)\left[\left(\int_0^{l_1}\phi_1'^2\,ds\right)^2 + 2\int_0^{l_1}\phi_1'^2\,ds\int_{l_1}^{l}\psi_1'^2\,ds + \left(\int_0^{l_1}\psi_1'^2\,ds\right)^2\right] \\
&\quad - e_{31}\Lambda_1 q_1^2\frac{3V}{2h_p}\int_0^{l_1}\phi_1'^2\phi_1''\,ds - e_{31}\Lambda_1\frac{V}{h_p}\int_0^{l_1}\phi_1''\,ds - \alpha_2\Lambda_2 q_1^2\frac{V}{2h_p}\int_0^{l_1}\phi_1'''^3\,ds \\
&\quad - \frac{1}{2}\alpha_1\Lambda_2 q_1^2\int_0^{l_1}\phi_1''^3\,ds + \alpha_3 I_p\frac{V}{h_p}q_1\int_0^{l_1}\phi_1''^2\,ds + \frac{1}{2}\alpha_4\Lambda_3 q_1^3\int_0^{l_1}\phi_1''^4\,ds \\
&+\rho_s(\dot{q}_1^2+q_1\ddot{q}_1)\left[\int_0^{l_1}{\phi_1}'^2\,ds\right]\left(\int_{l_1}^{l}\int_0^{\theta}\psi_1'^2\,dy\,d\theta\right) - \rho_{eq}q_1(\dot{q}_1^2+q_1\ddot{q}_1)\int_0^{l_1}\phi_1'^2\left(\int_{l_1}^{s}\int_0^{\theta}\phi_1'^2\,dy\,d\theta\right)ds \\
&-\rho_s q_1(\dot{q}_1^2+q_1\ddot{q}_1)\int_{l_1}^{l}\psi_1'^2\left(\int_{l}^{s}\int_0^{\theta}\psi_1'^2\,dy\,d\theta\right)ds = -\ddot{u}_b\left[m\psi_1(l) + \rho_{eq}\int_0^{l_1}\phi_1\,ds + \rho_s\int_{l_1}^{l}\psi_1\,ds\right]
\end{aligned} \tag{4.45}$$

and the corresponding electrical equation as

$$\begin{aligned}
&e_{31}\Lambda_1\left[\frac{q_1}{h_p}\int_0^{l_1}\phi_1''\,ds + \frac{q_1^3}{2h_p}\int_0^{l_1}{\phi_1'}^2\phi_1''\,ds\right] + \alpha_2\Lambda_2\frac{q_1^3}{6h_p}\int_0^{l_1}\phi_1'''^3\,ds \\
&\qquad + \int_0^{l_1}\frac{\varepsilon_{33}Vb}{h_p}\,ds - \alpha_3 I_p\frac{q_1^2}{2h_p}\int_0^{l_1}\phi_1''^2\,ds = Q(t)
\end{aligned} \tag{4.46}$$

Using the electrical damping arising from dissipation from the load resistance [88], $\dot{Q} = -\frac{V}{R}$, we modify the above equation to write

$$\begin{aligned}
&e_{31}\Lambda_1\left[\frac{\dot{q}_1}{h_p}\int_0^{l_1}\phi_1''\,ds + \frac{3q_1^2\dot{q}_1}{2h_p}\int_0^{l_1}{\phi_1'}^2\phi_1''\,ds\right] + \alpha_2\Lambda_2\frac{q_1^2\dot{q}_1}{2h_p}\int_0^{l_1}\phi_1'''^3\,ds \\
&\qquad + \int_0^{l_1}\frac{\varepsilon_{33}\dot{V}b}{h_p}\,ds - \alpha_3 I_p\frac{q_1\dot{q}_1}{h_p}\int_0^{l_1}\phi_1''^2\,ds + \frac{V}{R} = 0
\end{aligned} \tag{4.47}$$

4.2 Approximate solution - Method of Multiple Scales

To determine the nonlinear response to principal mode resonance and to study the stability characteristics of the system, we employ the method of multiple scales. To this end, we scale

the contributions of the different terms in the governing equations 4.45 and 4.46 appropriately and, by defining $u_b = f\cos(\Omega t + \tau_e)$, we re-write them as

$$\ddot{q} + \omega^2 q + 2\epsilon^2\mu_1\dot{q} + \epsilon\hat{\theta}V + \epsilon\delta_1 q^2 + \epsilon^2\delta_2 qV + \epsilon^2\delta_3 q^3 + \epsilon^2\delta_4 q(\dot{q}^2 + q\ddot{q}) = \epsilon\eta f\cos(\Omega t + \tau_e) \quad (4.48)$$

$$-\hat{\theta}_v\dot{q} + C_p\dot{V} - \epsilon\delta_{2v}q\dot{q} + \epsilon\frac{V}{R} = 0 \quad (4.49)$$

where

$$\epsilon^2\mu_1 = \frac{1}{2}c_1\left(\int_0^{l_1}\phi_1^2\,ds + \int_{l_1}^{l}\psi_1^2\,ds\right) \equiv \zeta\omega, \qquad \epsilon\hat{\theta} \equiv \hat{\theta}_v = -e_{31}\Lambda_1\frac{1}{h_p}\int_0^{l_1}\phi_1''\,ds, \quad (4.50a)$$

$$C_p = \frac{\varepsilon_{33}bl_1}{h_p}, \qquad \epsilon\delta_1 = -\frac{1}{2}\alpha_1\Lambda_2\int_0^{l_1}\phi_1'^3\,ds, \qquad \epsilon^2\delta_2 \equiv \epsilon\delta_{2v} = \frac{1}{h_p}\alpha_3 I_p\int_0^{l_1}\phi_1''^2\,ds, \quad (4.50b)$$

$$\epsilon^2\delta_3 = 2YI_{eq}\int_0^{l_1}\phi_1'^2\phi_1''^2\,ds + 2Y_{11}^s I_s\int_{l_1}^{l}\psi_1'^2\psi_1''^2\,ds + \frac{1}{2}\alpha_4\Lambda_3\int_0^{l_1}\phi_1''^4\,ds, \quad (4.50c)$$

$$\begin{aligned}\epsilon^2\delta_4 = m\left[\left(\int_0^{l_1}\phi_1'^2\,ds\right)^2 + 2\int_0^{l_1}\phi_1'^2\,ds\int_{l_1}^{l}\psi_1'^2\,ds + \left(\int_0^{l_1}\psi_1'^2\,ds\right)^2\right] + \\ \rho_s\left[\int_0^{l_1}{\phi_1}'^2\,ds\right]\left(\int_{l_1}^{l}\int_0^{\theta}\psi_1'^2\,dy\,d\theta\right) - \rho_{eq}\int_0^{l_1}\phi_1'^2\left(\int_{l_1}^{s}\int_0^{\theta}\phi_1'^2\,dy\,d\theta\right)ds \\ - \rho_s\int_{l_1}^{l}\psi_1'^2\left(\int_{l}^{s}\int_0^{\theta}\psi_1'^2\,dy\,d\theta\right)ds, \end{aligned} \quad (4.50d)$$

$$\eta = \Omega^2\left[m\psi_1(l) + \rho_{eq}\int_0^{l_1}\phi_1\,ds + \rho_s\int_{l_1}^{l}\psi_1\,ds\right], \text{ and} \qquad \Omega = \omega + \epsilon\sigma. \quad (4.50e)$$

We note that the subscripts representing mode numbers were removed from the equations for the sake of convenience.

We note that the piezoelectric coupling is usually small and one can scale the q^2V terms to $O(\epsilon^3)$ in equation 4.48 and to $O(\epsilon^2)$ in equation 4.49. We realize that this effect is not significant and can often be in the range of electrical and mechanical noise during experiments, hence these terms are neglected in the analysis.

To solve the equations 4.48 and 4.49, we introduce three independent time scales T_0, T_1 and T_2 defined by

$$T_n = \epsilon^n t \qquad n = 0, 1, 2$$

and expand the derivatives up to $O(\epsilon^2)$ and write:

$$\frac{D}{Dt} = \frac{\partial}{\partial T_0} + \epsilon\frac{\partial}{\partial T_1} + \epsilon^2\frac{\partial}{\partial T_2} \equiv D_0 + \epsilon D_1 + \epsilon^2 D_2 \quad (4.51a)$$

and

$$\frac{D^2}{Dt^2} = \frac{\partial^2}{\partial T_0^2} + 2\epsilon\frac{\partial^2}{\partial T_1 \partial T_0} + \epsilon^2\left(2\frac{\partial^2}{\partial T_0 \partial T_2} + \frac{\partial^2}{\partial T_1^2}\right) \equiv D_0^2 + 2\epsilon D_0 D_1 + \epsilon^2\left(D_1^2 + 2D_0 D_2\right) \quad (4.51b)$$

The solutions of $q(t)$ and $V(t)$ are then expressed as

$$q(t,\epsilon) = q_0(T_0,T_1,T_2) + \epsilon q_1(T_0,T_1,T_2) + \epsilon^2 q_2(T_0,T_1,T_2) + ... \quad (4.52a)$$

$$V(t,\epsilon) = V_0(T_0,T_1,T_2) + \epsilon V_1(T_0,T_1,T_2) + \epsilon^2 V_2(T_0,T_1,T_2) + ... \quad (4.52b)$$

Substituting equations 4.51a, 4.51b and 4.52a into the equations 4.48 and 4.49, retaining terms up-to $O(\epsilon^2)$, we obtain

ϵ^0- *order equation:*

$$D_0^2 q_0 + q_0\omega^2 = 0, \quad (4.53a)$$

$$C_p D_0 V_0 - \hat{\theta}_v D_0 q_0 = 0, \quad (4.53b)$$

ϵ^1- *order equation:*

$$D_0^2 q_1 + \omega^2 q_1 = -2\left(D_0 D_1 q_0\right) - \delta_1 q_0^2 - \hat{\theta} V_0 + \frac{1}{2} f\eta e^{i\tau_e + iT_0\Omega} + \frac{1}{2} f\eta e^{-i\tau_e - iT_0\Omega}, \quad (4.54a)$$

$$RC_p D_0 V_1 + RC_p D_1 V_0 - \delta_{2v} R q_0 D_0 q_0 - R\hat{\theta}_v D_0 q_1 - R\hat{\theta}_v D_1 q_0 + V_0 = 0, \quad (4.54b)$$

ϵ^2- *order equation:*

$$D_0^2 q_2 + \omega^2 q_2 = -\delta_4 q_0^2 D_0^2 q_0 - \delta_4 q_0 \left(D_0 q_0\right)^2 - 2\mu_1 D_0 q_0 - 2D_0 D_1 q_1 - D_1^2 q_0 - 2D_0 D_2 q_0 - \delta_3 q_0^3 - 2\delta_1 q_1 q_0 - \delta_2 V_0 q_0 - \hat{\theta} V_1, \text{ and} \quad (4.55a)$$

$$RC_p D_0 V_2 + RC_p D_1 V_1 + RC_p D_2 V_0 - \delta_{2v} R q_0 D_0 q_1 - \delta_{2v} R q_0 D_1 q_0 - \delta_{2v} R V_1 D_0 q_0 - R\hat{\theta}_v D_0 q_2 - R\hat{\theta}_v D_1 q_1 - R\hat{\theta}_v D_2 q_0 + V_1 = 0. \quad (4.55b)$$

From ϵ^0- order equations, we obtain,

$$q_0(T_0,T_1,T_2) = A(T_1,T_2)e^{j\omega T_0} + c.c, \text{ and} \quad (4.56a)$$

$$V_0 = \frac{\hat{\theta}_v}{C_p} A\left(T_1,T_2\right) e^{jT_0\omega} + c.c. \quad (4.56b)$$

By substituting q_0 and V_0 in ϵ^1- order equation 4.54a and eliminating secular terms we obtain

$$D_1 A = \frac{j}{4\omega C_p}\left(2A_1\hat{\theta}\hat{\theta}_v - f\eta C_p e^{j\tau_e + i\sigma T_1}\right) \tag{4.57}$$

and solving for q_1 and V_1 yields

$$q_1 = -\frac{A\delta_1\bar{A}}{\omega^2} + \frac{A^2\delta_1 e^{2iT_0\omega}}{3\omega^2} + c.c, \text{ and} \tag{4.58a}$$

$$V_1 = \frac{1}{6R\omega^2 C_p^2}\left[3\delta_{2v}R\omega^2 C_p A_1^2 e^{2iT_0\omega} + 2\hat{\theta}_v\left(A_1^2\delta_1 RC_p e^{2iT_0\omega} + 3iA_1\omega e^{iT_0\omega}\right)\right] + c.c. \tag{4.58b}$$

Next, by using q_1 and V_1 in the ϵ^2- order equation, 4.55a, and eliminating the secular terms, we obtain the relation for $D_2 A$. Using the relations for $D_1 A$ and $D_2 A$, we obtain the amplitude and phase modulation equations as

$$\dot{A} = \epsilon D_1 A + \epsilon^2 D_2 A \tag{4.59}$$

writing the complex amplitude, A, in polar coordinates, $A(T_1, T_2) = \frac{1}{2}a(T_0, T_2)e^{j\beta(T_1,T_2)}$ and defining $\gamma = \epsilon\sigma t + \tau_e - \beta$ to remove the explicit dependence of time in amplitude and phase modulation equations, we obtain

$$\dot{a} = -\epsilon\frac{f\eta(\Omega - 3\omega)}{4\omega^2}\sin\gamma + \epsilon^2\left[\frac{1}{2}a\left(-\frac{\hat{\theta}\hat{\theta}_v}{R\omega^2 C_p^2} - 2\mu_1\right) - \frac{f\eta\hat{\theta}^2}{8\omega^3 C_p}\sin\gamma\right], \text{ and} \tag{4.60}$$

$$\begin{aligned}\dot{\gamma} = -\epsilon\left[-\sigma + \frac{\hat{\theta}\hat{\theta}_v}{2\omega C_p} + \frac{f\eta(\Omega - 3\omega)}{4a\omega^2}\cos\gamma\right] \\ + \epsilon^2\left[\frac{a^2\left(6\delta_4\omega^4 - 9\delta_3\omega^2 + 10\delta_1^2\right)}{24\omega^3} + \frac{\hat{\theta}^2\hat{\theta}_v^2}{8\omega^3 C_p^2} - \frac{f\eta\hat{\theta}\hat{\theta}_v}{8a\omega^3 C_p}\cos\gamma\right].\end{aligned} \tag{4.61}$$

To consider the steady state amplitude a_0, for a given excitation, we set $\dot{a} = 0$ and $\dot{\gamma} = 0$ and eliminate γ in equations 4.60 and 4.61 to obtain the following steady state amplitude response relation

$$\begin{aligned}&\frac{16a_0^2\omega^2\epsilon^2\left(2\mu_1 R\omega^2 C_p^2 + \hat{\theta}\hat{\theta}_v\right)^2}{f^2\eta^2 R^2 C_p^2\left(2\omega C_p(3\omega - \Omega) - \hat{\theta}\epsilon\hat{\theta}_v\right)^2} \\ &+ \frac{a_0^2\left(-C_p^2\left[a^2\epsilon\left(6\delta_4\omega^4 - 9\delta_3\omega^2 + 10\delta_1^2\right) + 24\sigma\omega^3\right] + 12\hat{\theta}\omega^2 C_p\hat{\theta}_v - 3\hat{\theta}^2\epsilon\hat{\theta}_v^2\right)^2}{9f^2\eta^2 C_p^2\left(2\omega C_p(3\omega - \Omega) - \hat{\theta}\epsilon\hat{\theta}_v\right)^2} = 1\end{aligned} \tag{4.62}$$

where the approximate solutions are written as

$$w(s,t) = \begin{cases} \phi_1(s)\left[a_0\cos\left(\Omega t+\tau_e-\gamma_0\right)+\epsilon\frac{a_0^2\delta_1}{6\omega^2}\cos\left(2\left[\Omega t+\tau_e-\gamma_0\right]\right)-\epsilon\frac{a_0^2\delta_1}{2\omega^2}+...\right] & 0\le s\le l_1 \\ \psi_1(s)\left[a_0\cos\left(\Omega t+\tau_e-\gamma_0\right)+\epsilon\frac{a_0^2\delta_1}{6\omega^2}\cos\left(2\left[\Omega t+\tau_e-\gamma_0\right]\right)-\epsilon\frac{a_0^2\delta_1}{2\omega^2}+...\right] & l_1< s\le l \end{cases} \tag{4.63a}$$

$$V(t) = \frac{a_0\hat{\theta}_v}{C_p}\cos\left(\Omega t+\tau_e-\gamma_0\right)-\epsilon\frac{a_0\hat{\theta}_v}{R\omega C_p^2}\sin\left(\Omega t+\tau_e-\gamma_0\right)+\epsilon\frac{a_0^2\delta_1\hat{\theta}_v}{6\omega^2C_p}\cos\left(2\left[\Omega t+\tau_e-\gamma_0\right]\right) + \epsilon\frac{a_0^2\delta_{2v}}{4C_p}\cos\left(2\left[\Omega t+\tau_e-\gamma_0\right]\right)+... \tag{4.63b}$$

or can alternatively be represented in frequency domain as

$$w(s,\nu) = \begin{cases} \phi_1(s)\left[a_0\delta(\nu-\Omega)+\epsilon\frac{a_0^2\delta_1}{2\omega^2}\delta(\nu-0)+\epsilon\frac{a_0^2\delta_1}{6\omega^2}\delta(\nu-2\Omega)+...\right] & 0\le s\le l_1 \\ \psi_1(s)\left[a_0\delta(\nu-\Omega)+\epsilon\frac{a_0^2\delta_1}{2\omega^2}\delta(\nu-0)+\epsilon\frac{a_0^2\delta_1}{6\omega^2}\delta(\nu-2\Omega)+...\right] & l_1< s\le l \end{cases} \tag{4.64a}$$

$$V(\nu) = \frac{a_0\hat{\theta}_v}{C_p}\sqrt{1+\frac{\epsilon^2}{R^2\omega^2C_p^2}}\delta(\nu-\Omega)+\epsilon\frac{a_0^2}{2C_p}\sqrt{\frac{\delta_1^2\hat{\theta}_v^2}{9\omega^4}+\frac{\delta_{2v}^2}{4C_p^2}}\delta(\nu-2\Omega)+... \tag{4.64b}$$

where δ is the dirac delta function.

4.3 Parameter identification

In this section, we propose a systematic methodology to estimate material nonlinear parameters in the considered enthalpy density representation, i.e., α_1, α_2 and α_3. We assume that the linear parameters in governing equation including the damping ratio, natural frequency, capacitance and coupling coefficients can be estimated from free vibration tests, impedance measurements or frequency response functions under linear excitation. To this end, we point out that from the steady state amplitude response relation and the approximate solutions of equations 4.62, 4.63 and 4.64, contain δ_1, δ_2 and δ_3. Furthermore, these coefficients in the governing equations relate to the quantities of interest as shown in equations 4.50b and 4.50c. We wish to exploit the resonant response of the cantilever beam with tip mass system to identify δ_1, δ_2 and δ_3 and estimate the material nonlinear piezoelectric coefficients as described in the following paragraphs.

From the approximate solution of the transverse displacement $w(s,t)$, presented in equations 4.63a and 4.64a, it is interesting to note that the quadratic non linearity gives rise to a non-zero mean in the solution which corresponds to zero frequency in the frequency domain.

That is, in an experiment one can estimate a_0 from the component of the displacement at forcing frequency and then estimate δ_1 from the D.C component. The parameter α_1 can then be calculated from the estimated δ_1 value using the equation 4.50b. Once a_0 and δ_1 are estimated with a reasonable confidence, we analyze the voltage generated to gather more knowledge about the system. In particular, inspecting the approximate solution of voltage V, presented in the equations 4.63b and 4.64b, if $\delta_{2v}(\equiv \delta_2)$ is significant, it can be extracted from the component of voltage corresponding to twice the excitation frequency in the frequency domain. The parameter α_3 can then be calculated from the estimated δ_{2v} using equation 4.50b.

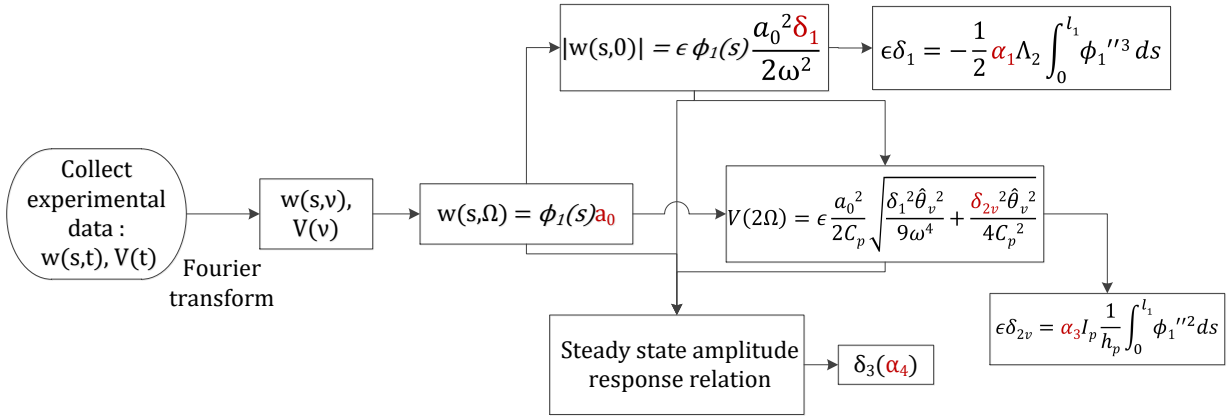

Figure 4.2: Flowchart presenting the systematic approach of analyzing data for parameter identification.

The parameter δ_3 corresponds to cubic nonlinearity and is a function of geometric nonlinearity due to curvature and material nonlinear parameter α_4. Although, δ_3 explicitly doesn't appear itself in the approximate solution of the response, it implicitly affects the amplitude of response, which can be understood by inspecting amplitude and phase modulation equations. In other words, for a given excitation conditions, one can solve for δ_3 from steady state amplitude response relation given by equation 4.62 by using estimates of the parameters of a_0, δ_1 and δ_2 obtained with the procedure defined above. The strategy and important relations discussed in this section towards parameter identification are summarized in figure 4.2.

4.4 Validation of parameter identification procedure

In this section, we consider a steel beam (substrate) and tip mass system with a piezoelectric layer and implement the parameter identification strategy mentioned in section 4.3. The geometric and material properties of the harvester are presented in table 4.1. Assumed

Table 4.1: Material and geometric properties of the energy harvester.

Parameter [units]	**Value**
Mass per unit length of substrate, ρ_s [g/m]	40.13
Mass per unit length of piezo, ρ_p [g/m]	20.28
Young's modulus of substrate, Y_{11}^s) [GPa]	210
Young's modulus of piezo, Y_{11}^p [GPa]	66
Length of substrate, l [mm]	60
Length of piezo, $l_1 = \frac{9l}{10}$ [mm]	54
Thickness of substrate, h_s [mm]	0.5
Thickness of piezo, h_p [mm]	0.26
width, b [mm]	10
Tip mass, m [gm]	10
Piezoelectric coupling coefficient, e_{31} [C/m^2]	-12.54
Piezoelectric permittivity, ε_{33} [F/m]	1.328×10^{-8}
Damping ratio, ζ	0.08
Load resistance, R [M Ohm]	10

values of the nonlinear constitutive parameters are presented in table 4.2. These parameters will be used in performing numerical simulations for the purpose of validating the proposed approach for parameter identification.

Table 4.2: Assumed nonlinear piezoelectric coefficients

Parameter [units]	**Value**
α_1 [Pa]	1×10^{14}
α_3 [C/m^2]	-5×10^3
α_4 [Pa]	-5×10^{16}

For the geometric and material property parameters presented in tables 4.1 and 4.2, the coefficients in the governing equation of the first mode and the electrical circuit responses are listed in table 4.3. The corresponding mass normalized linear mode shapes are determined as

$$\phi_1(s) = 14.56\,[\cos(16.71s) - \cosh(16.71s)] + 15\,[\sinh(16.71s) - \sin(16.71s)] \;\; \forall \;\; 0 \leq s \leq l_1 \tag{4.65a}$$

$$\psi_1(s) = 22.7\cos(17.98s) - 27.26\cosh(17.98s) - 17.63\sin(17.98s) + 30.69\sinh(17.98s) : \forall\ l_1 < s \leq l \quad (4.65b)$$

Table 4.3: Coefficients in the governing equations corresponding to the parameters presented in tables 4.1 and 4.2.

Parameter [units]	**Value**
ω [rad]	238.68
$\epsilon^2\mu_1$ [s^{-1}]	1.91
$\epsilon\hat{\theta} \equiv \hat{\theta}_v$ [$CKg^{-\frac{1}{2}}\ m^{-1}$]	-9.71×10^{-3}
$\epsilon\delta_1$ [$Kg^{-1/2}m^{-1}s^{-2}$]	41.15×10^6
$\epsilon^2\delta_2 \equiv \epsilon\delta_{2v}$ [$CKg^{-1}\ m^{-2}$]	-7.23
$\epsilon^2\delta_3$ [$Kg^{-1}\ m^{-2}s^{-2}$]	-4.83×10^{10}
$\epsilon^2\delta_4$ [$Kg^{-1}\ m^{-2}$]	8.37×10^5
$\epsilon\eta$ [$Kg^{-1/2}s^{-2}$]	$-0.11\Omega^2$
C_p [nF]	27.58

First, we examine the response and investigate the significance of material and geometric nonlinearities. In particular, by inspecting figures 4.3(b) and 4.3(d), we note the spectral content in the response at twice and thrice the forcing frequency. The response at twice the forcing frequency is related to the quadratic nonlinearity and that at thrice the forcing frequency is related to the cubic terms. Although not explicit in the response, as discussed earlier, the cubic nonlinearity affects the response at forcing frequency by causing internal resonances which can be noted by inspecting the equation 4.62.

Following the parameter identification strategy described in section 4.3, we first identify the component of the displacement at forcing frequency as $w(s,\Omega)|_{s=5\text{ cm}} \approx 1.097$ mm, which is used to calculate $a_0^* = 1.51 \times 10^{-4}$ $Kg^{1/2}m$. From figure 4.3(b), $w(s,0)|_{s=5cm} \approx 6.58 \times 10^{-2}$ mm, which yields

$$w(s,0) = \phi_1(s)\frac{a_0^{*2}\epsilon\delta_1^*}{2\omega^2} \implies \epsilon\delta_1^* = 45.33 \times 10^7\ Kg^{-1/2}m^{-1}s^{-2} \quad (4.66)$$

We then use equation 4.50b to evaluate $\alpha_1^* \approx 1.1 \times 10^{14}$ Pa.

Next, we estimate $\epsilon^2\delta_2(\equiv \epsilon\delta_{2v}^*)$ from the voltage generated in the frequency domain presented in the figure 4.3(d), by noting that the parameters C_p, ω and θ_v are known and that $V(2\Omega) = 2.53$ V and by using equation 4.64b

$$V(2\Omega) = \frac{a_0^{*2}}{2C_p}\sqrt{\frac{\left(\epsilon\delta_1^*\right)^2\hat{\theta}_v^2}{9\omega^4} + \frac{\left(\epsilon\delta_{2v}\right)^2}{4C_p^2}} \quad (4.67)$$

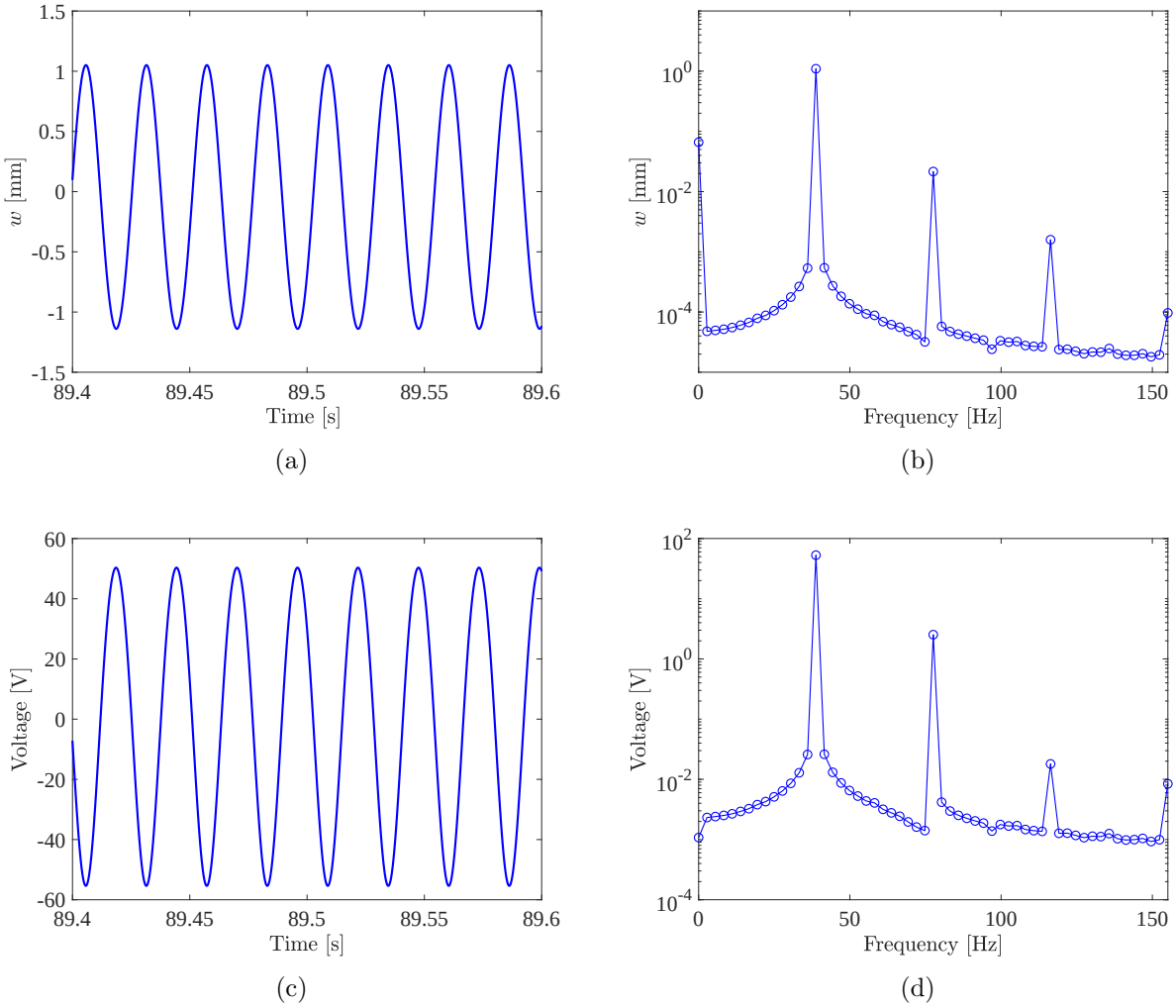

Figure 4.3: Principal mode resonant response represented by the displacement at 5 cm away from the fixed end and the corresponding harvested voltage for a detuning value $\epsilon\sigma = 5$ rad/s and excitation amplitude of $f\Omega^2 = 2$ m/s^2 in time domain (a and c) and frequency domain (b and d).

and the values of a_0^* and $\epsilon\delta_1^*$ and $V(2\Omega)$, we determine $\epsilon\delta_{2v}^* \approx -7.54$ CKg^{-1} m^{-2}. Using equation 4.50c, we evaluate $\alpha_3^* \approx -5.22 \times 10^3$ C/m^2.

As discussed in section 4.3, equation 4.62 has to be used to estimate α_4 which requires the value of $\epsilon^2\delta_4$. We point that for a given problem, we can numerically evaluate $\epsilon^2\delta_4$ using the equation 4.50d. Using all the necessary parameters and by numerically solving for $\epsilon^2\delta_3$, we obtain two solutions as $\epsilon^2\delta_3^* \approx -4.49 \times 10^{10}$ Kg^{-1} m^{-2}s^{-2} and $\epsilon^2\delta_3^* \approx 7.39 \times 10^{10}$ Kg^{-1} m^{-2}s^{-2} respectively corresponding to a softening and hardening response. One solution can

be eliminated by performing a frequency sweep for various values of detuning $\epsilon\sigma$. In this analysis, we assume a softening response and hence choose the solution for cubic nonlinear parameter as $\epsilon^2\delta_3^* \approx -4.49 \times 10^{10}$ Kg^{-1} $\mathrm{m}^{-2}\mathrm{s}^{-2}$. Subsequently, using equation 4.50c, we determine $\alpha_4 \approx -4.85 \times 10^{16}$ Pa.

Table 4.4: Summary of the results and efficiency of the parameter identification scheme proposed.

Parameter [units]	**Value**	**Parameter [units]**	**Value**	**% error**
α_1 [Pa]	1×10^{14}	α_1^* [Pa]	1.1×10^{14}	10
α_3 [C/m^2]	-5×10^3	α_3^* [C/m^2]	-5.22×10^3	4.4
α_4 [Pa]	-5×10^{16}	α_4^* [Pa]	-4.85×10^{16}	3

Table 4.4 compares the identified values of nonlinear piezoelectric coefficients with values used in the numerical simulations. It is noted that, the nonlinear constitutive relation parameters are estimated with a maximum error of 10%. We shall note here that using different values of the detuning parameters can reduce the percentage errors or yield a trend in the identification procedure that can be effectively exploited for more accurate prediction.

The MATHEMATICA file *firstmodeeqs9lby10*, and the MATLAB file *final.m*, used for generating the results can be found in Appendices A and B.

4.5 Conclusions

In this paper, we considered a beam with tip mass and a piezoelectric layer subjected to direct excitation as an unsymmetrical energy harvester to identify nonlinear piezoelectric coefficients. We derived the governing equations considering the electric enthalpy density derived by Wagner and Hagedorn [34] followed by a Galerkin weighted residual method. We note that the cubic nonlinearity is a combined affect of material and geometric nonlinearity and that the geometric nonlinearity can be determined from the equations 4.50c and 4.50d. Next, we used the method of multiple scales and determined the steady state amplitude response relation and approximate solutions for displacement and voltage generated. We then used the response characteristics in the frequency domain and approximate solutions obtained with the method of multiple scales to implement a systematic procedure to identify the nonlinear piezoelectric coefficients in section 4.3 and summarized it in the figure 4.2. Next, we chose a numerical example, with properties of the beam with tip mass energy harvester as mentioned in the tables 4.1-4.2 and performed numerical simulations to illustrate the nonlinear response of the system. We showed that the proposed identification scheme estimates the nonlinear parameters with a maximum error of 10%.

Chapter 5

Conclusions and future work

In this work, we first presented theoretical modeling of a cantilever beam with tip mass system subjected to parametric excitation. We showed that, though neglecting nonlinear boundary conditions can simplify the math in determining the governing equations, the representation of the response can be significantly altered. In particular, we demonstrated that for the problem under consideration, the nature of the Hopf bifurcation is exactly opposite and that the amplitude of the response is considerably different.

We then performed a sensitivity analysis of a cantilever beam with tip mass system subjected to parametric excitation for small variations in the values of the elasticity and tip mass. For the problem considered, we illustrated that a decrease in elasticity and very small increase in tip mass can alter the response of a system that is designed to yield a supercritical bifurcation to result in a sub-critical bifurcation. This observation can potentially be applied for using parametrically excited micro-cantilever beams as sensing devices. We also noted that the sensitivity to small variations in the tip mass can be increased by decreasing σ.

Finally, we considered the cantilever beam with tip mass and a piezoelectric layer subjected to direct excitation as an unsymmetrical energy harvester to identify nonlinear piezoelectric coefficients. We derived the governing equations considering the electric enthalpy density derived by Wagner and Hagedorn [34]. We then used the response characteristics in the frequency domain and approximate solutions obtained with the method of multiple scales to implement a systematic procedure to identify the nonlinear piezoelectric coefficients. By choosing a numerical example, we showed that the proposed identification scheme estimates the nonlinear parameters with a maximum error of 10%.

For future work, it is proposed that approaches and results presented here are to be validated further with experiments and higher-fidelity models such as finite elements.

Appendix A

MATHEMATICA files

Below are the hyperlinked MATHEMATICA files:

- *Genhamilton1.0*
- *mass vary*
- *mass vary 0p0096*
- *Genhamilton2.0*
- *firstmodeeqs9lby10*

These above listed files are tested in MATHEMATICA 11.2 and 11.3.

Appendix B

MATLAB files

Below are the hyperlinked MATLAB files:

final.m, which needs the following two functions:

- *ppx.m*
- *forced43peizoWHD9lby10.m*

Bibliography

[1] Francois E Cellier and Jurgen Greifeneder. *Continuous system modeling*. Springer Science & Business Media, 2013.

[2] Ali Hasan Nayfeh. *Nonlinear interactions: analytical, computational and experimental methods*. Wiley, 2000.

[3] Ali H Nayfeh and Balakumar Balachandran. *Applied nonlinear dynamics: analytical, computational and experimental methods*. John Wiley & Sons, 2008.

[4] Ali H Nayfeh and P Frank Pai. *Linear and nonlinear structural mechanics*. John Wiley & Sons, 2008.

[5] Lawrence N Virgin. *Introduction to experimental nonlinear dynamics: a case study in mechanical vibration*. Cambridge University Press, 2000.

[6] SK Dwivedy and RC Kar. Non-linear dynamics of a slender beam carrying a lumped mass under principal parametric resonance with three-mode interactions. *International journal of non-linear mechanics*, 36(6):927–945, 2001.

[7] SK Dwivedy and RC Kar. Simultaneous combination and 1: 3: 5 internal resonances in a parametrically excited beam–mass system. *International journal of non-linear mechanics*, 38(4):585–596, 2003.

[8] CWS To. *The response of mast antenna structures to transient disturbances*. PhD thesis, University of Southampton, 1979.

[9] CWS To. Vibration of a cantilever beam with a base excitation and tip mass. *Journal of Sound and Vibration*, 83(4):445–460, 1982.

[10] Kiun Kim and Thomas W Strganac. Nonlinear responses of a cantilever wing with an external store. In *44th AIAA Structures, Structural Dynamics, and Materials Conference, Norfolk, VA, AIAA Paper*, number 2003-1708, 2003.

[11] Philip S Beran, Thomas W Strganac, Kiun Kim, and Chetan Nichkawde. Studies of store-induced limit-cycle oscillations using a model with full system nonlinearities. *Nonlinear Dynamics*, 37(4):323–339, 2004.

[12] LK Abbas, Q Chen, P Marzocca, and A Milanese. Non-linear aeroelastic investigations of store (s)-induced limit cycle oscillations. *Proceedings of the Institution of Mechanical Engineers, Part G: Journal of Aerospace Engineering*, 222(1):63–80, 2008.

[13] AH Nayfeh, BK Hammad, and MR Hajj. Discretization effects on flutter aspects and control of wing/store configurations. *Journal of Vibration and Control*, 18(7):1043–1055, 2012.

[14] Ali H Nayfeh, Mehdi Ghommem, and Muhammad R Hajj. Normal form representation of the aeroelastic response of the goland wing. *Nonlinear Dynamics*, 67(3):1847–1861, 2012.

[15] Sungsoo Na and Liviu Librescu. Dynamic response of adaptive cantilevers carrying external stores and subjected to blast loading. *Journal of Sound and Vibration*, 231(4):1039–1055, 2000.

[16] Dongna Shen, Jyoti Ajitsaria, Song-Yul Choe, and Dong-Joo Kim. The optimal design and analysis of piezoelectric cantilever beams for power generation devices. *MRS Online Proceedings Library Archive*, 888, 2005.

[17] Alper Erturk and Daniel J Inman. *Piezoelectric energy harvesting*. John Wiley & Sons, 2011.

[18] Miso Kim, Mathias Hoegen, John Dugundji, and Brian L Wardle. Modeling and experimental verification of proof mass effects on vibration energy harvester performance. *Smart Materials and Structures*, 19(4):045023, 2010.

[19] Mohammed F Daqaq, Christopher Stabler, Yousef Qaroush, and Thiago Seuaciuc-Osório. Investigation of power harvesting via parametric excitations. *Journal of Intelligent Material Systems and Structures*, 20(5):545–557, 2009.

[20] A Abdelkefi, AH Nayfeh, and MR Hajj. Effects of nonlinear piezoelectric coupling on energy harvesters under direct excitation. *Nonlinear Dynamics*, 67(2):1221–1232, 2012.

[21] Abdessattar Abdelkefi, Zhimiao Yan, and Muhammad R Hajj. Modeling and nonlinear analysis of piezoelectric energy harvesting from transverse galloping. *Smart materials and Structures*, 22(2):025016, 2013.

[22] Michael I Friswell, S Faruque Ali, Onur Bilgen, Sondipon Adhikari, Arthur W Lees, and Grzegorz Litak. Non-linear piezoelectric vibration energy harvesting from a vertical cantilever beam with tip mass. *Journal of Intelligent Material Systems and Structures*, 23(13):1505–1521, 2012.

[23] Xinxin Li, Minhang Bao, Heng Yang, Shaoqun Shen, and Deren Lu. A micromachined piezoresistive angular rate sensor with a composite beam structure. *Sensors and Actuators A: Physical*, 72(3):217–223, 1999.

[24] Heng Yang, Minhang Bao, Hao Yin, and Shaoqun Shen. A novel bulk micromachined gyroscope based on a rectangular beam-mass structure. *Sensors and Actuators A: Physical*, 96(2):145–151, 2002.

[25] Rashid Bashir. Biomems: state-of-the-art in detection, opportunities and prospects. *Advanced drug delivery reviews*, 56(11):1565–1586, 2004.

[26] Sandeep Kumar Vashist. A review of microcantilevers for sensing applications. *J. of Nanotechnology*, 3:1–18, 2007.

[27] Blake N Johnson and Raj Mutharasan. Biosensing using dynamic-mode cantilever sensors: A review. *Biosensors and bioelectronics*, 32(1):1–18, 2012.

[28] Mai Duc Dai, Kilho Eom, and Chang-Wan Kim. Nanomechanical mass detection using nonlinear oscillations. *Applied Physics Letters*, 95(20):203104, 2009.

[29] N Kacem, J Arcamone, F Perez-Murano, and S Hentz. Dynamic range enhancement of nonlinear nanomechanical resonant cantilevers for highly sensitive nems gas/mass sensor applications. *Journal of Micromechanics and Microengineering*, 20(4):045023, 2010.

[30] Wenhua Zhang, Rajashree Baskaran, and Kimberly L Turner. Effect of cubic nonlinearity on auto-parametrically amplified resonant mems mass sensor. *Sensors and Actuators A: Physical*, 102(1):139–150, 2002.

[31] Wenhua Zhang and Kimberly L Turner. Application of parametric resonance amplification in a single-crystal silicon micro-oscillator based mass sensor. *Sensors and Actuators A: Physical*, 122(1):23–30, 2005.

[32] N Aurelle, D Guyomar, C Richard, P Gonnard, and L Eyraud. Nonlinear behavior of an ultrasonic transducer. *Ultrasonics*, 34(2-5):187–191, 1996.

[33] D Guyomar, N Aurelle, and L Eyraud. Piezoelectric ceramics nonlinear behavior. application to langevin transducer. *Journal de Physique III*, 7(6):1197–1208, 1997.

[34] U Von Wagner and P Hagedorn. Piezo–beam systems subjected to weak electric field: experiments and modelling of non-linearities. *Journal of Sound and Vibration*, 256(5):861–872, 2002.

[35] O Cuvalci and A Ertas. Pendulum as vibration absorber for flexible structures: experiments and theory. *Journal of vibration and acoustics*, 118(4):558–566, 1996.

[36] Zhimiao Yan and Muhammad R Hajj. Energy harvesting from an autoparametric vibration absorber. *Smart Materials and Structures*, 24(11):115012, 2015.

[37] Zhimiao Yan, Haithem E Taha, and Ting Tan. Nonlinear characteristics of an autoparametric vibration system. *Journal of Sound and Vibration*, 390:1–22, 2017.

[38] Iván Delgado-Velázquez. Nonlinear vibration of a cantilever beam. 2007.

[39] Perngjin F Pai and Ali H Nayfeh. Three-dimensional nonlinear vibrations of composite beamsii. flapwise excitations. *Nonlinear Dynamics*, 2(1):1–34, 1991.

[40] TJ Anderson, AH Nayfeh, and B Balachandran. Experimental verification of the importance of the nonlinear curvature in the response of a cantilever beam. *Journal of Vibration and Acoustics*, 118(1):21–27, 1996.

[41] Ali H Nayfeh and Walter Lacarbonara. On the discretization of distributed-parameter systems with quadratic and cubic nonlinearities. *Nonlinear Dynamics*, 13(3):203–220, 1997.

[42] Hiroshi Yabuno, Yoshiro Ide, and Nobuharu Aoshima. Nonlinear analysis of a parametrically excited cantilever beam: Effect of the tip mass on stationary response (special issue on nonlinear dynamics). *JSME International Journal Series C Mechanical Systems, Machine Elements and Manufacturing*, 41(3):555–562, 1998.

[43] Hiroshi Yabuno and Ali H Nayfeh. Nonlinear normal modes of a parametrically excited cantilever beam. In *Normal Modes and Localization in Nonlinear Systems*, pages 65–77. Springer, 2001.

[44] Lawrence D Zavodney. *A theoretical and experimental investigation of parametrically excited nonlinear mechanical systems*. PhD thesis, Virginia Polytechnic Institute and State University, 1987.

[45] Samir A Emam and Ali H Nayfeh. Nonlinear responses of buckled beams to subharmonic-resonance excitations. *Nonlinear Dynamics*, 35(2):105–122, 2004.

[46] Ali H Nayfeh. *Introduction to perturbation techniques*. John Wiley & Sons, 2011.

[47] Leonard Meirovitch. *Fundamentals of vibrations*. Waveland Press, 2010.

[48] C Chin and SA Nayfeh. Nonlinear normal modes of a cantilever beam. *Journal of vibration and acoustics*, 117:477, 1995.

[49] AH Nayfeh and SA Nayfeh. Nonlinear normal modes of a continuous system with quadratic nonlinearities. *TRANSACTIONS-AMERICAN SOCIETY OF MECHANICAL ENGINEERS JOURNAL OF VIBRATION AND ACOUSTICS*, 117:199–199, 1995.

[50] Ali H Nayfeh and Dean T Mook. *Nonlinear oscillations*. John Wiley & Sons, 2008.

[51] Mohammad Ibrahim Younis and AH Nayfeh. A study of the nonlinear response of a resonant microbeam to an electric actuation. *Nonlinear Dynamics*, 31(1):91–117, 2003.

[52] Ali H Nayfeh. Resolving controversies in the application of the method of multiple scales and the generalized method of averaging. *Nonlinear Dynamics*, 40(1):61–102, 2005.

[53] Nathan S Shenck and Joseph A Paradiso. Energy scavenging with shoe-mounted piezoelectrics. *IEEE micro*, 21(3):30–42, 2001.

[54] P Glynne-Jones, SP Beeby, EP James, and NM White. The modelling of a piezoelectric vibration powered generator for microsystems. In *Transducers 01 Eurosensors XV*, pages 46–49. Springer, 2001.

[55] Geffrey K Ottman, Heath F Hofmann, and George A Lesieutre. Optimized piezoelectric energy harvesting circuit using step-down converter in discontinuous conduction mode. *IEEE Transactions on power electronics*, 18(2):696–703, 2003.

[56] Shad Roundy and Paul K Wright. A piezoelectric vibration based generator for wireless electronics. *Smart Materials and structures*, 13(5):1131, 2004.

[57] Daniel J Inman and Benjamin L Grisso. Towards autonomous sensing. In *Smart Structures and Materials 2006: Sensors and Smart Structures Technologies for Civil, Mechanical, and Aerospace Systems*, volume 6174, page 61740T. International Society for Optics and Photonics, 2006.

[58] Nader Jalili. *Piezoelectric-based vibration control: from macro to micro/nano scale systems*. Springer Science & Business Media, 2009.

[59] Thomas Bailey and JE Ubbard. Distributed piezoelectric-polymer active vibration control of a cantilever beam. *Journal of Guidance, Control, and Dynamics*, 8(5):605–611, 1985.

[60] Nesbitt W Hagood and Andreas von Flotow. Damping of structural vibrations with piezoelectric materials and passive electrical networks. *Journal of Sound and Vibration*, 146(2):243–268, 1991.

[61] William W Clark. Vibration control with state-switched piezoelectric materials. *Journal of intelligent material systems and structures*, 11(4):263–271, 2000.

[62] Victor Giurgiutiu. Review of smart-materials actuation solutions for aeroelastic and vibration control. *Journal of Intelligent Material Systems and Structures*, 11(7):525–544, 2000.

[63] Liviu Librescu and Sungsoo Na. Active vibration control of doubly tapered thin-walled beams using piezoelectric actuation. *Thin-Walled Structures*, 39(1):65–82, 2001.

[64] SO Reza Moheimani. A survey of recent innovations in vibration damping and control using shunted piezoelectric transducers. *IEEE transactions on control systems technology*, 11(4):482–494, 2003.

[65] Alper Erturk, Jamil M Renno, and Daniel J Inman. Modeling of piezoelectric energy harvesting from an l-shaped beam-mass structure with an application to uavs. *Journal of intelligent material systems and structures*, 20(5):529–544, 2009.

[66] Samuel C Stanton, Clark C McGehee, and Brian P Mann. Nonlinear dynamics for broadband energy harvesting: Investigation of a bistable piezoelectric inertial generator. *Physica D: Nonlinear Phenomena*, 239(10):640–653, 2010.

[67] S Adhikari, MI Friswell, and DJ Inman. Piezoelectric energy harvesting from broadband random vibrations. *Smart Materials and Structures*, 18(11):115005, 2009.

[68] AF Arrieta, P Hagedorn, Alper Erturk, and DJ Inman. A piezoelectric bistable plate for nonlinear broadband energy harvesting. *Applied Physics Letters*, 97(10):104102, 2010.

[69] Masato Abe, Gyuhae Park, and Daniel J Inman. Impedance-based monitoring of stress in thin structural members. *UNIT 45002 APO AP 96337-5002*, page 285, 2001.

[70] Gyuhae Park, Hoon Sohn, Charles R Farrar, Daniel J Inman, et al. Overview of piezoelectric impedance-based health monitoring and path forward. *Shock and Vibration Digest*, 35(6):451–464, 2003.

[71] Mohsen Safaei and Steven R Anton. Sensing and energy harvesting performance, and fatigue life of embedded piezoelectric transducer in total knee arthroplasty. In *ASME 2016 Conference on Smart Materials, Adaptive Structures and Intelligent Systems*, pages V002T07A010–V002T07A010. American Society of Mechanical Engineers, 2016.

[72] Elias Hoummadi, Mohsen Safaei, and Steven R Anton. Design, analysis, and fabrication of a piezoelectric force plate. In *Health Monitoring of Structural and Biological Systems 2017*, volume 10170, page 101700W. International Society for Optics and Photonics, 2017.

[73] Teimour Maleki, Ning Cao, Seung Hyun Song, Chinghai Kao, Song-Chu Ko, and Babak Ziaie. An ultrasonically powered implantable micro-oxygen generator (imog). *IEEE transactions on Biomedical Engineering*, 58(11):3104–3111, 2011.

[74] Maurice GL Roes, Jorge L Duarte, Marcel AM Hendrix, and Elena A Lomonova. Acoustic energy transfer: A review. *IEEE Transactions on Industrial Electronics*, 60(1):242–248, 2013.

[75] S Shahab, M Gray, and A Erturk. Ultrasonic power transfer from a spherical acoustic wave source to a free-free piezoelectric receiver: Modeling and experiment. *Journal of Applied Physics*, 117(10):104903, 2015.

[76] Mohammed F Daqaq, Ravindra Masana, Alper Erturk, and D Dane Quinn. On the role of nonlinearities in vibratory energy harvesting: a critical review and discussion. *Applied Mechanics Reviews*, 66(4):040801, 2014.

[77] S Leadenham and A Erturk. M-shaped asymmetric nonlinear oscillator for broadband vibration energy harvesting: Harmonic balance analysis and experimental validation. *Journal of Sound and Vibration*, 333(23):6209–6223, 2014.

[78] RL Harne and KW Wang. A review of the recent research on vibration energy harvesting via bistable systems. *Smart materials and structures*, 22(2):023001, 2013.

[79] Stephen Leadenham and Alper Erturk. Unified nonlinear electroelastic dynamics of a bimorph piezoelectric cantilever for energy harvesting, sensing, and actuation. *Nonlinear Dynamics*, 79(3):1727–1743, 2015.

[80] Ali H Nayfeh. Parametric identification of nonlinear dynamic systems. In *Advances and Trends in Structures and Dynamics*, pages 487–493. Elsevier, 1985.

[81] Lawrence D Zavodney. Identification of nonlinearity in structural systems: Theory, simulation, and experiment. *Applied Mechanics Reviews*, 44(11S):S295–S303, 1991.

[82] MR Hajj, J Fung, AH Nayfeh, and SO'F Fahey. Damping identification using perturbation techniques and higher-order spectra. *Nonlinear Dynamics*, 23(2):189–203, 2000.

[83] Gaetan Kerschen, Keith Worden, Alexander F Vakakis, and Jean-Claude Golinval. Past, present and future of nonlinear system identification in structural dynamics. *Mechanical systems and signal processing*, 20(3):505–592, 2006.

[84] F Ayela and T Fournier. An experimental study of anharmonic micromachined silicon resonators. *Measurement Science and Technology*, 9(11):1821, 1998.

[85] AJ Dick, B Balachandran, DL DeVoe, and CD Mote Jr. Parametric identification of piezoelectric microscale resonators. *Journal of Micromechanics and Microengineering*, 16(8):1593, 2006.

[86] Stephen H Crandall. *Dynamics of mechanical and electromechanical systems*. McGraw-Hill, 1968.

[87] Nesbitt W Hagood, Walter H Chung, and Andreas Von Flotow. Modelling of piezoelectric actuator dynamics for active structural control. *Journal of Intelligent Material Systems and Structures*, 1(3):327–354, 1990.

[88] Henry Angelo Sodano. *Macro-fiber composites for sensing, actuation and power generation*. PhD thesis, Virginia Tech, 2003.

[89] Steven Robert Anton. *Multifunctional piezoelectric energy harvesting concepts*. PhD thesis, Virginia Tech, 2011.